DISCRETE MODELING AND ANALYSIS OF SWITCHING REGULATORS

Thesis by

Dennis John Packard

In partial fulfillment of the requirements

for the degree of

Doctor of Philosophy

California Institute of Technology

Pasadena, California

1976

(Submitted May 24, 1976)

ACKNOWLEDGMENTS

I first wish to thank my advisor, Professor R. D. Middlebrook, for his kind support and suggestions in the development of this work. In addition to this, special thanks are due to Hughes Aircraft Co. for supplying me with financial support through a Hughes Staff Doctoral Fellowship and for providing me with part-time employment during the time of this research. The support and encouragement of Hughes management together with the assistance of the Hughes Engineering Publications Department, Culver City, are also greatly appreciated.

ABSTRACT

A simplified method for finding and using discrete small-signal models for switching regulators is presented. With introduction of a new "straight-line" approximation, and application of root locus techniques, it is demonstrated that discrete models may be used accurately to predict wide bandwidth closed-loop behavior with methods simple enough to be useful in the initial design phase of a switching regulator. The principal result is a set of converter transfer functions comparable to the set derived by describing function techniques, but not subject to the low frequency restriction of describing function models. Also presented is a set of pulse-width modulator transfer functions which indicates that the potential small-signal transient behavior of a switching regulator is independent of the choice of modulator.

TABLE OF CONTENTS

INTRODUCTION

In recent years a new class of power processing circuits called switching regulators has emerged. Advantages such as higher efficiency, lighter weight, and in some cases lower cost when compared with linear regulators, are making these "switchers" more important in a variety of applications. Today these regulators may be found in space satellites, office equipment, computers, and even in hand-held calculators.

So rapid has been their penetration into a wide range of areas that the analysis for switching regulator design has often been done on an ad hoc basis with varying results. In particular, a recurring problem in any switching regulator design is proper choice of the feedback to yield good regulation and fast recovery from various source and load transients. Attempts to extend the bandwidth of such regulators to frequencies near the switching frequency have sometimes resulted in control loop oscillation, quite often at half the switching frequency. This in turn has resulted in sometimes conservative bandwidth design simply for want of an accurate picture of closed-loop behavior near half the switching frequency.

The principal motivation for this thesis is that to date there has not been a single analysis technique applicable to the transient design of switching regulators that is both simple enough for the practicing

engineer to use in an initial design, and accurate enough to model behavior for wide bandwidth regulators.

The transient analysis of a switching regulator is a nonlinear control problem, because regulation is achieved with pulse-width modulation control. Because of this, a number of the standard techniques for analyzing nonlinear control systems have been applied to the problem by various investigators.

The phase plane method, for example, has been used by Bábaá, Wilson, and Yu [1], to demonstrate stability for certain classes of switching regulators. From a design point of view, though, this is a cumbersome method yielding little design information about the actual transient response. Furthermore, the phase plane is limited to second order systems and hence is usually not able to handle a regulator with additional compensation.

Functional analytical methods by Skoog and Blankenship [2], and more recently by Rootenburg and Walk [3] have been used to establish stability bounds for general types of pulse-width modulated systems. Again, these methods give little information about the transient response of a switching regulator other than whether or not it will be stable. Of equal importance is that the mathematics of these techniques are in forms foreign to the circuit designer who is usually more familiar with Bode plots than Banach spaces.

One may conclude then that sufficient literature exists on various large-signal analysis techniques applied to the regulator problem to make a convincing case that the large-signal analysis of switching regulators is excessively complex for initial design purposes.

This leads one to the conclusion that if there is a design technique that meets the criterion of simplicity, it is likely to be a linear small-signal technique.

If one agrees with this argument, then one is confronted with a choice of two approaches.

The approach that has to date shown the greatest simplicity is the describing function (df) method in which the switching regulator components are replaced by linear continuous elements.

Using describing function methods, Middlebrook and Wester [4] have developed equivalent linear continuous models for many types of switch and filter combinations.

From a design standpoint, this approach is currently dominant in the field and may continue to be so principally because df models are often obtained entirely by pictorial circuit manipulation without the necessity of explicit equations. The main disadvantage of this approach is that it suffers from inaccuracy as the closed-loop bandwidth of a switching regulator approaches half the switching frequency. This inaccuracy springs from the assumption that harmonics

generated by pulse-width modulation are attenuated much more than the fundamental modulation frequency in traversing the control loop shown in Fig. 1.

This assumption need only be valid for frequencies below the unity gain bandwidth of the regulator because, beyond the unity gain frequency, attenuation in the loop is sufficient to make both the fundamental and its harmonics insignificant.

It can be shown that the sampling behavior of a pulse-width modulator introduces significant harmonics which are not far beyond the fundamental input frequency, as the fundamental approaches half the switching frequency. Because in the converter these harmonics are attenuated little more than is the fundamental, the assumption of

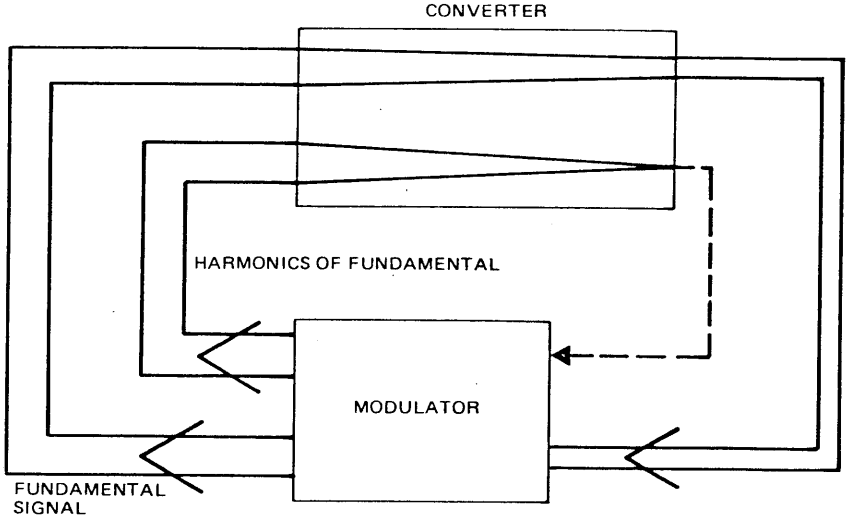

Fig. 1. Harmonic attenuation assumption of describing function models.

Fig. 1 is no longer valid, and if there is sufficient loop gain at these frequencies then the closed-loop behavior will differ from df model predictions.

It is the harmonic attenuation assumption that chiefly limits the valid frequency range of df methods.

One might be content with the describing function approach, regardless of its restricted range of validity, were it not for the fact that particular regulators have been reported in the literature which have transient response superior to those generally designed with df methods [5,6].

These "fast" regulators have often been the product of the second approach to linearization of a switching regulator, which may be called the discrete modeling approach. As will be shown at the beginning of this work, there are no assumptions necessary to derive discrete models other than the small-signal assumption, so that they are capable of accurately describing wide bandwidth behavior. In its present state of definition, however, this technique has only been successfully applied in conjunction with a computer because of its mathematical complexity. Consequently, it is rarely, if ever, used in the initial design phases of a switching regulator.

The conclusion that one is led to then is that, of the two linear approaches, the df models are simple but not accurate at high frequencies, and the discrete models are accurate but not simple enough for general use.

It seemed to this author that the accuracy limitation of the df approach was of a more fundamental nature than the complexity limitation of the discrete approach, and this investigation is the result of that belief.

Basically, the goal of this thesis is to redefine the discrete approach and by removal of as much mathematical complexity as possible make the discrete method applicable as a synthesis tool.

A secondary aim is to fashion the discrete models into forms comparable to the df models to allow comparisons between the two approaches. Knowing that the discrete models are more accurate, we can then use them as a yardstick to measure the accuracy of various df results.

The idea that is the basis for this thesis is to utilize in a new way a type of approximation that designers routinely make when finding the steady state condition of a switching regulator. This is the "straight-line" approximation.

To ensure adequate filtering of switching harmonics, the switching frequency f_s in a regulator is usually much higher than the resonant or cutoff frequency f_c of the filtering components. As will be illustrated in Chapter 1, in the time domain the condition $f_s >> f_c$ results in some of the steady state regulator waveforms appearing very much like straight lines. Use of this fact allows designers to do a simple and accurate analysis to find the steady state waveforms.

It is shown here that application of a generalization of the straight line approximation during a discrete model derivation greatly simplifies computation of the discrete model parameters without sacrifice of the inherent accuracy of the discrete model at high frequencies. It is this result more than any of the others presented here that makes it possible to use discrete modeling as a synthesis tool.

In addition, it is shown that the analysis of a regulator may be broken into separate simpler parts. One can independently arrive at discrete models for a portion of the regulator called the "converter" consisting of the electronic switch and power filtering components. In a similar manner, one can independently derive discrete models for various kinds of pulse-width modulators. Finally, through the use of a "non-loading" approximation, Appendix 2 demonstrates that the compensation problem may be isolated to a certain extent from the basic converter models. Following is a brief summary of the contents of each chapter and its contribution to the discrete model development.

We begin with what a switching regulator is and how it works in Chapter 1, concluding with a discussion of stability and a heuristic argument on why the discrete method should be appropriate for a pulse-width modulated (PWM) system. This chapter also introduces the basic method that designers use to find the approximate steady

state conditions in a switching regulator. It is necessary to know this method because various parameters of the steady state solution often occur in the small-signal discrete models. Also in Chapter 1 a boost converter is introduced as an example for the steady state analysis method. This converter is used as an example throughout the thesis to demonstrate in a concrete way methods which are often derived first in a general form.

In the second chapter it is shown how a generalized switch and filter combination may be exactly described on a small-signal basis by a system of linear difference equations. The difference equations are then derived for the boost converter.

In the third chapter a variety of standard pulse-width modulators are shown to be characterized by simple linear difference equations on a small-signal basis.

Chapter 4 introduces the use of the z-transform to the discrete modeling method. In this chapter the z-transform is used to formulate the closed-loop transient problem for a switching regulator in the z-plane. The notion of transfer functions and loop gain are introduced to make the discrete model seem less strange to the practicing engineer. When the z-transform is applied to the modulators introduced in Chapter 3, the surprising result is that their discrete models all have no poles, zeros, or phase shift in the z-plane.

An example of the discrete method as a design aid is presented in Chapter 5 with use of the boost converter again as an example. A review of the discrete model derivation is given to clarify the technique. Next, explicit solutions for the discrete converter transfer functions are used to motivate the "straight-line" approximation. Application of this approximation then allows easy computation of the converter transfer functions. Finally, the root locus technique is applied to these transfer functions in the z-plane to predict potential closed-loop switching regulator transient performance. It is shown that conditions for high frequency behavior such as half switching frequency oscillation and an optimally fast transient response are predicted by use of the root locus technique on the discrete converter model.

The results predicted in Chapter 5 are verified in Chapter 6 by comparison of the discrete model against the large-signal boost converter in a digital simulation.

Various conclusions and a review of the discrete results are summarized in Chapter 7.

Additional information about and extensions of the discrete method are presented in the appendices.

Appendix 1 shows a systematic way by which state equations for a switching regulator may be derived.

Appendix 2 shows how reactive regulator compensation may be analyzed with discrete models simple enough that the method remains useful to the designer.

Finally, Appendix 3 uses a physical argument to motivate the proof of an invariance property of the discrete models.

Chapter 1

Basic Operation of Switching Regulators

In this chapter the basics of what a switching regulator is and how it operates are described. A steady state analysis of a boost converter is performed to illustrate the simplicity of the analysis method and the accuracy of the result. This is also meant to familiarize the reader with the specific operation of this converter, because it will be used as an example for the techniques developed in later chapters of this thesis.

With this analysis complete, some of the advantages of switching regulators over their linear counterparts become more obvious and are noted. The chapter concludes with a qualitative discussion of the stability problems one can expect when closing a feedback loop around a switching converter.

A switching regulator is a piece of electronic equipment which processes some unregulated or partly regulated source of ac or dc electrical power. The output of the regulator is ac or dc power where generally the voltage (or sometimes current) is constrained to be constant under a variety of loading conditions. The key to what makes a regulator a switching regulator is that the active power handling devices are operated in either closed or open conditions so that they may be characterized as switches.

Herein the term "regulator" will refer to a complete power processing unit incorporating some form of feedback. As shown in Fig. 1.1, the regulator may be considered to be composed of three parts.

The power handling part of the regulator is called a "converter". This consists of electronic switches and any power filtering components. From Fig. 1.1 we note that any significant power that a switching regulator handles flows into and out of the converter only. Inputs to a converter consist of a source of power usually unregulated,

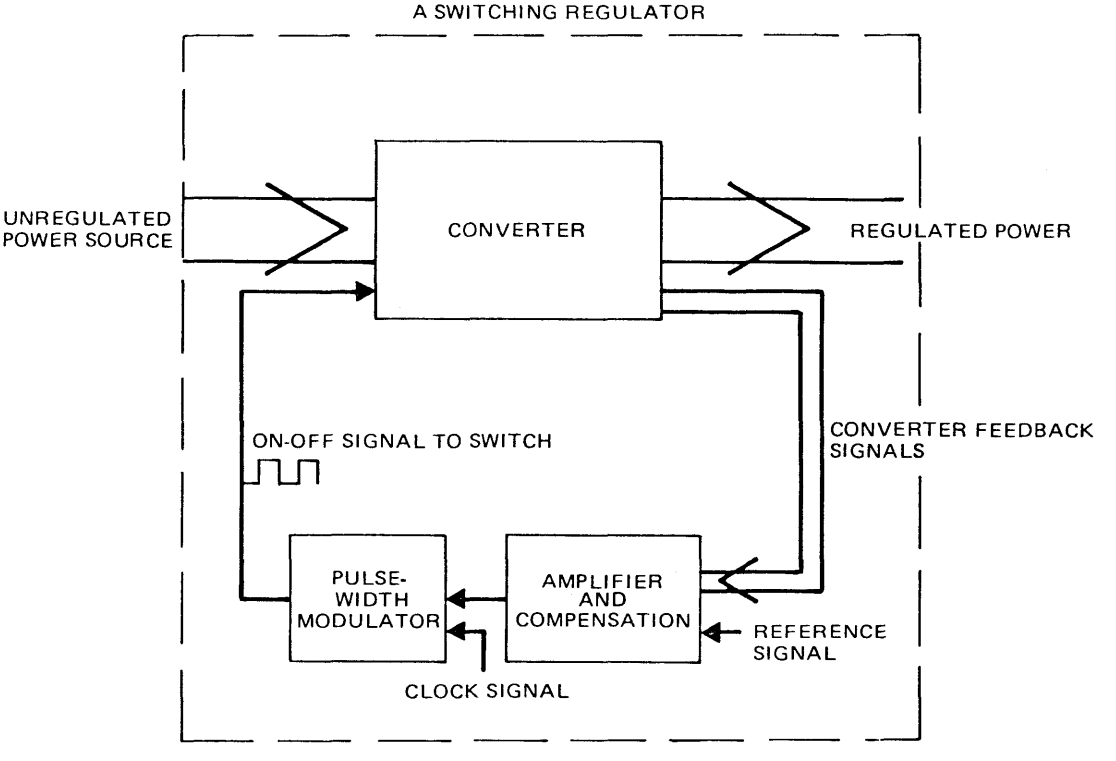

Fig. 1.1. Block diagram of the constituent parts of a switching regulator.

and an on-off signal that drives the switch inside the converter. The converter outputs are the regulated power and a set of feedback signals which in general will be some measure of the capacitor voltages and inductor currents in the converter.

The second part of a regulator is labelled "compensation" in Fig. 1.1. "Compensation", as it is used here, includes any additional reactive elements (usually capacitors) used to alter and improve the closed loop performance of a switching regulator. Inputs to the compensation are the various converter feedback signals and usually a reference signal, while its output is a single analog signal which serves as input to the pulse-width modulator. In its simplest form the compensation output may be just a linear combination of its inputs. This will be the case for the examples in the main body of this thesis. Treatment of more complex compensation is given in Appendix 2.

The third part of a switching regulator shown in Fig. 1.1 is the pulse-width modulator. Its inputs are the combined feedback signal produced by the compensation and sometimes, but not always, a clock signal which can set the switching frequency of the regulator. The modulators considered in this thesis will all be of the "clocked" type, since control of the switching frequency is mandatory for many applications. Also, the analysis seems to yield more useful results for clocked regulators. The output of the pulse-width modulator is a sequence of on-off signals which drives the switch in the converter.

These three blocks, the converter, compensation, and the pulse-width modulator, are the consituent parts of any switching regulator.

To illustrate the importance of the switching regulator, consider the linear regulator of Fig. 1.2. In this circuit the series pass element behaves as a variable resistor which maintains a constant output voltage for source and load variations. If, as shown, the load current is 1 A and the source voltage is 14 V, then the pass element must support 9 V to maintain the 5 V output voltage. Under this condition the regulator absorbs 9 watts of power while delivering only 5 watts of power to the load. If we define η, the efficiency, as load power/total input power, then $\eta = 5/14 = 0.36$. Hence, the efficiency is only 36%.

This efficiency is costly in terms of power wasted. Furthermore, since the wasted power is dissipated in the regulator, adequate means to dispose of the resultant heat must be provided. This

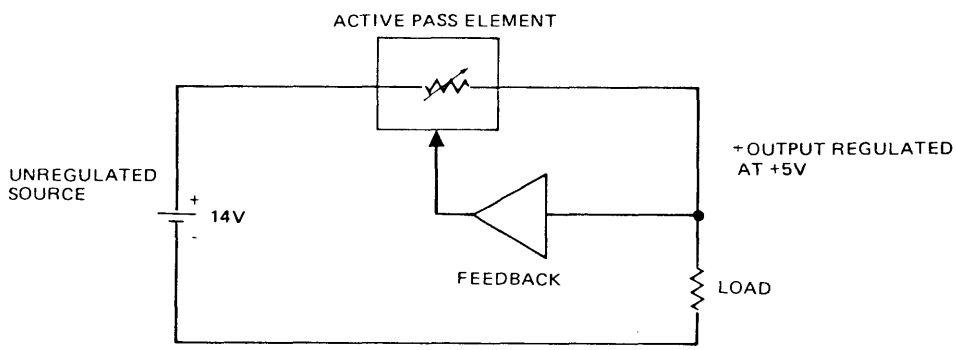

Fig. 1.2. Equivalent circuit for a 5 V linear regulator.

typically means greater volume and weight when compared with switching regulators of an equivalent power handling capacity.

To understand how a switching regulator works we will first examine a converter, since this is the part of a switching regulator through which the power flows.

Figure 1.3 is an example of a type of converter known as a "boost" converter because its output voltage is always greater than or equal to its input voltage. It has a number of features typical of most switching converters. First, the control element is operated as a switch. In this case the element is a bipolar transistor. In most converters a diode is required along with the switch to carry reactive current when the switch is open. This is noted in Fig. 1.3 as DI and is known as the commutating diode. The other necessary parts of a converter are the filtering elements to smooth the step-like waveforms produced at the switch. The converter power source is a voltage source of magnitude V_s, and its load is shown in Fig. 1.3 as a resistor R.

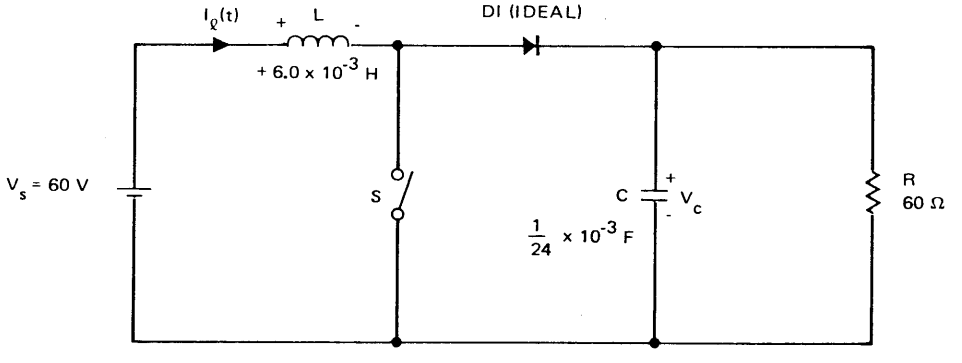

Fig. 1.3. Circuit schematic for a boost converter.

We now derive the steady state solution for this converter, because it is in doing this that its basic operation is understood.

At a steady state condition, the switch S in Fig. 1.3 is driven by the periodic on-off signal shown in Fig. 1.4, which is the output of a pulse-width modulator. This periodic on-off signal establishes the switching frequency of the converter, and ultimately of the regulator when a loop is closed around the converter as in Fig. 1.1. At a steady state condition the on-time τ_1, and the off-time τ_2, are constant from period to period.

The ratio of the on-time of the switch τ_1 to the total switching period T as is defined as D, the duty ratio:

$$D \triangleq \frac{\tau_1}{T}$$

To begin the steady state analysis we find an approximation for the average output voltage $\overline{V}_c$ by the following argument.

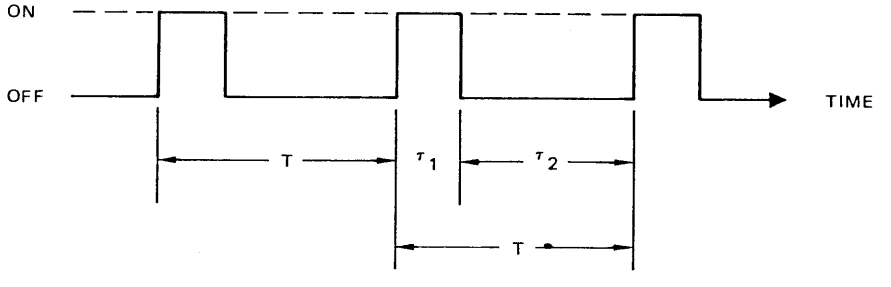

Fig. 1.4. Steady state on-off signal to converter switch.

If the converter in Fig. 1.3 is at its steady state, then the average voltage across the inductor per period must be zero. If this were not so, inductor current would continue to build up or decay until this condition is met. During the on-time τ_1 a voltage of V_s is impressed across the inductor. The energy stored in the inductor cannot change instantaneously, requiring continuity of inductor current when the switch opens. Thus as the switch opens, the voltage across the switch rises to V_c plus a diode drop. For the analysis in this work all diodes will be assumed to be ideal, and hence their forward voltage drops will be neglected.

Since the inductor current increases during the switch on-time, it must decrease during the off-time if the converter is to be at a steady state. Thus V_c must be larger in magnitude than V_s, which demonstrates the "boost" property of the circuit of Fig. 1.3.

With one further assumption and one more approximation, we shall have the first result. If the inductor current $I_\ell(t)$ decreases during the off time of the switch, it is possible that it may go to zero before the switch closes again. At zero inductor current the diode no longer conducts and the voltage across the inductor is zero until the switch turns on again. This mode of operation is known as the "discontinuous" or "light" conduction mode. If the steady state inductor current does not become zero during the switch off-time,

this is known as the "continuous" or "heavy" conduction mode. It can be shown that the methods developed in this thesis are applicable to both cases.

For simplicity, we shall assume throughout this thesis that the converters are always in the continuous conduction mode. With this assumption, the reverse voltage across the inductor is $V_c - V_s$ throughout the switch off-time.

If the boost converter is to do an adequate job in reproducing a dc voltage at its output, the ripple voltage on V_c should be small compared with the average $\overline{V}_c$. Hence it is a good approximation during the off-time τ_2 that the inductor supports a constant reverse voltage $\overline{V}_c - V_s$.

The requirement for zero average voltage across the inductor over a complete period $\tau_1 + \tau_2 = T$ then gives a formula for the average output voltage:

$$V_s \tau_1 = (\overline{V}_c - V_s) \tau_2$$

$$\overline{V}_c = \frac{T}{\tau_2} V_s = \frac{T}{1-\tau_1} V_s = \frac{V_s}{1-D} \qquad (1.1)$$

Equation (1.1) establishes why the converter of Fig. 1.3 is called a "boost" converter. We see that as the switch is closed for a larger and larger portion of each period (D increasing) the average output voltage is increased for a constant input voltage. Thus the

boost converter behaves like a step-up dc transformer. If we can find the steady-state time waveforms $\overline{I}_\ell(t)$ and $\overline{V}_c(t)$, then the steady state converter behavior is completely known. So far we have found $\overline{V}_c$, the approximate average of $\overline{V}_c(t)$. Next $\overline{I}_\ell$, the average of $\overline{I}_\ell(t)$ will be found.

At the steady state, the net current into the output capacitor must be zero. The average current flowing out of the capacitor to the load is $\overline{V}_c/R$. Current only flows into the capacitor from the inductor when the switch is open so that the average current flowing into the capacitor is $\overline{I}_\ell \tau_2/T$. This gives a relation for $\overline{I}_\ell$, the average inductor current in terms of the average output voltage $\overline{V}_c$.

$$\frac{\tau_2}{T}\overline{I}_\ell = \frac{\overline{V}_c}{R} \tag{1.2}$$

Use of specific values shown in Fig. 1.3, and $\tau_1 = \tau_2 = 0.5 \times 10^{-4}$ sec. so that $T = 10^{-4}$ sec. (f_s = 10 kHz), gives $D = \tau_1/T = 0.5$. Evaluation of Eq. (1.1) leads to an average output voltage $\overline{V}_c$ of 120 V. If the resistance R is 60 Ω, then Eq. (1.2) indicates that the average inductor current $\overline{I}_\ell$ should be 4 A.

It is now possible to sketch a fairly accurate picture of $\overline{I}_\ell(t)$, as shown in Fig. 1.5.

Because the source V_s is constant and the steady state output voltage $\overline{V}_c(t)$ must be nearly constant for the converter to be useful, the slope of the inductor current is nearly constant as shown in

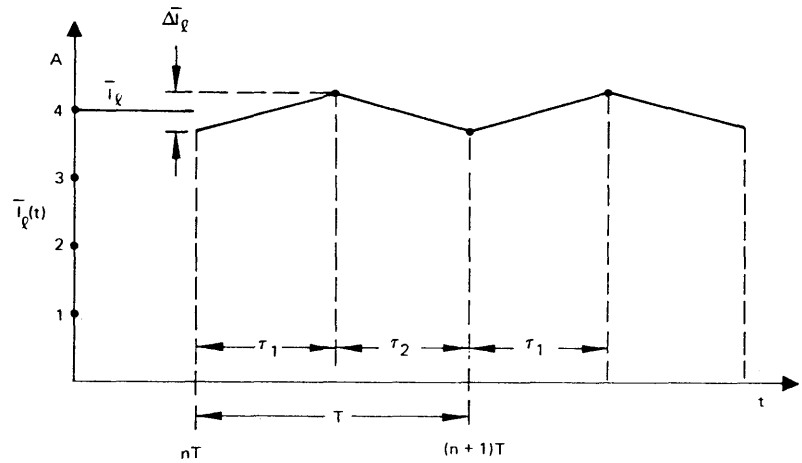

Fig. 1.5. Steady state inductor current $\bar{I}_\ell(t)$ for boost converter.

Fig. 1.5 whether the switch is open or closed. During the time τ_1 when the switch is closed, the slope of $I_\ell(t)$ is determined by:

$$V_s = L\frac{d\bar{I}_\ell(t)}{dt} = L\frac{\Delta\bar{I}_\ell}{\Delta t} = L\frac{\Delta\bar{I}_\ell}{\tau_1}$$

For the element values in Fig. 1.3 and with $\tau_1 = 0.5 \times 10^{-4}$ sec, the change in inductor current $\Delta\bar{I}_\ell$ during τ_1 is calculated to be $\Delta\bar{I}_\ell = 0.5$ A.

Knowledge of the average inductor current $\bar{I}_\ell$ and its change $\Delta\bar{I}_\ell$ is sufficient for completion of the picture of $\bar{I}_\ell(t)$. In particular, we can say that if the time when the switch closes is called t = nT,

then $\bar{I}_\ell(nT) \sim 3.75$ A. The approximate solution for $\bar{I}_\ell(t)$ is accurate to the extent that the voltage ripple on $\bar{V}_c(t)$ is small compared with its average $\bar{V}_c$.

We can compute $\bar{V}_c(t)$ to see if the small ripple assumption is valid. If the ripple is small, then the assumptions are consistent, and the resulting steady state solutions are accurate.

During the time when the switch is closed, the capacitor discharges into the load resistor. The slope of the output voltage during this time is governed by:

$$\frac{d\bar{V}_c(t)}{dt} = -\frac{\bar{V}_c(t)}{RC}$$

However, if $\bar{V}_c(t)$ does not change much during this time, then the slope is nearly constant and we may approximate it as follows:

$$\frac{d\bar{V}_c(t)}{dt} \simeq -\frac{\bar{V}_c}{RC} \simeq \frac{\Delta\bar{V}_c}{\Delta t} = \frac{\Delta\bar{V}_c}{\tau_1}$$

$$\Delta\bar{V}_c = -\tau_1 \frac{\bar{V}_c}{RC}$$

For the element values shown in Fig. 1.3 and $\tau_1 = 0.5 \times 10^{-4}$ sec, $\Delta\bar{V}_c$ is 2.4 V which is only 2% of $\bar{V}_c = 120$ V. Thus the results are consistent and we may sketch $\bar{V}_c(t)$ as shown in Fig. 1.6.

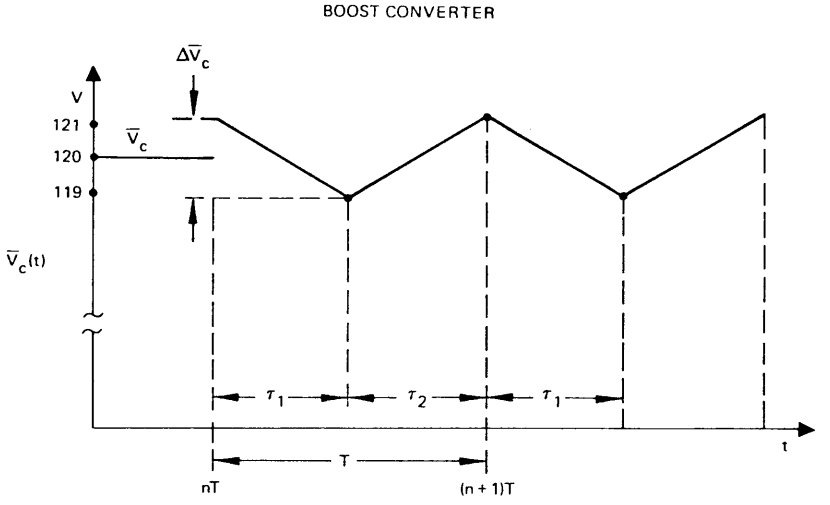

Fig. 1.6. Steady state capacitor voltage $\bar{V}_c(t)$ for boost converter.

In addition, knowing $\bar{V}_c$ and $\Delta\bar{V}_c$ we can say that if the time when the switch closes is t = nT then $\bar{V}_c(nT) \sim 121.2$ V.

As a check on the accuracy of this approach to finding the steady state solutions, a computer program was used to simulate this converter and calculate the exact (or at least more exact than this approach) values for $\bar{I}_\ell(nT)$ and $\bar{V}_c(nT)$, with the following results:

	Predicted	Exact
$\bar{I}_\ell(nT)$	3.750	3.7478
$\bar{V}_c(nT)$	121.200	121.145

So we see that with some very simple analysis it is possible to find quite accurately the steady state conditions for a switching converter.

Before consideration of the problem of making a regulator out of this converter, something should be said about the advantages these circuits enjoy over their linear competitors. As was noted in the example shown in Fig. 1.2, a linear regulator may absorb a significant amount of power in performing a regulation function. In a switching converter such as the boost converter, if the switch, diode, and filtering elements were ideal, the efficiency would be 100%. Indeed, in practical circuits efficiencies on the order of 80% are easy to achieve. For state-of-the-art equipment, efficiencies as high as 95% have been reported [7].

In addition to their usually higher operating efficiency, switching regulators offer an extra degree of flexibility over linear regulators in that various topologies exist which can step the input voltage up (as with the boost converter), down, or both.

Now that we understand how the converter part of a switching regulator works and its advantages over linear regulators, this chapter will conclude with a discussion of the stability problems that occur when one tries to close a feedback loop around a converter to make it a regulator.

To make the converter of Fig. 1.3 a voltage regulator, a signal loop is made by choosing a pulse-width modulator and compensation as shown in Fig. 1.1. The feedback is set up such that an increase in the steady state output voltage tends to decrease the duty ratio of

the modulator. With sufficient gain in this loop, the output voltage of the regulator may be made insensitive to both source and load changes.

The basic steady state behavior of a great variety of switching regulators is well understood by designers in the field. However, analysis of the closed-loop dynamics of such circuits is another story. Because the control loop contains what is well approximated as a switch, analysis of the dynamics of the loop is a nonlinear control problem.

The problem of designing compensation to stabilize such a feedback loop would be much easier if the problem were linear. Two things favor this approach. First, in any well-designed switching regulator, regardless of topology, the switching frequency is deliberately designed to be much higher than the natural frequencies of the power handling filtering components. This is done so that ac components due to the switching will be small relative to the desired output. Second, in many cases the type of instability that commonly occurs is some relatively low-frequency modulation of the duty cycle which, after filtering, results in a nearly sinusoidal output.

The presence of a low-pass element along with generally low frequency phenomena being observed suggests that a describing function representation of the feedback and stability problem would be fruitful. The method as described by Middlebrook and Wester has

indeed shown itself to be both easy to work with and reasonably accurate in the prediction of performance at frequencies well below the switching frequency.

The problem is that engineers (and their customers), as a group are never satisfied with a regulator that merely works. There is always the urge to extend the performance of these circuits. One thing which seems easy enough to do is to improve the transient response. To do this one may increase the closed-loop bandwidth. However, as the closed-loop bandwidth approaches half the switching frequency, the linear continuous model gives erroneous results.

For a simple example of why this happens, imagine a regulator whose pulse-width modulator (PWM) is implemented as shown in Fig. 1.7. Here the on-off signal to the switch is produced by comparison of a sawtooth clock waveform with the feedback signal. Under steady state conditions the feedback signal is a voltage containing a ripple at the sawtooth frequency, if the modulator is not saturated (i.e., always on or always off). Since the time at which the switch turns off is determined by the sawtooth, information from the feedback is passed through the modulator once per cycle at the instant the switch is turned on.

Roughly speaking, information about the feedback signal flows through the modulator at discrete instants at a rate equal to the switching frequency. In other words, the pulse-width modulation

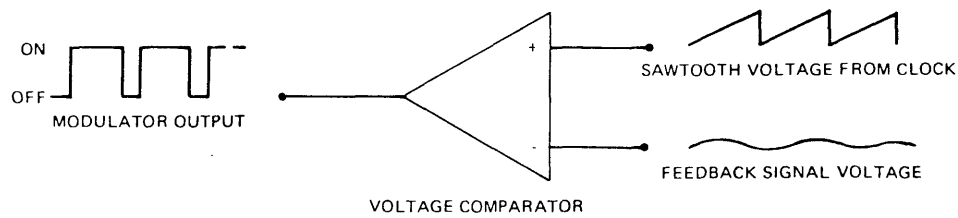

(a) SAWTOOTH PULSE WIDTH MODULATOR CIRCUIT

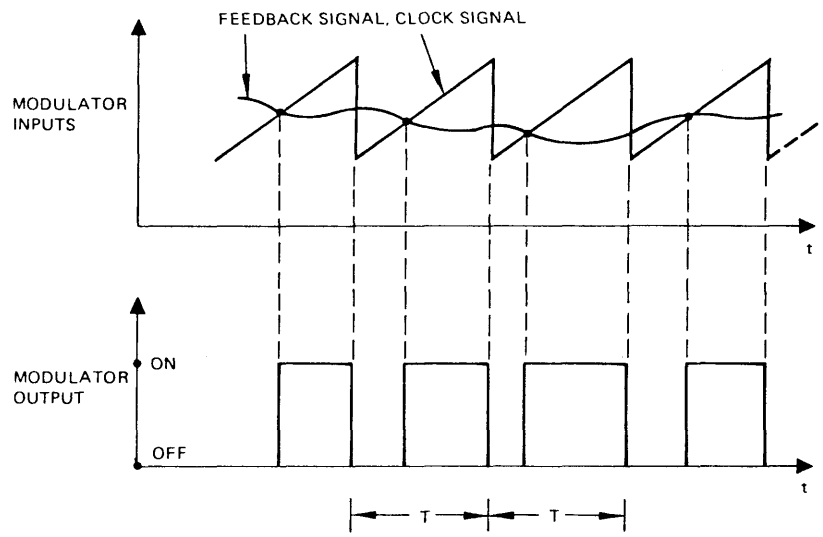

(b) MODULATOR TIMING

Fig. 1.7. Sawtooth modulator circuit and timing.

behaves as a sampler which samples the feedback signal at the switching frequency. Unlike the ideal analog sampler, the PWM does not have to sample uniformly (i.e., time between samples constant) nor is its output a series of impulse functions. Nevertheless, one might expect that signals entering the modulator with bandwidth greater than half the switching frequency would be in for trouble, which is indeed the case. If the information coming out of the modulator is contained in the time location of one of the switching instants per cycle, then periodic motion of this switching edge with respect to its steady-state location can occur at a maximum rate of half the switching frequency. Clearly, if a switching regulator is unstable with a small oscillation in duty ratio, the maximum possible frequency of oscillation is half the modulator switching frequency.

We may surmise that since the PWM in a switching regulator is part of the feedback loop, a linear small-signal continuous model of the loop dynamics will become increasingly inaccurate at higher frequencies in describing loop behavior, because of the sampling nature of the PWM. Chapter 2 will show how this inaccuracy at frequencies near half the switching frequency may be overcome by using a linear small-signal discrete model for the regulator. This is done by replacing the approximate differential equations of the continuous model with a set of exact difference equations.

Chapter 2

Derivation of Converter Difference Equations

This chapter introduces the discrete analysis of a switching converter. The first part of the chapter shows how one can derive the exact set of small-signal linear difference equations which characterizes a generalized switching converter about a steady state operating point. Equivalent derivations have been done before, but by means of somewhat different arguments and notation [6,8]. Also, to point out the differences between the discrete converter models, and describing function or "averaged" converter models, their derivations are compared.

To add concreteness to the general converter model derivation, the difference equations for the boost converter introduced in Chapter 1 are found. This derivation is done briefly to illustrate how a designer would proceed; the derivation will be reviewed in Chapter 5.

Although the general derivation requires a substantial amount of algebra and matrix manipulation, most of the math is in the general derivation and very little is shown to be necessary in putting the method into practice.

The conclusions to be drawn from this chapter are: first, a difference equation model of a converter is a true small-signal linear model with no "low-frequency" approximations necessary for its

validity, and second, at least in form, the difference equations are not difficult to derive.

The idea that a nonlinear system containing a switch might be analyzed with discrete techniques is not a new one. It has an interesting history, first being described by Y. S. Zypkin [9] in the analysis of the stability of limit cycles in certain relay control systems. A large-signal approximate extension of the idea for a particular type of PWM system was later used by R. E. Andeen [10]. Later, McVey and Nurre [11] used the method to locate possible limit cycles in relay-type systems. More recently Sucena-Paiva et al [12] have successfully demonstrated the method in studying the stability of silicon-controlled-rectifier regulator circuits. Finally, Prajoux, Capel, and Ferrante [6], and Iwens, Yu, and Triner [8] have developed the analysis in exact form for several special types of switching regulators such as the one mentioned in Chapter 1.

The discrete model of a switching converter, like any other small-signal model, is useful in describing the local behavior about some operating point of what is basically a nonlinear system. For sufficiently small disturbances from the operating point the discrete model gives an accurate description of how the actual converter behaves.

We begin the derivation of the converter difference equations by introducing the large-signal mathematical model of Eqs. (2.1):

$$\dot{x}(t) = D_1(t)\left[A_1 x(t) + B_1 u\right] + D_2(t)\left[A_2 x(t) + B_2 u\right] \qquad (2.1)$$

in which

$$x(t) = \begin{bmatrix} x_1(t) \\ \cdot \\ \cdot \\ \cdot \\ x_m(t) \end{bmatrix} \qquad \dot{x}(t) = \begin{bmatrix} \frac{dx_1(t)}{dt} \\ \cdot \\ \cdot \\ \cdot \\ \frac{dx_m(t)}{dt} \end{bmatrix}$$

This set of matrix equations characterizes the behavior of most switching converters. The notation is as follows: $x(t)$ is an m^{th} order column vector containing the state variables of the converter at time t. Its components $x_1(t)$ through $x_m(t)$ are chosen such that they are all <u>continuous</u> functions of time. The functions $D_1(t)$ and $D_2(t)$ are scalar functions which may be termed pulse-width modulation functions or simply modulation functions. These functions are described pictorially in Fig. 2.1. They have the following properties:

1. They are binary valued, being either zero or unity.
2. Their sum $D_1(t) + D_2(t)$ is unity for all t.

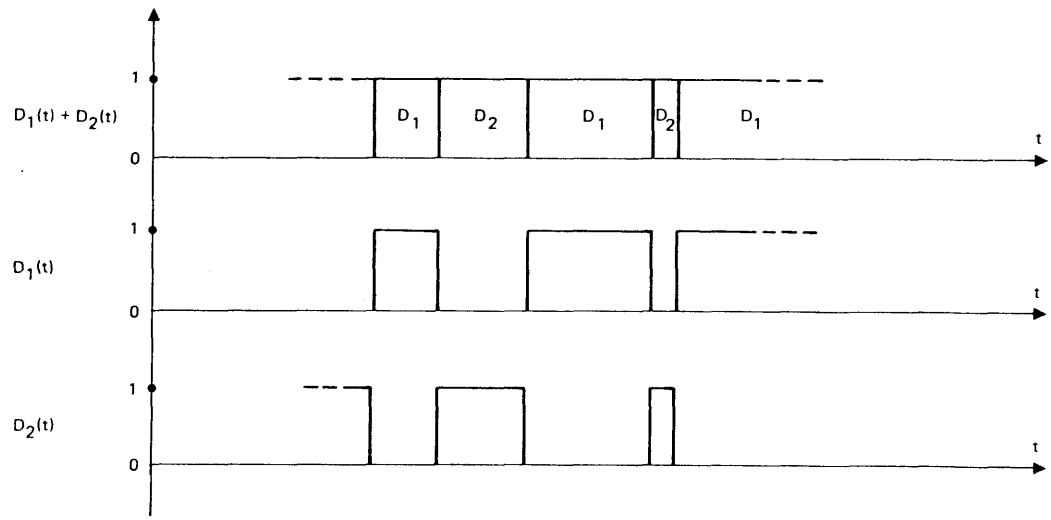

Fig. 2.1. Modulation function timing diagram.

Physically these functions represent the alteration of the converter topology as ideal switches are opened and closed, and in general there is no requirement for periodicity.

The matrices A_1 and A_2 are m x m constant matrices, while B_1 and B_2 are m x r constant matrices. Independent voltage and current sources are contained in u an r^{th} order column vector. For simplicity these sources are taken to be dc sources in this derivation. This choice is adequate to treat many types of converters, although it can be shown that the only necessary assumption about the sources is that they are periodic at the converter switching frequency. During a time interval when $D_1(t) = 1$, A_1 and B_1 indicate the current network topology. At the instant when D_1 becomes zero and D_2

becomes unity, the new network topology is described by A_2 and B_2, and reverts to A_1, B_1 when again D_1 becomes unity and D_2 zero. As already stated, the components of x(t) are chosen so that they are continuous across each switching transition. The operation of this generalized open loop converter is summarized in Fig. 2.2.

Formulation of the large-signal converter model of Eqs. (2.1) is the first step in the difference equation derivation. The next step is choice of a steady state operating condition for the converter.

The boost converter example in Chapter 1 showed that the signal that "drives" the converter is the on-off signal from the pulse-width modulator. We were able to find the steady state converter waveforms when this modulator signal was periodic with constant duty ratio. This on-off signal is modeled in Eqs. (2.1) by the modulation

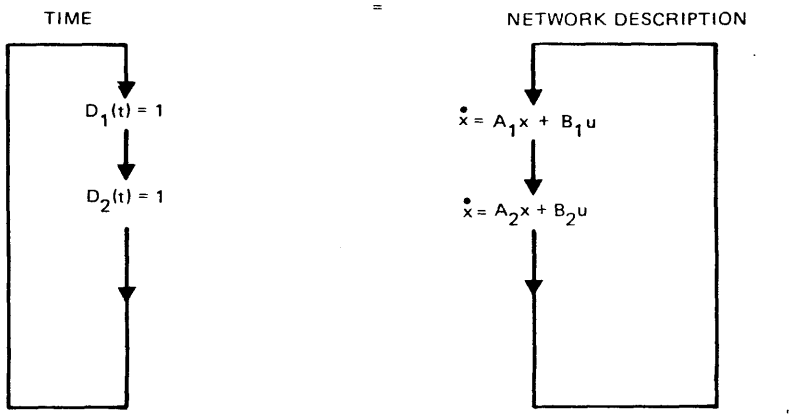

Fig. 2.2. Operation of generalized open-loop converter.

functions $D_1(t)$ and $D_2(t)$. We therefore conclude that to choose a particular steady state condition, $D_1(t)$ and $D_2(t)$ must be periodic functions of t. These functions are denoted as $\bar{D}_1(t)$ and $\bar{D}_2(t)$, each being unity for a time τ_1 and τ_2 respectively, as shown in Fig. 2.3.

From the example in Chapter 1 we know that if a boost converter is excited by a periodic switch drive, the steady state inductor current $\bar{I}_\ell(t)$ and capacitor voltage $\bar{V}_c(t)$ are also periodic functions of time. Hence, we conclude that the steady state solution of Eqs. (2.1) which we call $\bar{x}(t)$ is periodic with the same period as $\bar{D}_1(t)$ and $\bar{D}_2(t)$. Thus, the second step in the derivation is to specify

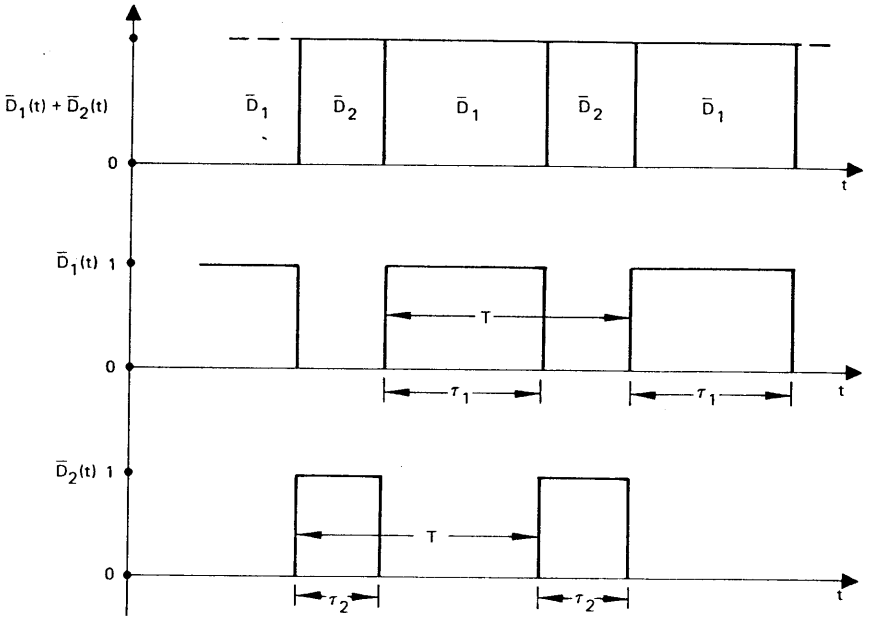

Fig. 2.3. Steady state modulation function timing.

steady state modulation functions $\bar{D}_1(t)$ and $\bar{D}_2(t)$ which give rise through Eqs. (2.1) to a steady state solution $\bar{x}(t)$. The steady state quantities $\bar{D}_1$, $\bar{D}_2$ and $\bar{x}$ then satisfy Eqs. (2.2):

$$\dot{\bar{x}} = \bar{D}_1 [A_1\bar{x} + B_1u] + \bar{D}_2 [A_2\bar{x} + B_2u] \qquad (2.2)$$

The next step in the derivation is description of the behavior of perturbations about the steady state condition. The source of the perturbations $\tilde{x}(t)$ is modulation of the widths of the D(t) functions about their steady state values. Figures 2.4a, b and c show that there are three different ways of doing this. The crosshatched edges in these figures indicate that these switching instants are moved about their steady state time locations from cycle to cycle.

In later examples in this work the time when the converter switch is closed is taken as the $D_1 = 1$ interval. The words "leading" and "trailing" are defined with respect to when the switch is closed so that "leading-edge" modulation is of the instant when D_1 becomes unity and "trailing-edge" modulation is of the instant when D_1 becomes zero.

For this derivation we choose the type of modulation to be leading-edge modulation as shown in Fig. 2.4a. The difference equation derivation for trailing-edge modulation is identical to that of leading-edge modulation except for a change in the time reference, so the result for this case will simply be stated. Although it can be

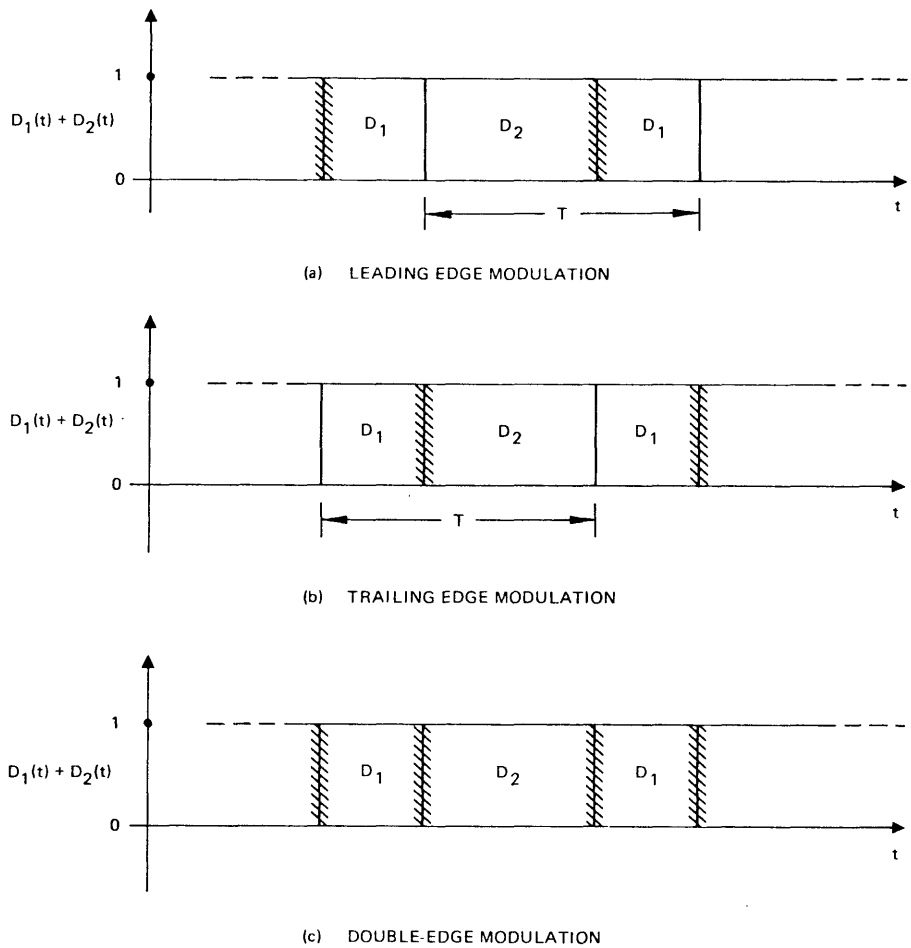

Fig. 2.4. Three types of pulse-width modulation.

shown that the double-edge modulation of Fig. 2.4c can be analyzed with discrete models, the results are more complex and they contribute little additional understanding to the difference equation derivation, so this case is ignored here.

Having chosen leading-edge modulation, we continue toward describing the behavior of perturbations on the steady state solution by modeling perturbations on the steady state modulation functions. Figure 2.5 shows two consecutive leading-edge perturbations in detail. The width of the n^{th} perturbation is a time Δt_n, but instead of using this variable in the derivation we use a normalized variable d_n defined by the relation $d_n = \Delta t_n / T$. The modulation being small compared with the converter period T then implies $|d_n| \ll 1$. The steady state location of the leading edge of the n^{th} converter cycle is chosen as the reference time nT.

Figure 2.5 shows that leading-edge modulation is equivalent to addition of a stream of pulses d(t) to $\bar{D}_2(t)$ and subtraction of this

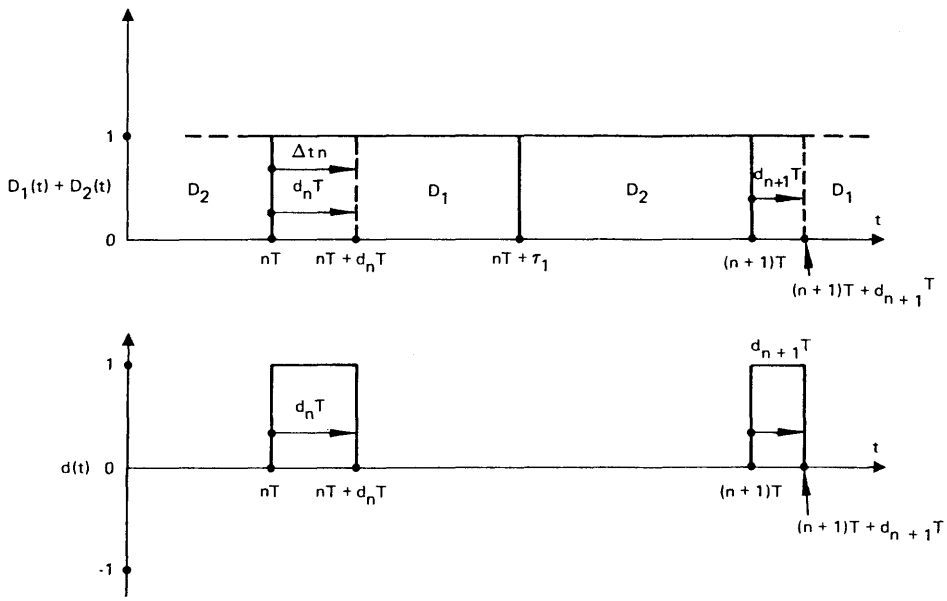

Fig. 2.5. Detail of leading-edge pulse-width modulation timing.

same stream of pulses from $\bar{D}_1(t)$, that is, $D_2(t) = \bar{D}_2(t) + d(t)$ and $D_1(t) = \bar{D}_1(t) - d(t)$.

To determine the effects of the modulation shown in Fig. 2.5, we substitute $D_1(t) = \bar{D}_1(t) - d(t)$ and $D_2(t) = \bar{D}_2(t) + d(t)$ into Eqs. (2.1). Since this perturbation in the steady state modulation should give rise to a perturbation $\tilde{x}(t)$ on the steady state solution $\bar{x}(t)$, we also substitute $x(t) = \bar{x}(t) + \tilde{x}(t)$ into Eqs. (2.1) to yield Eqs. (2.3):

$$\dot{\bar{x}} + \dot{\tilde{x}} = \left(\bar{D}_1 - d\right)\left[A_1(\bar{x} + \tilde{x}) + B_1 u\right] + \left(\bar{D}_2 + d\right)\left[A_2(\bar{x} + \tilde{x}) + B_2 u\right] \tag{2.3}$$

Subtraction of the steady state Eqs. (2.2) from Eqs. (2.3) leaves Eqs. (2.4), which describe the behavior of the perturbation $\tilde{x}(t)$ caused by the modulation $d(t)$:

$$\dot{\tilde{x}} = \overset{1}{\bar{D}_1 A_1 \tilde{x}} + \overset{2}{\bar{D}_2 A_2 \tilde{x}} + d\left[\left(A_2 - A_1\right)\bar{x} + \left(B_2 - B_1\right)u\right] + \overset{3}{d\left[\left(A_2 - A_1\right)\tilde{x}\right]} \tag{2.4}$$

The right-hand side of Eqs. (2.4) consists of three parts. The first part represents the steady state dynamics of the open-loop converter when there is no modulation. The second part may be thought of as a forcing function or input. It consists of a stream of pulses $d(t)$ with gain coefficients dependent in general on the steady state solution $\bar{x}(t)$ and on the independent sources. Finally, there is a third part which is a "small" stream of pulses compared with the second part if the components of $\tilde{x}$ are "small".

It can be shown that the third part of Eqs. (2.4) ultimately makes a negligible contribution to small-signal equations, so we neglect this term and complete this part of the difference equation derivation by writing the differential equations for "small" perturbations as Eqs. (2.5):

$$\dot{\tilde{x}} = \bar{D}_1 A_1 \tilde{x} + \bar{D}_2 A_2 \tilde{x} + d\left[\left(A_2 - A_1\right)\bar{x} + \left(B_2 - B_1\right)u\right] \qquad (2.5)$$

At this point if a continuous small signal model of the system is desired, an averaging operator may be applied to both sides of Eqs. (2.5) resulting in the set of continuous differential equations (2.6):

$$\langle\dot{\tilde{x}}\rangle = \left[\frac{T_1}{T} A_1 + \frac{T_2}{T} A_2\right]\langle\tilde{x}\rangle + \langle d\rangle\left[\left(A_2 - A_1\right)\langle\bar{x}\rangle + \left(B_2 - B_1\right)\langle u\rangle\right] \qquad (2.6)$$

In Eqs. (2.6) $\langle\tilde{x}\rangle$ indicates the new set of variables and is some average of $\tilde{x}$ such as $\frac{1}{T}\int_{t-T}^{t} \tilde{x}\, dt$.

This is the averaging method of Middlebrook and Wester. One result of this method of linearization is that there is a disparity between the actual average perturbation and $\langle\tilde{x}\rangle$, its average as computed by Eqs. (2.5), which increases as $\tilde{x}$ changes more rapidly in one converter cycle. This is because the average of the product of $\bar{D}_i(t)\tilde{x}$ in general is <u>not</u> equal to the product of the averages of

$\tilde{D}_i$ and $\tilde{x}$ unless $\tilde{x}$ is constant. Thus an approximation is made to get from Eqs. (2.5) to Eqs. (2.6), which requires the switching frequency of the converter to be much higher than the cutoff frequency of the power filtering components. This approximation is well satisfied for most converters, making measurements of open-loop averaged quantities agree well with predictions at frequencies up to half the switching frequency. Yet experience shows that the averaged converter models give erroneous predictions of regulator transient response as the closed-loop bandwidth nears half the switching frequency. The reason for this paradoxical behavior is that the averaged models also require the harmonic assumption discussed in the introduction to describe closed-loop behavior. So, rather than average the Eqs. (2.5), we continue with the difference equation derivation here.

The final step in the derivation of the converter difference equations is to integrate the "small" perturbation equations (2.5) across one complete converter period in the time domain. With reference to Fig. 2.5, this is done in two parts; first, across the d(t) pulse from nT to $nT + d_nT$, and then across the remainder of the period from $nT + d_nT$ to $(n + 1)T$.

In performing this integration extensive use is made of the fact that the width d_nT becomes vanishingly small for small signals. This small-signal approximation limits the resultant discrete

convertor model to the approximate description of local behavior about a steady state condition; but, in return for this limitation the integration of Eqs. (2.5) is simplified and the resultant small-signal difference equations are linear.

Integration of Eqs. (2.5) first across the narrow d(t) pulse leads to the following expression:

$$\int_{nT}^{nT + d_n T} \dot{\tilde{x}}\, dt = \int_{nT}^{nT + d_n T} \left(\bar{D}_1 A_1 \tilde{x} + \bar{D}_2 A_2 \tilde{x}\right) dt$$

$$+ \int_{nT}^{nT + d_n T} d\left[\left(A_2 - A_1\right)\bar{x} + \left(B_2 - B_1\right)u\right] dt \qquad (2.7)$$

The left-hand side of Eqs. (2.7) is simply equal to $\tilde{x}(nT + d_n T) - \tilde{x}(nT)$. The right-hand side may be evaluated for the small-signal result by repeated application of the integral mean value theorem, but it is more instructive if we reason that since the first integral contains "small" quantities $\tilde{x}(t)$ integrated over a "small" time $d_n T$, its contribution to Eqs. (2.7) is of <u>second order</u> and hence negligible for small signals.

We can similarly argue that the second integral on the right-hand side of Eqs. (2.7) contains "large" quantities $\bar{x}$ and u integrated

over "small" time, producing a first order contribution to Eqs. (2.7). Consequently, the result of integration of Eqs. (2.7) for small signals is:

$$\tilde{x}\left(nT + d_n T\right) - \tilde{x}(nT) = d_n T\left[\left(A_2 - A_1\right)\bar{x}(nT) + \left(B_2 - B_1\right)u\right] \quad (2.8)$$

Note that in Eqs. (2.8) the steady state solution is evaluated at nT. As the modulation becomes vanishingly small, it matters little whether we evaluate $\bar{x}$ at $nT + d_n T$ or nT because its components are all continuous.

To complete the integration we integrate Eqs. (2.5) from time $nT + d_n T$ to $(n + 1)T$ in Fig. 2.5. Because this is between d(t) pulses, Eqs. (2.5) reduce to Eqs. (2.9):

$$\dot{\tilde{x}} = \bar{D}_1 A_1 \tilde{x} + \bar{D}_2 A_2 \tilde{x} \quad (2.9)$$

When $\bar{D}_1 = 1$, Eqs. (2.9) become $\dot{\tilde{x}} = A_1 \tilde{x}$. The solution of $\dot{\tilde{x}} = A_1 \tilde{x}$ in terms of its initial condition $\tilde{x}(nT + d_n T)$ is given by Eqs. (2.10):

$$\tilde{x}(t) = e^{A_1 t}\,\tilde{x}\left(nT + d_n T\right) \quad (2.10)$$

The symbol e^{At} represents the exponential matrix. It has many properties reminiscent of the scalar exponential function. Among them are:

1. Series definition: $e^{At} \triangleq I + A + A^2\frac{t^2}{2!} + \cdots = \sum_{k=0}^{\infty} A^k \frac{t^k}{k!}$

2. Matrix differential equation: e^{At} solves $\dot{Y} = AY$

3. Behavior at $t = 0$: $e^{A \cdot 0} = I$, the identity matrix;

4. Commutivity: $e^{At_1} e^{At_2} = e^{At_2} e^{At_1} = e^{A(t_2 + t_1)}$

5. Inverse: $e^{At} e^{-At} = e^{A(t-t)} = I$

$\therefore$ Inverse of e^{At} is e^{-At}

Note: $e^{At} e^{Bt} \neq e^{(A + B)t}$ unless $AB = BA$

If the widths of the d(t) pulses in Fig. 2.5 become vanishingly small, then integration from $nT + d_nT$ to $nT + \tau_1$ is nearly the same as integration from nT to $nT + \tau_1$. It is easily shown then that the small-signal equations that take the states of the converter from $nT + d_nT$ to $nT + \tau_1$ are Eqs. (2.11):

$$\tilde{x}(nT + \tau_1) = e^{A_1 \tau_1} \tilde{x}(nT + d_nT) \qquad (2.11)$$

Application of the same argument to Eqs. (2.9) when $\bar{D}_2 = 1$ yields Eqs. (2.12):

$$\tilde{x}\Big((n+1)T\Big) = e^{A_2\tau_2}\tilde{x}(nT+\tau_1) \tag{2.12}$$

Because x(t) was chosen to be continuous for all t, then $\bar{x}$ and $\tilde{x}$ are also continuous for all t. This means that the small-signal integration results of Eqs. (2.8), (2.11) and (2.12) can be connected end to end to form the complete set of small-signal converter difference equations (2.13) for leading-edge modulation:

$$\tilde{x}\Big((n+1)T\Big) = e^{A_2\tau_2}e^{A_1\tau_1}\Big[\tilde{x}(nT) + d_nT\big[(A_2 - A_1)\bar{x}(nT) + (B_2 - B_1)u\big]\Big] \tag{2.13}$$

With this result our derivation is complete, but because there are many symbols in Eqs. (2.13), the reader may understand the meaning of this result more clearly if it is expressed in words.

What Eqs. (2.13) say is as follows:

We are given $\tilde{x}(nT)$, the perturbation on the steady state solution at a time nT just before a small modulation d_nT occurs. The modulation adds an additional perturbation to $\tilde{x}(nT)$ if the circuit topology changes at the switching instant (i.e., $(A_2 - A_1) \neq [0]$) and the steady state solution $\bar{x}(nT)$ at the steady state switching instant is not zero, or if independent sources u are switched in or out around this time (i.e., $(B_2 - B_1) \neq [0]$).

The resultant perturbations are taken as initial conditions at the beginning of one cycle and used to find the final conditions at the end of this cycle just before the next modulation occurs.

The results for trailing-edge modulation are found by following the same procedures. For this case the reference time nT is chosen to be at the beginning of the $\bar{D}_2$ - $\underline{1}$ pulses. The result is stated in Eqs. (2.14):

$$x\,(n+1)T = e^{A_1 T_1} e^{A_2 T_2} \left[\tilde{x}(nT) + d_n T \left[(A_1 - A_2)\bar{x}(nT) + (B_1 - B_2)u \right] \right] \qquad (2.14)$$

Both of these sets of linear difference equations become exact descriptions of the effect of pulse-width modulation on perturbations from the steady state solution as the modulation d_n becomes vanishingly small. Though for the derivation d_n was taken as positive, one finds the same formal result of Eqs. (2.13) and (2.14) for d_n negative, so that the modulation may be on either side of the steady state switching instant. The important thing to note about these linear converter models is that no assumptions about the switching frequency relative to the natural frequencies of the filter were necessary. Also note that a solution of Eqs. (2.13) defines the state of the converter only at a sequence of the time points nT, rather than for all time.

However, it is clear that if the state is known at one time during each period, its behavior at other times during the period may be found by use of exponential matrices. Hence, the behavior of this sequence of points is sufficient to imply the local behavior of the continuous converter.

An additional conclusion from the difference equations for both leading and trailing edge modulation is that they are both of the form

$$\tilde{x}\Big((n+1)T\Big) = M\Big[\tilde{x}(nT) + d_n K\Big]$$

where M is a constant matrix called the transition matrix and K is a constant column vector. From Eqs. (2.13) and (2.14) it is clear that even if there is no modulation (i.e., $d_n = 0$ for all n), these formulations produce two different transition matrices. Yet, if the difference equation formulation is to be correct these two different transition matrices should indicate the same dynamic behavior. In Appendix 3 this argument is used as motivation to show that the eigenvalues of all transition matrices for the same converter are the same.

Up to this point we have shown that one can start with a large-signal mathematical model for virtually any kind of switching converter and with a step-by-step approach ultimately derive a small-signal difference equation model of the converter's behavior about some steady state condition.

Once the ideas are understood the derivation for a particular case may be done rapidly.

As an example of the procedure to develop the difference equations for a specific converter, consider the circuit of Fig. 2.6. Details on the steady state operation of this converter may be found in Chapter 1. Following the general derivation we first cast the equations for this regulator in the form of Eqs. (2.1). The inductor current $I_\ell(t)$ and the capacitor voltage $V_c(t)$ are chosen as the state variables $x(t)$ because they remain continuous as switch S is opened and closed. Consider the interval when S is closed as the

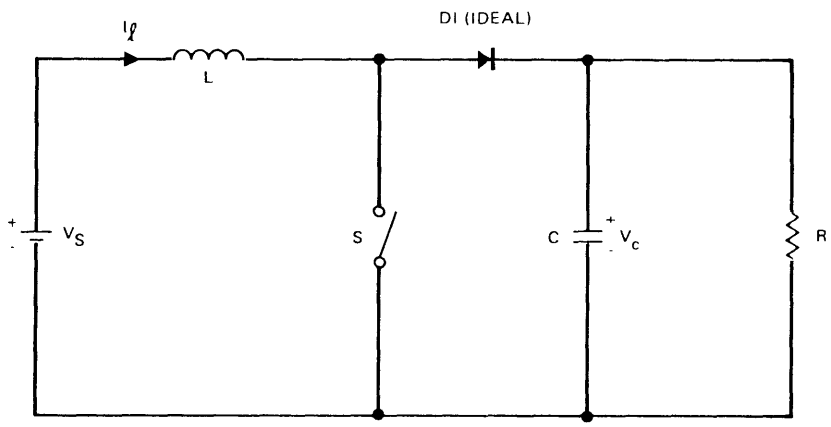

Fig. 2.6. Boost converter simplified model.

$D_1 = 1$ interval. During this interval the state equations of the boost circuit are:

$$\begin{bmatrix} I_\ell \\ V_c \end{bmatrix} = \begin{bmatrix} 0 & 0 \\ 0 & \frac{-1}{RC} \end{bmatrix} \begin{bmatrix} I_\ell \\ V_c \end{bmatrix} + \begin{bmatrix} \frac{1}{L} \\ 0 \end{bmatrix} \begin{bmatrix} V_s \end{bmatrix}$$

$$\dot{x} = A_1 x + B_1 u$$

When the switch is open, $D_2 = 1$. The state equations for this interval are:

$$\begin{bmatrix} \dot{I}_\ell \\ V_c \end{bmatrix} = \begin{bmatrix} 0 & \frac{1}{L} \\ \frac{1}{C} & \frac{-1}{RC} \end{bmatrix} \begin{bmatrix} I_\ell \\ V_c \end{bmatrix} + \begin{bmatrix} \frac{1}{L} \\ 0 \end{bmatrix} \begin{bmatrix} V_s \end{bmatrix}$$

$$\dot{x} = A_2 x + B_2 u$$

As in Chapter 1 we treat here the "continuous conduction" mode in which the inductor current never is zero.

The combination of the equations for the D_1 and D_2 intervals yields Eqs. (2.15):

$$\begin{bmatrix} \dot{I}_\ell \\ \dot{V}_c \end{bmatrix} = D_1 \left(\begin{bmatrix} 0 & 0 \\ 0 & \frac{-1}{RC} \end{bmatrix} \begin{bmatrix} I_\ell \\ V_c \end{bmatrix} + \begin{bmatrix} \frac{1}{L} \\ 0 \end{bmatrix} \begin{bmatrix} V_s \end{bmatrix} \right)$$

$$+ D_2 \left(\begin{bmatrix} 0 & -\frac{1}{L} \\ \frac{1}{C} & -\frac{1}{RC} \end{bmatrix} \begin{bmatrix} I_\ell \\ V_c \end{bmatrix} + \begin{bmatrix} \frac{1}{L} \\ 0 \end{bmatrix} \begin{bmatrix} V_s \end{bmatrix} \right) \qquad (2.15)$$

In the next step of the derivation the steady state condition is specified by choosing periodic modulation functions $\bar{D}_1$ and $\bar{D}_2$. Then if necessary we can find the steady state current and voltage $I_\ell(t)$ and $\bar{V}_c(t)$ which correspond to $\bar{D}_1$ and $\bar{D}_2$ by the methods shown in Chapter 1.

In the third part of the derivation we first choose the type of modulation (see Figs. 2.4a, b, c), then make the appropriate substitutions into the large signal Eqs. (2.17) to extract the equations describing the continuous perturbations.

For the choice of leading edge modulation we form Eqs. (2.16):

$$\begin{bmatrix} \dot{\bar{I}}_\ell \\ \dot{\bar{V}}_c \end{bmatrix} + \begin{bmatrix} \dot{\tilde{i}}_\ell \\ \dot{\tilde{v}}_c \end{bmatrix} = \left(\bar{D}_1 - d\right)\left(\begin{bmatrix} 0 & 0 \\ 0 & \frac{-1}{RC} \end{bmatrix}\begin{bmatrix} \bar{I}_\ell + \tilde{i}_\ell \\ \bar{V}_c + \tilde{v}_c \end{bmatrix} + \begin{bmatrix} \frac{1}{L} \\ 0 \end{bmatrix}\begin{bmatrix} V_s \end{bmatrix}\right)$$

$$+ \left(\bar{D}_2 + d\right)\left(\begin{bmatrix} 0 & -\frac{1}{L} \\ \frac{1}{C} & \frac{-1}{RC} \end{bmatrix}\begin{bmatrix} \bar{I}_\ell + \tilde{i}_\ell \\ \bar{V}_c + \tilde{v}_c \end{bmatrix} + \begin{bmatrix} \frac{1}{L} \\ 0 \end{bmatrix}\begin{bmatrix} V_s \end{bmatrix}\right) \quad (2.16)$$

Removal of the steady state part from these equations leaves Eqs. (2.17), in which we ignore the group of "small" terms as shown:

$$\begin{bmatrix} \dot{\tilde{i}}_\ell \\ \dot{\tilde{v}}_c \end{bmatrix} = \bar{D}_1\begin{bmatrix} 0 & 0 \\ 0 & -\frac{1}{RC} \end{bmatrix}\begin{bmatrix} \tilde{i}_\ell \\ \tilde{v}_c \end{bmatrix} + \bar{D}_2\begin{bmatrix} 0 & -\frac{1}{L} \\ \frac{1}{C} & -\frac{1}{RC} \end{bmatrix}\begin{bmatrix} \tilde{i}_\ell \\ \tilde{v}_c \end{bmatrix}$$

$$+ d\begin{bmatrix} 0 & -\frac{1}{L} \\ \frac{1}{C} & 0 \end{bmatrix}\begin{bmatrix} \bar{I}_\ell \\ \bar{V}_c \end{bmatrix} \quad (2.17)$$

This set corresponds to Eqs. (2.5) for the general case.

The final step in the derivation is to integrate Eqs. (2.17) across a complete converter period from the beginning of the n^{th} d(t) pulse to the beginning of the $(n + 1)^{th}$ d(t) pulse as shown in Fig. 2.7.

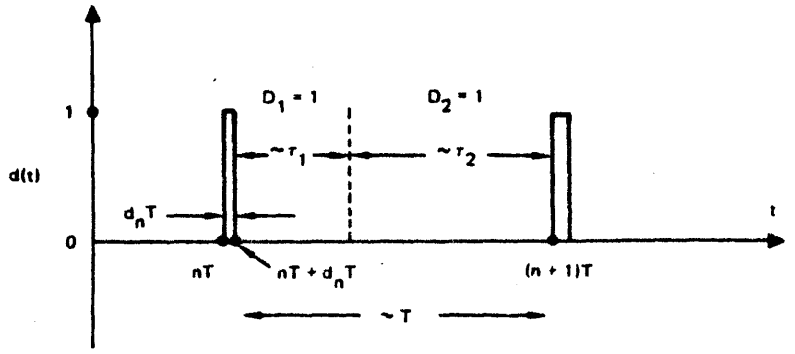

Fig. 2.7. Modulation timing for boost converter.

To do this we ignore the fact that the d(t) pulses can encroach on the length of the n^{th} period, and say that for small signals the matrix which carries the states at time $nT + d_nT$ across to $(n + 1)T$ is the transition matrix $M = e^{A_2T_2} e^{A_1T_1}$.

$$\begin{bmatrix} \tilde{i}_\ell \left((n + 1)T\right) \\ \tilde{v}_c \left((n + 1)T\right) \end{bmatrix} = e^{A_2T_2} e^{A_1T_1} \begin{bmatrix} \tilde{i}_\ell \left(nT + d_nT\right) \\ \tilde{v}_c \left(nT + d_nT\right) \end{bmatrix} \tag{2.18}$$

Next we simplify Eqs. (2.17) for the time period nT to $nT + d_n T$ by ignoring all terms except the "full size" coefficients of d:

$$\begin{bmatrix} \dot{\tilde{i}}_\ell \\ \dot{\tilde{v}}_c \end{bmatrix} \simeq d \begin{bmatrix} 0 & -\frac{1}{L} \\ \frac{1}{C} & -\frac{1}{RC} \end{bmatrix} \begin{bmatrix} \bar{I}_\ell \\ \bar{V}_c \end{bmatrix}$$

This approximation only ignores second order terms which would ultimately be neglected anyway in a small-signal model.

Finally, because $\bar{I}_\ell(t)$ and $\bar{V}_c(t)$ are continuous, they cannot change very much during the short time from nT to $nT + d_n T$. So if d(t) is very narrow, we can replace $\bar{I}_\ell(t)$ with $\bar{I}_\ell(nT)$ (or $\bar{I}_\ell(T)$ since $\bar{I}_\ell(t)$ is periodic) and replace $\bar{V}_c(t)$ with $\bar{V}_c(nT)$ (or $\bar{V}_c(T)$) in the integration over the d(t) pulse width:

$$\begin{bmatrix} \dot{\tilde{i}}_\ell \\ v_c \end{bmatrix} \simeq d \begin{bmatrix} 0 & -\frac{1}{L} \\ \frac{1}{C} & 0 \end{bmatrix} \begin{bmatrix} \bar{I}_L(nT) \\ \bar{V}_c(nT) \end{bmatrix}$$

This approximation also ignores only second order terms.

This expression then allows us to write the result of integration of (2.17) across from nT to nT + d_nT by inspection:

$$\begin{bmatrix} \tilde{i}_\ell\left(nT + d_nT\right) \\ \tilde{v}_c\left(nT + d_nT\right) \end{bmatrix} = \begin{bmatrix} \tilde{i}_\ell\,(nT) \\ \tilde{v}_c(nT) \end{bmatrix} + d_nT \begin{bmatrix} 0 & \frac{1}{L} \\ \frac{1}{C} & 0 \end{bmatrix} \begin{bmatrix} \bar{I}_\ell\,(nT) \\ \bar{V}_c(nT) \end{bmatrix}$$

$$= \begin{bmatrix} \tilde{i}_\ell(nT) - d_nT\,\dfrac{\bar{V}_c(T)}{C} \\ \tilde{v}_c(nT) + d_nT\,\dfrac{\bar{I}_\ell(T)}{L} \end{bmatrix}$$

The result is then combined with Eq. (2.18) to yield the complete boost converter small-signal difference equations (2.19) for leading-edge modulation:

$$\begin{bmatrix} \tilde{i}_\ell\left((n+1)T\right) \\ \tilde{v}_c\left((n+1)T\right) \end{bmatrix} = e^{A_2\tau_2}\, e^{A_1\tau_1} \begin{bmatrix} \tilde{i}_\ell\,(nT) - d_nT\,\dfrac{\bar{V}_c(T)}{L} \\ \tilde{v}_c(nT) + d_nT\,\dfrac{\bar{I}_\ell(T)}{C} \end{bmatrix} \qquad (2.19)$$

These equations say two separate things for the case of small-signal pulse-width modulation:

1. Small-signal perturbations on the steady state solutions are carried across each period by the transition matrix corresponding to d(t) = 0 for all t.

2. The only significant perturbations caused by modulation are due to interaction between the pulse-width modulation and the steady state solutions.

In summary, it has been shown in this chapter that an exact linear small-signal model of a generalized open-loop switching converter may be derived by characterization of the converter by a set of linear difference equations rather than by a set of linear differential equations.

The steps in this derivation are:

1. Write the large-signal equations of the converter.
2. Choose a steady state operating point.
3. Find the nonlinear differential equations for perturbations about the operating point.
4. Use the small-signal approximation to integrate the perturbation equations across one complete cycle including modulation to find the small-signal difference equations.

The feature of this discrete analysis that makes it potentially very useful is that the only approximation used to linearize the model is the small-signal approximation of step 4. This means that although a discrete model is valid only for small signals, it does not have the frequency limitations of the describing function models.

The extended range of frequency validity only makes the discrete converter model potentially useful. What ultimately affects its use

in a design mode is the amount of work one has to do to derive this model. Because ease of use is one goal of this thesis, it is worthwhile to assess the difficulty in the various steps of derivation of the converter difference equations.

The first step in writing the large-signal converter equations is generally quite easy if one is familiar with the state variable formulation. Since the practicing engineer may not be so familiar with this characterization, a simple systematic technique for finding converter state equations is included in Appendix 1.

Many types of switching converters have only two basic state variables (usually an inductor current and a capacitor voltage), so that the effort is not much more involved than the boost converter example at the end of this chapter. We may thus conclude that step 1 in the derivation, although being unfamiliar to some, is generally easy to do.

The second step amounts simply to choosing a set of symbols to stand for the steady state conditions (e.g., $\bar{I}_\ell(t)$ and $\bar{V}_c(t)$ in this example). Ultimately in using the final difference equations one will need to know the steady state solution at the time of modulation in the period, for example $\bar{I}_\ell(nT)$ and $\bar{V}_c(nT)$. It was demonstrated in Chapter 1, however, that accurate values for these quantities can be found easily by analysis that designers are familiar with. So we conclude that the second step in the model derivation is easy.

The third step consists of subtraction of the steady state solution from the total solution to find a characterization for the various perturbations. This step is trivial, only requiring the designer to decide where during the converter cycle the modulation will be placed.

The last step integration of the perturbation equations, is easy in principle but difficult to implement. The final answer is easily written in the form of Eqs. (2.19) shown in the boost converter example, but the practical problem in utilization of the difference equations such as Eqs. (2.19) is that ultimately one needs to know the exponential matrices explicitly. Computation of even one of these in exact symbolic form for a simple two-state converter can be a formidable task. An indication of this will be given in Chapter 5.

It has been this difficulty that has resulted in discrete converter models being little used for initial design purposes.

We shall show in Chapter 5 that use of a generalization of the simple "straight-line" approximations used in Chapter 1 to find the steady state conditions of a converter effectively solves the difficulty of finding explicit forms for the exponential matrices.

Chapter 3

Derivation of Pulse-Width Modulator Difference Equations

The contents of this chapter are a companion to the principal work of the last chapter. In that chapter a four-step derivation was introduced to show how nearly any kind of switching converter could be modeled by a set of small-signal linear difference equations. In this chapter we show that three different pulse-width modulators may also be modeled by small-signal difference equations.

In earlier work by Yuh [13] the three modulators treated here have been characterized by describing function methods. Because of the complicated frequency spectrum produced by pulse-width modulation, a significant amount of effort is necessary to derive the exact df models and in the end they seem to offer little additional insight over one's original intuitive feeling about a particular modulator.

In contrast to the difficulty presented by df analysis of pulse-width modulators, this chapter shows that discrete modulator models are remarkably easy to derive, principally because their behavior in the time domain is usually simple to describe mathematically. This ease of derivation leads us to conclude that modeling the modulator introduces no new problems in the use of discrete models for design purposes.

As with the converter difference equation derivation of the last chapter, the only approximation used in this discrete modulator derivation is the small-signal approximation. So once again the result is linear, but has no frequency limitations.

To allow more explicit forms for the modulator models to be presented we take the regulator compensation to consist of a linear combination of the converter state variables x(t) and a dc reference signal V_r:

$$V(t) = h_1x_1 + h_2x_2 + \ldots h_mx_m + V_r = H^Tx(t) + V_r \qquad (3.1)$$

In Eq. (3.1) V(t) is the signal input to the modulator and H^T is a row vector containing the gain (or attenuation) constants applied to the components $x_1 \ldots x_m$ of x(t).

Compensation of the form of Eqs. (3.1) is the most general kind of compensation that one can consider for a regulator short of the inclusion of reactive frequency-shaping components in the compensation. Treatment of this "reactive" compensation is reserved for Appendix 2. With the compensation form of Eq. (3.1) noted, the modulator model derivations begin with the sawtooth modulator.

We first discussed the behavior of this modulator at the end of Chapter 1. In its simplest form the sawtooth modulator is a voltage comparator that switches when the feedback signal V(t) is equal to a

sawtooth clock signal R(t). A detailed picture of the timing for this modulator is given in Fig. 3.1.

The difference equation derivation for this modulator has been done by others, but is included here as a starting point. We first write the large-signal equation that describes the switching time t_s:

$$R(t_s) - V(t_s) = 0 \tag{3.2}$$

If the falling edge of the sawtooth is fast, then essentially only a single transition is modulated in each period. This is arbitrarily chosen to be at the beginning of the $D_1 = 1$ interval.

In the steady state condition, reference to Fig. 3.1 shows that the modulator inputs satisfy Eq. (3.3):

$$R(nT) - \overline{V}(nT) = 0 \tag{3.3}$$

If a small perturbation is added to the steady state modulator input, the output switches at a slightly different time, which may be computed with the following line of reasoning.

First, the new switching time in the n^{th} period is defined by the relation $R(nT + d_nT) - V(nT + d_nT) = 0$. Since the input V is a combination of steady state $\overline{V}$ and perturbation $\tilde{v}$, the relation for the switching time may also be expressed by Eq. (3.4):

$$R(nT + d_nT) - \left[\overline{V}(nT + d_nT) + \tilde{v}(nT + d_nT)\right] = 0 \tag{3.4}$$

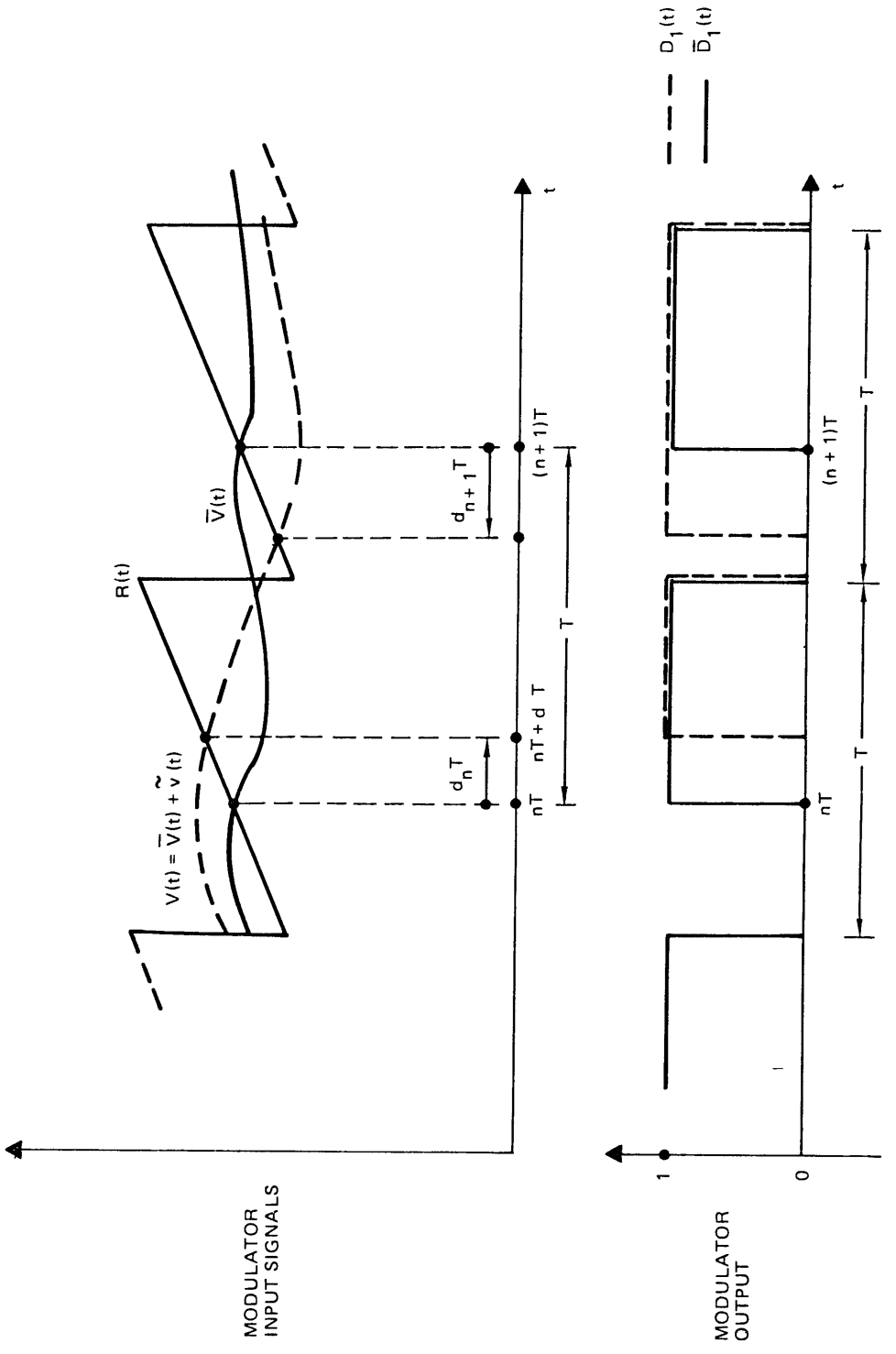

Fig. 3.1. Sawtooth modulation timing diagram.

If the input perturbation $\tilde{v}$ is small, then the modulation $d_n T$ is also small; hence we may approximate R, $\bar{V}$ and $\tilde{v}$ in Eq. (3.4) with part of their Taylor series expansions about the steady state switching time nT as shown in Eq. (3.5):

$$R(nT) + R'(nT)d_n T$$

$$- \left[\bar{V}(nT) + \bar{V}'(nT)d_n T + \tilde{v}(nT) + \tilde{v}'(nT)d_n T\right] = 0 \qquad (3.5)$$

Next, we subtract the steady state relation Eq. (3.3) from Eq. (3.5) and neglect the term $\tilde{v}'(nT)d_n T$ as being of second order. Then we rearrange terms to obtain the final result given in Eq. (3.6):

$$d_n = \frac{\tilde{v}(nT)}{T(R' - \bar{V}'(nT))} \qquad (3.6)$$

where R' is the constant slope of the sawtooth, and $\bar{V}'(nT)$ is the slope of the steady state modulator input signal evaluated at nT.

Note that if the modulator input V(t) or its first derivative contain switching discontinuities at nT, then in place of $\tilde{v}(nT)$ or $\bar{V}'(nT)$ we use their values just before the discontinuity. This reflects the fact that the modulator makes its switching decision before it switches, which in turn may cause discontinuities at the modulator input.

Since R and $\bar{V}$ are periodic, the proportionality between a small input perturbation and the resultant modulation is merely a constant

for this modulator. Note, the only assumption necessary to derive the difference equation (3.6) is that the input perturbation be small.

Two important characteristics of the sawtooth modulator that we see from Eq. (3.6) are: first, that it samples its input just before it produces modulation, and second, the modulator small signal gain depends partly on the derivative of its steady state input at the time nT when it samples the input.

If we consider the compensation to be of the form given in Eq. (3.1) it follows that:

$$\tilde{v}(nT) = H^T \tilde{x}(nT)$$

and

$$\bar{V}'(nT) = H^T \bar{x}'(nT)$$

So the characterizations of the compensation and modulator may be combined to yield Eq. (3.7):

$$d_n = \frac{H^T \tilde{x}(nT)}{T\left(R' - H^T \bar{x}'(nT)\right)} \tag{3.7}$$

This expression will be compared with those of the other modulators at the end of this chapter.

The next modulator whose difference equations we derive is called the uniformly sampled modulator. Its timing is pictured in Fig. 3.2. This modulator periodically samples the amplitude of its

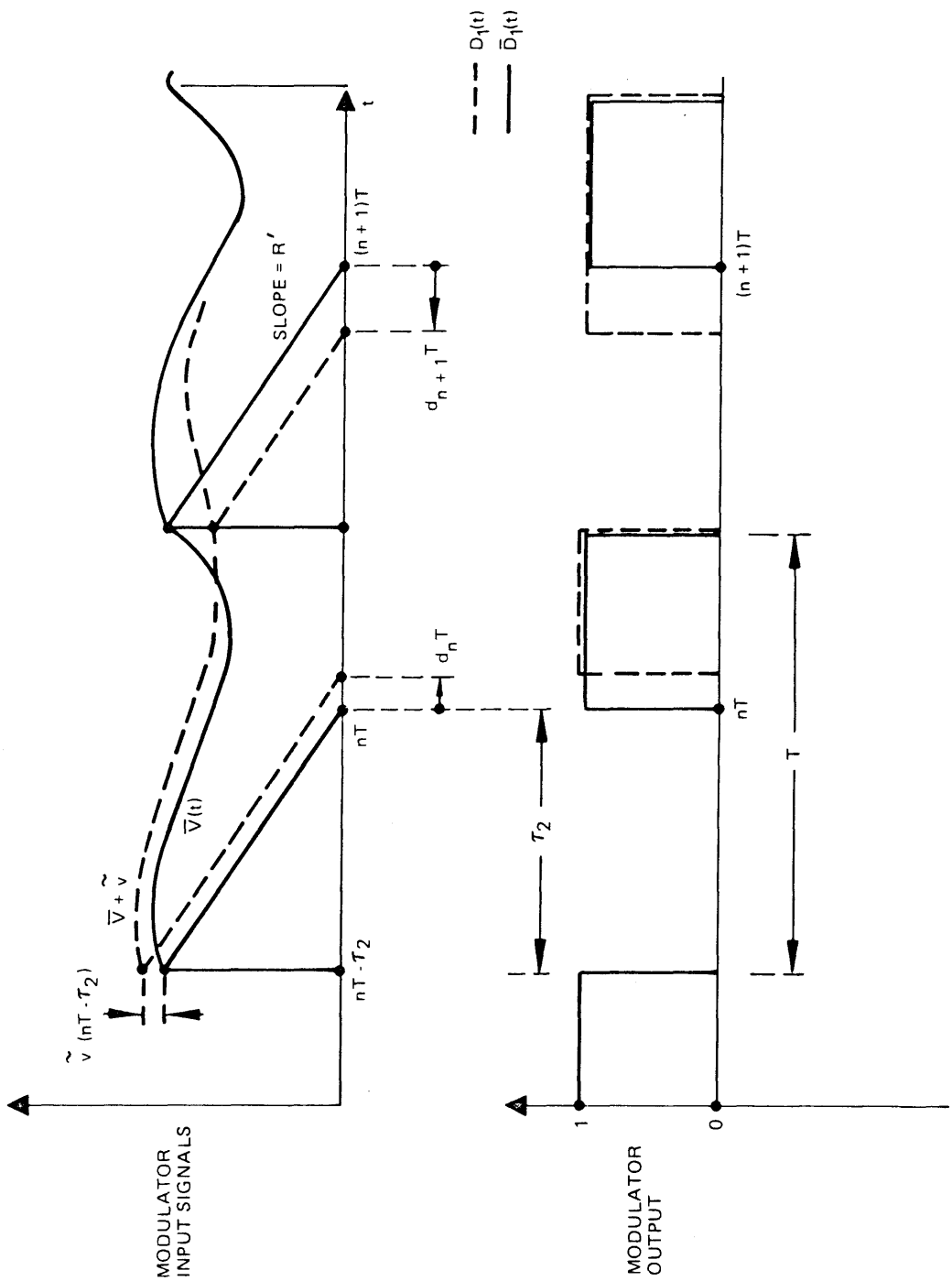

Fig. 3.2. Timing diagram for a uniformly sampled pulse-width modulator.

input and determines a switching instant whose time location is proportional to the sampled input amplitude. In Fig. 3.2 the waveform R(t) could be the voltage on a capacitor which is periodically charged up to the input voltage V(t), and then allowed to discharge through a constant current source until it has zero volts across it, at which instant the modulator switches. Clearly, from the geometry of the picture, the modulation d_nT is again proportional to the perturbation $\tilde{v}$, but to $\tilde{v}(nT - \tau_2)$ rather than to $\tilde{v}(nT)$. If R' is the slope of R(t), the modulator may be characterized by Eq. (3.8):

$$d_n = \frac{\tilde{v}\left(nT - \tau_2\right)}{TR'} \tag{3.8}$$

The important characteristics of this modulator are: first, that it has a time delay τ_2 between when it samples and when it modulates, and second, its small-signal gain does not depend at all on its steady state input $\overline{V}(t)$, in contrast to the sawtooth modulator.

The time delay inherent in this modulator has led many designers to decide that the uniformly sampled modulator is a poor choice for wide bandwidth switching regulators. However, with the expression for the state-space compensation Eq. (3.1), it will now be shown that the delay can be made to disappear.

If the feedback is chosen as in Eq. (3.1), then for small signals the modulator input is $\tilde{v} = H^T\tilde{x}$. Substitution of this relation for $\tilde{v}$ in Eq. (3.8) gives:

$$d_n = \frac{H^T\tilde{x}(nT - \tau_2)}{TR'}$$

Since $nT - \tau_2$ is the beginning of a $D_2 = 1$ interval and nT is at the end of the $D_2 = 1$ interval then, we may write:

$$\tilde{x}(nT) = e^{A_2\tau_2} \cdot \tilde{x}(nT - \tau_2)$$

This is simply carrying the converter perturbations across the $\bar{D}_2 = 1$ interval as done in Chapter 2. Running time backwards, however, allows the starting conditions to be computed from the ending conditions as:

$$\tilde{x}(nT - \tau_2) = e^{-A_2\tau_2}\tilde{x}(nT)$$

So in terms of its input just before modulation occurs at time nT the uniformly sampled modulator may be characterized by Eq. (3.9):

$$d_n = \frac{H^T e^{-A_2\tau_2}\tilde{x}(nT)}{TR'} \qquad (3.9)$$

From Eq. (3.9) we observe that the gain is now dependent on the steady state width of the $D_2 = 1$ interval, but there is no delay between the occurrence of a sample and the modulation instant.

The fact that the discrete equations for this modulator with the compensation can be put in the form of Eq. (3.9) has some important consequences which we investigate in the next chapter.

The last modulator that we consider here is called the integrated error modulator. The steady state switching time, nT, for this modulator is defined by Eq. (3.10):

$$\int_{nT - \tau_2}^{nT} \bar{V}(t)\, dt = V_t \tag{3.10}$$

A picture of the timing for the modulator is given in Fig. 3.3. The operation is as follows: Periodically a clock begins the $D_2 = 1$ interval and the modulator input is integrated. When this integrated input reaches some threshold value V_t the modulator switches, ending the $D_2 = 1$ interval, and the integrator is reset to some initial value. If a perturbation $\tilde{v}(t)$ is present, the modulation $d_n T$ is defined by Eq. (3.11):

$$\int_{nT - \tau_2}^{nT + d_n T} \left(\bar{V}(t) + \tilde{v}(t) \right) dt = V_t \tag{3.11}$$

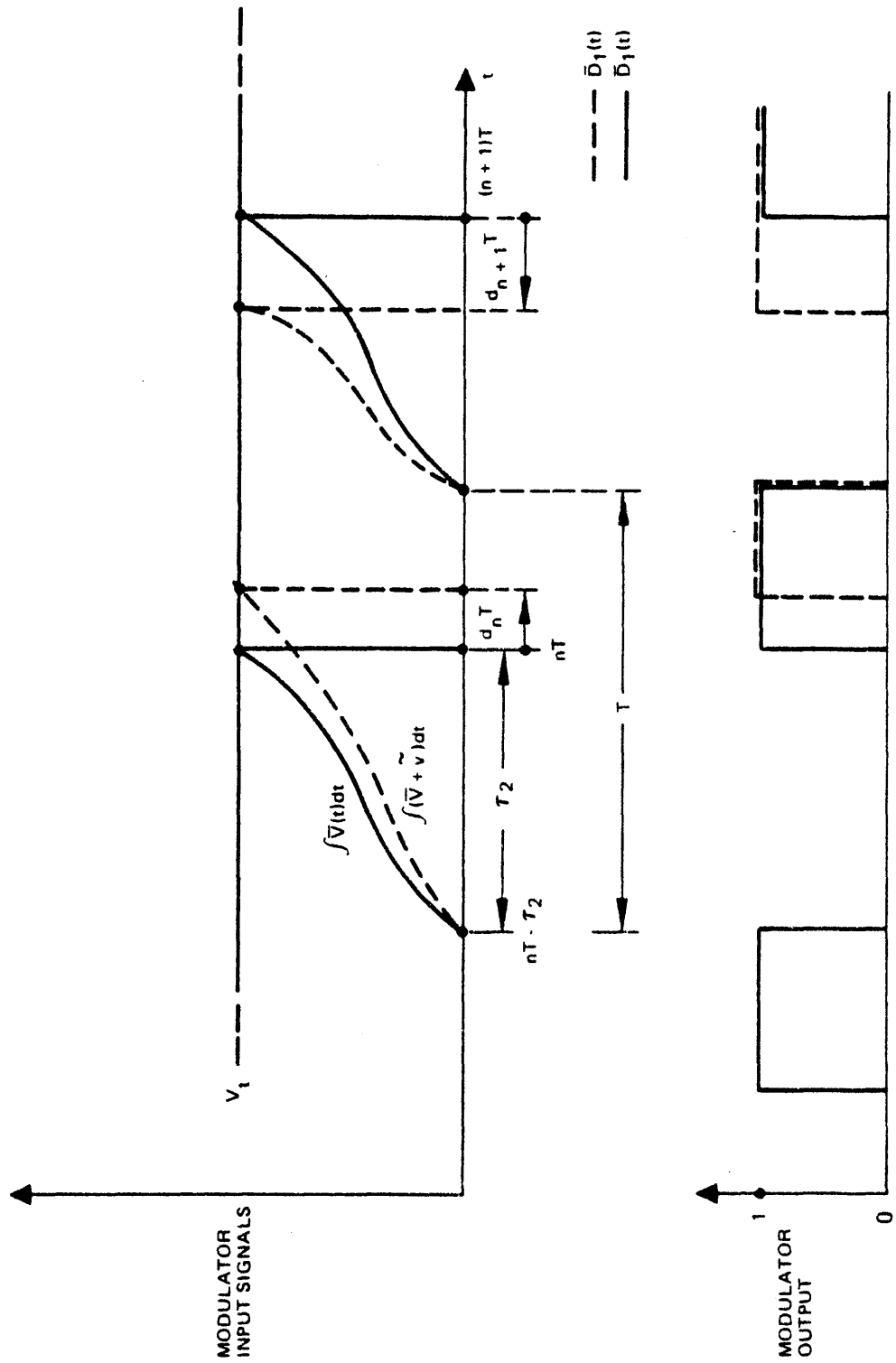

Fig. 3.3. Integrated error modulator timing.

This may be expanded as follows:

$$\int_{nT - \tau_2}^{nT} \bar{V}dt + \int_{nT}^{nT + d_nT} \bar{V}dt + \int_{nT - \tau_2}^{nT} \tilde{v}dt + \int_{nT}^{nT + d_nT} \tilde{v}dt = V_t$$

Subtraction of the steady state Eq. (3.10) gives:

$$\int_{nT}^{nT + d_nT} \bar{V}dt + \int_{nT - \tau_2}^{nT} \tilde{v}dt + \int_{nT}^{nT + d_nT} \tilde{v}dt = 0$$

If d_nT is small, then two of the integrals may be approximated as follows:

$$d_nT\ \bar{V}(nT) + \int_{nT - \tau_2}^{nT} \tilde{v}dt + d_nT\ \tilde{v}(nT) = 0$$

The third term is of second order for small d_n and $\tilde{v}$, and may be neglected. The final result is the difference Eq. (3.12):

$$d_n = \frac{-1}{T\bar{V}(nT)} \int_{nT - \tau_2}^{nT} \tilde{v}(t)dt \qquad (3.12)$$

It is difficult to say from Eq. (3.12) exactly where the input is effectively sampled because of the integral in the result, but we can

say that the modulator small-signal gain depends on the steady state input, rather than its derivative as in the sawtooth modulator, or not at all as in the uniformly sampled modulator.

To find a more explicit formula for the behavior of the integrated error modulator we again assume the compensation is of the form of Eq. (3.1). Then we may say that

$$\tilde{v}(t) = H^T \tilde{x}(t)$$

Since the integral in Eq. (3.12) is over the $D_2 = 1$ interval we may write:

$$\tilde{x}(t) = e^{A_2 t} \tilde{x}\left(nT - \tau_2\right)$$

and therefore

$$\tilde{x}\left(nT - \tau_2\right) = e^{-A_2 \tau_2} \tilde{x}(nT)$$

Connection of these last three relations provides an expression for $\tilde{v}(t)$:

$$\tilde{v}(t) = H^T e^{A_2\left(t - \tau_2\right)} \tilde{x}(nT) \qquad (3.13)$$

Substitution of Eq. (3.13) into Eq. (3.12) and integration then leads to the following exact expression for the small-signal discrete gain of an integrated error modulator with compensation:

$$d_n = \frac{H^T A_2^{-1} \left(I - e^{-A_2 \tau_2}\right) \tilde{x}(nT)}{T\left(H^T \bar{x}(nT) + V_r\right)} \tag{3.14}$$

If τ_2 is short compared to the natural time constants of the converter, then the exponential matrix may be approximated by the first three terms in time,

$$e^{-A_2 \tau_2} \simeq I - A_2 \tau_2 + A_2^2 \frac{\tau_2^2}{2}$$

Then there results an approximate expression for Eq. (3.14):

$$d_n \quad \frac{\tau_2 H^T \cdot \left(I - A_2 \tau_2/2\right) \tilde{x}(nT)}{T\left(H^T \bar{x}(nT) + V_r\right)} \simeq \frac{\tau_2 H^T e^{-A_2 \tau_2/2} \tilde{x}(nT)}{T\left(H^T \bar{x}(nT) + V_r\right)} \tag{3.15}$$

The exponential matrix in the approximate result means that this modulator behaves as if it had a delay of $\tau_2/2$ if the approximation $e^{-A_2 \tau_2} \simeq I - A_2 \tau_2$ is valid. This agrees with the approximate continuous model for this modulator developed by Yuh.

A summary of the results of the modulator derivations is given in Table 3.1. A conclusion is that one can make a trade-off between the effective delay of a modulator and its sensitivity to the steady state input.

We note that, from sawtooth to integrated error to uniformly sampled modulator, the effective delay increases from zero to $\sim\tau_2/2$ to τ_2 while the dependence on the steady state input decreases from dependence on its slope to dependence on its amplitude to no dependence at all.

It is also seen from Table 3.1 that, with assumption of state variable feedback as the compensation, explicit difference formulas can easily be determined for all three modulators. We also note that time delay may be treated as a gain factor in the difference equations.

In Chapter 6 use of some of these modulator equations as design formulas will enable the physical feedback H^T to be chosen to yield an optimal small-signal transient response.

Modulator Type	Difference Eq.	Difference Eq. with Compensation	
Sawtooth:	$d_n = \frac{\tilde{v}(nT)}{T(R' - \bar{V}'(nT))}$	$= \frac{H^T \tilde{x}(nT)}{T\left(R' - H^T \bar{x}'(nT)\right)}$	$= H_e^T \tilde{x}(nT)$
Uniformly Sampled:	$d_n = \frac{\tilde{v}\left(nT - \tau_2\right)}{TR'}$	$= \frac{H^T e^{-A_2 \tau_2} \tilde{x}(nT)}{TR'}$	$= H_e^T \tilde{x}(nT)$
Integrating Error:	$d_n = \frac{-\int_{nT-\tau_2}^{nT} \tilde{v}(t)dt}{T\,\bar{V}(nT)}$	$= \frac{\tau_2 H^T e^{-A_2 \tau_2/2} \tilde{x}(nT)}{T\left(H^T \bar{x}(nT) + V_r\right)}$	$= H_e^T \tilde{x}(nT)$

Table 3.1. Small signal discrete modulator models.

Chapter 4

Application of z-Transform to the Difference Equations

In this chapter the z-transform is applied to the discrete models developed in the previous two chapters to obtain a frequency domain representation of the closed-loop behavior of a switching regulator. The idea behind using the z-transform is to simplify the use of the discrete models by shifting their characterization from the time domain to the frequency domain. To give those more familiar with the Laplace transform a "feel" for the discrete frequency domain, the beginning material also includes comparisons between the z-plane and the s-plane. A review of the stability discussion of Chapter 1 shows that the z-plane is a natural setting for the small-signal stability problem of switching regulators.

We begin with a definition of the z-transform and then show how it may be applied to transform difference equations into algebraic equations.

After these preliminaries, the z-transform is applied to the converter difference equations to show that a converter may be characterized by a set of scalar transfer functions G(z), as shown in Eqs. (4.1):

$$\tilde{x}^* = \begin{bmatrix} \tilde{x}_1^* \\ \cdot \\ \cdot \\ \cdot \\ \tilde{x}_m^* \end{bmatrix} = G(z)d^* = \begin{bmatrix} G_1(z) \\ \cdot \\ \cdot \\ \cdot \\ G_m(z) \end{bmatrix} d^* \qquad (4.1)$$

where d^* is the z-transform of the input modulation d_n and $\tilde{x}^*$ is the transform of the perturbations $\tilde{x}$ on the state variables. These transfer functions emphasize the idea that for feedback loop design the input to a switching converter is the modulation and its outputs are the various converter state variable perturbations.

When the transform is applied in a similar manner to the combined difference equations of a pulse-width modulator with compensation of the form introduced in Chapter 3, we find that unlike the s-plane descriptions of these modulators, their models in the z-plane have no poles, or zeros, or phase shift. Instead, the gain is constant and in general dependent on the steady state operating condition.

Finally, a "loop gain" quantity is introduced which allows the designer to use the root locus technique in the z-plane to position the closed-loop poles of a regulator. With a general expression for loop gain as the goal of this chapter, we now proceed with a brief description of the z-transform and some of its properties.

Formally, the z-transform is defined for a sequence of numbers S_n, where n is an integer ranging from zero to infinity. In its use here, the sequence of numbers will be points on a function of time, f(t), taken at points in time labeled nT in keeping with the derivations in Chapters 2 and 3. We define the z-transform of f(nT) as f* according to Eq. (4. 2):

$$Z\left\{f(nT)\right\} = f^* = \sum_{n=0}^{\infty} f(nT)\, z^{-n} \qquad (4.2)$$

A crucial property of the transform which follows from its definition is the relation of Eq. (4. 3):

$$Z\left\{f\Big((n+1)\,T\Big)\right\} = z\left(f^* - f(0)\right) \qquad (4.3)$$

This relation allows a set of difference equations to be transformed into a set of algebraic equations.

After application of the z-transform to a set of difference equations, the algebraic results may be described by pole-zero plots in the z-plane. To understand how the z-plane poles relate to various types of transient responses, we compare the s-plane and the z-plane in Fig. 4. 1. It can be shown that the two planes are related by the mapping $z = e^{sT}$. In Fig. 4. 1 a contour is drawn and numbered to indicate how a semi-infinite strip in the s-plane

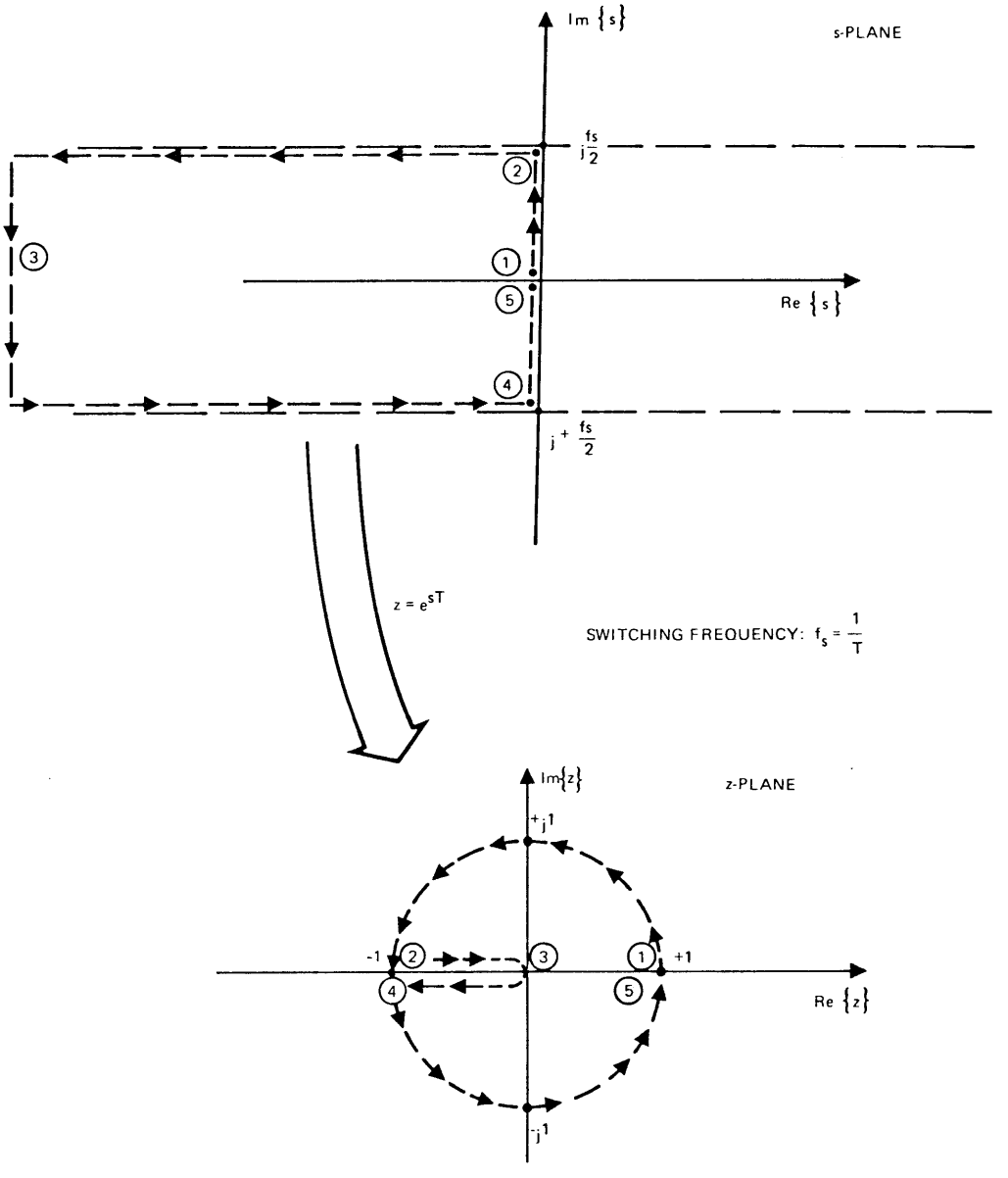

Fig. 4. 1. Mapping between s-plane and z-plane.

between plus and minus half of the switching frequency is mapped inside the unit circle in the z-plane. Zero frequency s = 0 maps into z = 1 in the z-plane. Traversal of the positive imaginary axis in the s-plane which is done when finding the frequency response of a network, maps into a counter-clockwise trajectory around the edge of the unit circle in the z-plane. Finally, stability, which corresponds to all poles in the left half of the s-plane, implies all poles inside the unit circle in the z-plane.

Important to note is that just the strip of the s-plane between plus and minus half of the switching frequency is enough to uniquely describe the entire z-plane. The left half s-plane strip fills the inside of the unit circle and the right half plane strip fills the remaining z-area outside the unit circle.

This means that all frequencies in the z-plane can be thought of as being less than or equal to half the switching frequency, which is precisely the real limitation on small oscillations in duty ratio as given in Chapter 1. This limitation can be restated in terms of the quantities introduced in Chapter 2. Basically, a small amount of pulse-width modulation may be thought of as adding or subtracting a stream of narrow pulses d(t) to the steady state modulation functions $\bar{D}_i(t)$. The width of the n^{th} d(t) pulse is given by the normalized variable d_n, so that the modulation may be thought of as a sequence of numbers $\ldots d_{n-1} d_n d_{n+1} \cdots$.

The fastest possible periodic variation in d(t) then is a sequence of numbers such as . . . ababab . . . . Since there is only one

pulse produced per switching period T, the fastest possible variation in d(t) requires 2T for its period. Hence, the maximum possible frequency of pulse-width oscillation, assuming that its amplitude is small, is half the switching frequency.

Since the z-plane can only uniquely describe frequencies up to half the switching frequency, there is a consistency with the physical constraints of the problem built into the z-plane. With this introduction to the z-transform, we may proceed to apply it to the difference equation models. First we show how the general converter introduced in Chapter 2 may be characterized by a set of transfer functions.

Recall that the main result of Chapter 2 was that about some steady state condition a generalized converter can be represented by the set of small-signal linear difference Eqs. (4.4):

$$\tilde{x}\left((n+1)T\right) = M\left[\tilde{x}\,(nT) + Kd_n\right] \qquad (4.4)$$

where $\tilde{x}$ is a vector of the perturbations on the converter state variables, M is a matrix called the transition matrix which carries the small-signal initial conditions of a converter across one cycle to determine its final conditions, and K is a vector of constants describing the effect of the input modulation d_n on each of the components of $\tilde{x}$ at the beginning of a cycle.

Application of the z-transform to the converter Eqs. (4.4), and use of the result of Eq. (4.3) gives:

$$Z\left\{\tilde{x}\left((n+1)T\right)\right\} = Z\left\{M\left[\tilde{x}\,(nT) + Kd_n\right]\right\}$$

$$z\left(\tilde{x}^* - \tilde{x}(0)\right) = M\left[\tilde{x}^* + Kd^*\right]$$

A rearrangement of terms yields Eqs. (4. 5):

$$\tilde{x}^* = (zI - M)^{-1} MKd^* + z(zI - M)^{-1} \tilde{x}(0) \qquad (4.5)$$

If the initial conditions on the converter states $\tilde{x}(0)$ are all zero, the remainder of Eqs. (4. 5) are z-plane transfer functions describing the effect of the modulation d^* on each of the converter state variables. If G(z) is defined to be the vector of the converter transfer functions for an m-state converter, then the steady state part of Eqs. (4. 5) may be written as:

$$\tilde{x}^* = G(z)\,d^*$$

in which

$$\begin{bmatrix} x_1^* \\ \vdots \\ x_m^* \end{bmatrix} = \begin{bmatrix} G_1(z) \\ \vdots \\ G_m(z) \end{bmatrix} d^* \qquad (4.6)$$

$$G(z) = (zI - M)^{-1} MK \qquad (4.7)$$

If the converter possesses only two states, as do many of the basic types such as boost converters, Eqs. (4.7) may be expressed more explicitly as:

$$\begin{bmatrix} G_1(z) \\ G_2(z) \end{bmatrix} = \frac{1}{(z - z_1)(z - z_2)} \left[zM - z_1 z_2 I \right] K \qquad (4.8)$$

where z_1 and z_2 are the eigenvalues of M or the roots of Det. $(zI - M) = 0$.

With the results summarized in Eqs. (4.7) and (4.8) the development of a discrete converter model is complete. We now proceed to model the modulators with compensation presented in Chapter 3.

In Table 3.1 explicit results were included for three different types of pulse-width modulators with compensation consisting of state variable feedback. All of these results were in the form:

$$d_n = H_e^T \tilde{x}(nT) = a\tilde{x}_1(nT) + b\tilde{x}_2(nT) + \ldots \qquad (4.9)$$

where $\tilde{x}$ is the converter state vector and H_e^T is a row vector of effective gain constants dependent on the type of modulator, the physical compensation H^T and the steady state conditions of the converter.

Application of the z-transform to Eq. (4.9) yields the simple but remarkable result

$$d^* = H_e^T \tilde{x}^* \tag{4.10}$$

Equation (4.10) implies that if a linear combination of the converter states is physically fed back to any of the modulators considered in Chapter 3, the resultant modulation d^* is merely a somewhat different linear combination of the states with no additional poles, zeros or phase shift in the z-plane.

What this means in practical terms is that if the physical feedback for two different types of modulators is chosen such that the "effective" feedback given by H_e^T is the same for both, then the small-signal transient behavior of regulators with either modulator should be identical. In more concise terms we may say that with regard to potential small-signal transient performance all the modulators considered in Chapter 3 are equal.

At first this seems a bit peculiar, particularly for modulators such as the uniformly sampling variety which have time delay between when the input is sampled and when the actual pulse-width modulation occurs. We note, however, that in the difference equation representation a time delay τ is taken into account by means of a factor $e^{-A\tau}$ in the gain of the modulator. As the duty ratio of a delay type modulator varies, its effective delay varies. So,

although a small-signal discrete model of a delaying type of modulator has no phase shift in the z-plane, its small-signal gain changes with steady state pulse width.

To summarize this part of the chapter, the introduction of the z-transform has accomplished two important goals. First, it has allowed the replacement of the difference equation characterization of a converter with a set of small-signal transfer functions in the z-plane describing the effect of pulse-width modulation on each of the state variables of the converter.

Next, it was observed that with state variable feedback, the model for all of the modulators in Chapter 3 in the z-plane is a set of constants describing the modulator output d^* as a linear combination of the state variables $\tilde{x}^*$.

At this point the theoretical development is nearly done. The last step, which in some ways is the most important one, is to introduce the discrete equivalent of loop gain which will be noted as $T^*(z)$ and should not be confused with T, the symbol for the steady state switching period.

To find the loop gain, first consider the z-plane description of the switching regulator signal loop shown in Fig. 4.2. The sign inversion after the modulator is provided to make the feedback negative. Traversal of the loop as indicated in the figure yields Eq. (4.11) for the loop gain:

$$T^*(z) = H_e^T G(z) = aG_1(z) + bG_2(z) + \ldots \qquad (4.11)$$

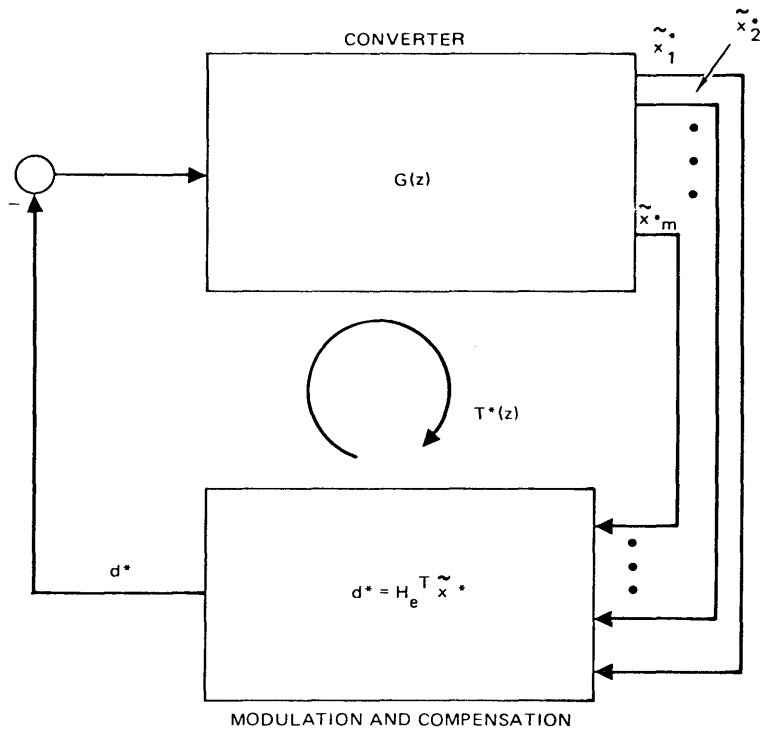

Fig. 4. 2. Block diagram of the z-transformed signal loop for a switching regulator with state variable feedback.

To verify the expression for T*(z) we may combine the results of Eqs. (4. 5) and Eq. (4. 10) as follows:

$$d^* = H_e^T \tilde{x}^* = H_e^T \left[G(z)\,(-d^*) + z(zI - M)^{-1}\,\tilde{x}(0) \right]$$

↑ negative feedback

$$d^* \left(1 + H_e^T G(z)\right) = H_e^T z(zI - M)^{-1} \tilde{x}(0)$$

$$d^* = \frac{H_e^T z(zI - M)^{-1} \tilde{x}(0)}{1 + H_e^T G(z)}$$

$$= \frac{H_e^T z(zI - M)^{-1} \tilde{x}(0)}{1 + T^*(z)} \qquad (4.12)$$

Equation (4.12) describes the closed-loop regulator transient which occurs when a distrubance $\tilde{x}(0)$ is introduced on the steady state condition. The important point to note about Eq. (4.12) is that the closed-loop poles of the regulator are the zeros of $1 + T^*(z)$, which makes $T^*(z)$ a true loop gain quantity.

We can infer information about the closed-loop transient response of a switching regulator by knowledge of the location of its closed-loop poles in the z-plane. Since the closed-loop poles in the z-plane are shown to be the zeros of $1 + T^*(z)$ in Eq. (4.12), it is possible to use root locus techniques on $T^*(z)$ to find the closed-loop poles. In fact, the root locus gives the designer a means to design the closed loop poles of a switching regulator, and is important in making the discrete formulation of the regulator problem useful for synthesis as well as analysis. All of the transfer functions of the converter have the same poles which are the eigenvalues of the converter transition matrix. Since with state variable

feedback the loop gain T*(z) is a linear combination of these transfer functions, the poles of the loop gain are those of the converter by itself. It will be shown in Chapter 5 that with the right combination of state variable feedback to place the zeros of the loop gain, and by proper choice of the magnitude of T*(z), one can sometimes place closed-loop poles in an optimal manner.

The results of this chapter conclude the theoretical part of this investigation. The basic idea is to develop a more accurate means of designing switching regulators for proper stability and transient response. The introduction and Chapter 1 indicated that linear continuous models lose their validity for describing small-signal closed-loop behavior as frequencies approach half the switching frequency. In Chapter 2 a general converter was presented and it was shown that a small-signal model consisting of linear difference equations could be derived which characterizes the converter in a way which requires no "low-frequency" approximation. Chapter 3 showed that similar characterizations are possible for a variety of different pulse-width modulators.

Finally, in this chapter the z-transform was used to obtain a frequency domain representation of the transient design problem. Using the transform one can work with transfer functions in the z-plane rather than sets of difference equations in the time domain. Also, a loop gain quantity T*(z) was introduced which enables the

designer to use the root locus to place closed loop z-plane poles. The notion of loop gain and poles and zeros are brought into the regulator problem to make the discrete formulation seem less strange to the practicing designer. Besides making the models more familiar, the z-transform produces some startling results such as the fact that certain delay type pulse-width modulators may be modeled by a constant transfer function in the z-plane with no poles or zeros or phase shift.

Knowing how to formulate discrete models in a general way, we go from the general to the specific in Chapter 5 with an example of a performance analysis approach.

Chapter 5

The Straight-Line Approximation, and a Performance Analysis Example of the Discrete Method

In this chapter the results derived in Chapters 2, 3, and 4 are applied to the analysis of the boost converter of Fig. 5.1a. With use of the root locus the potential transient performance of this converter is investigated, which leads to a simple prediction of wide bandwidth phenomena such as subharmonic oscillation and optimal transient response.

Of equal importance in this chapter is the introduction of the powerful "straight-line" approximation, which greatly reduces the computation necessary to obtain the converter transfer functions. This makes the approximate transfer functions simple enough that in symbolic form they may be used for design purposes. Because this chapter is meant to tie together the results of the previous chapters with a specific example, we shall begin with a review of the derivation of the boost converter discrete model.

As a first step the converter of Fig. 5.1a is modeled by the large signal Eqs. (5.1):

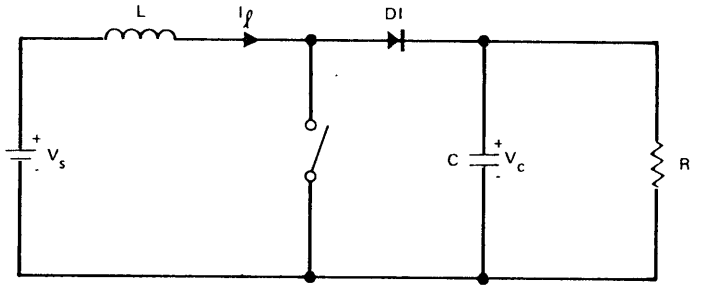

(a) BOOST CONVERTER SCHEMATIC

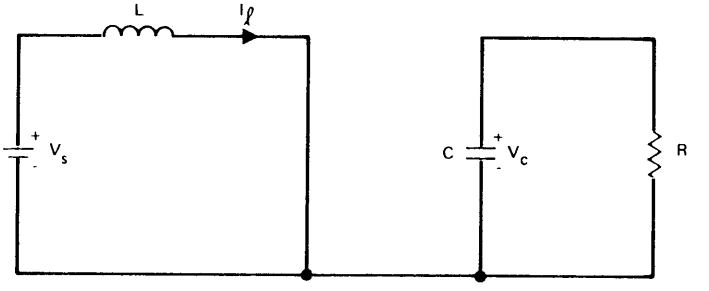

(b) CONVERTER TOPOLOGY WITH SWITCH CLOSED ($D_1(t) = 1$)

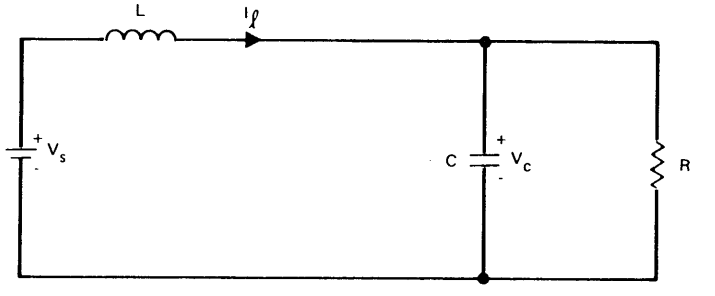

(c) CONVERTER TOPOLOGY WITH SWITCH OPEN ($D_2(t) = 1$)

Fig. 5.1. Boost converter schematic with topologies for each switching interval.

$$\begin{bmatrix} \dot{I}_\ell \\ \dot{V}_c \end{bmatrix} = D_1\left(\begin{bmatrix} 0 & 0 \\ 0 & -\frac{1}{RC} \end{bmatrix}\begin{bmatrix} I_\ell \\ V_c \end{bmatrix} + \begin{bmatrix} \frac{1}{L} \\ 0 \end{bmatrix}\begin{bmatrix} V_s \end{bmatrix}\right)$$

$$+ D_2\left(\begin{bmatrix} 0 & -\frac{1}{L} \\ \frac{1}{C} & -\frac{1}{RC} \end{bmatrix}\begin{bmatrix} I_\ell \\ V_c \end{bmatrix} + \begin{bmatrix} \frac{1}{L} \\ 0 \end{bmatrix}\begin{bmatrix} V_s \end{bmatrix}\right) \qquad (5.1)$$

The alteration of the converter topology by the switch is shown in Figs. 5.1b and c and is modeled in Eqs. (5.1) by the modulation functions $D_1(t)$ and $D_2(t)$.

The large signal converter model, of Eqs. (5.1) is nonlinear and too complicated to yield design information about transient response. So, with a linear model objective, a steady state operating point is chosen and denoted by $\overline{I}_\ell(t)$ and $\overline{V}_c(t)$, which correspond to a particular choice of $D_1(t) = \overline{D}_1(t)$ and $D_2(t) = \overline{D}_2(t)$. The timing of $\overline{D}_1(t)$ and $\overline{D}_2(t)$ is shown in Fig. 5.2.

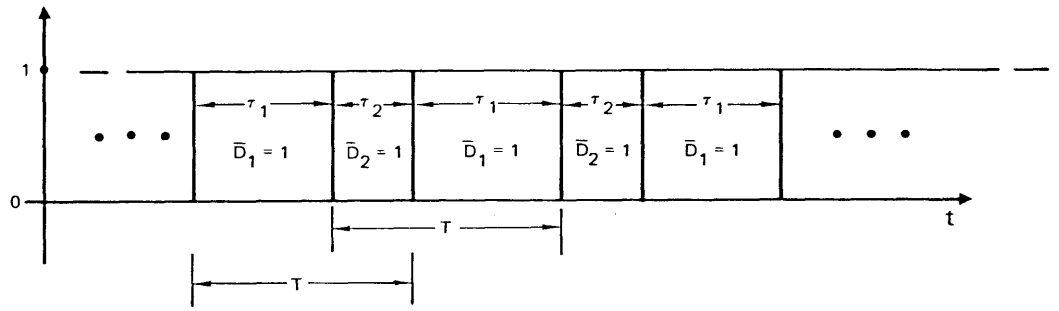

Fig. 5.2. Boost converter timing diagram.

Once the converter is modeled by a set of large-signal equations and an operating point is chosen, then we decide where pulse-width modulation will occur during a switching cycle. For our example the modulation is taken to move the time location at the beginning of $\overline{D}_1 = 1$ interval about its steady state location.

Next we find the differential equations which describe perturbations about the steady state condition. This is done by noting that both the steady state solution and the steady state solution plus perturbations must satisfy Eqs. (5. 1). By subtraction of the former from the latter and neglect of second order terms, one is left with Eqs. (5. 2) which describe the perturbations only:

$$\begin{bmatrix} \tilde{i}_\ell \\ \tilde{v}_c \end{bmatrix} = \overline{D}_1 \underbrace{\begin{bmatrix} 0 & 0 \\ 0 & -\frac{1}{RC} \end{bmatrix}}_{A_1} \begin{bmatrix} \tilde{i}_\ell \\ \tilde{v}_c \end{bmatrix} + \overline{D}_2 \underbrace{\begin{bmatrix} 0 & -\frac{1}{L} \\ \frac{1}{C} & -\frac{1}{RC} \end{bmatrix}}_{A_2} \begin{bmatrix} \tilde{i}_\ell \\ \tilde{v}_c \end{bmatrix}$$

$$+ d \underbrace{\begin{bmatrix} 0 & -\frac{1}{L} \\ \frac{1}{C} & 0 \end{bmatrix}}_{(A_2 - A_1)} \begin{bmatrix} \overline{I}_\ell \\ \overline{V}_c \end{bmatrix} \qquad (5.2)$$

The difference equations of the discrete model are then found by integration of Eqs. (5. 2) over one complete converter cycle. To do this a reference time is chosen for the n^{th} cycle to be at the part of the cycle where the pulse-width modulation modeled by d(t) occurs. We note that as d(t) becomes very narrow the integration may be carried out in two parts over the n^{th} cycle yielding the final small-signal converter difference result Eqs. (5. 3):

$$\begin{bmatrix} \tilde{i}_\ell\left((n+1)T\right) \\ \tilde{v}_c\left((n+1)T\right) \end{bmatrix} = e^{A_2\tau_2} e^{A_1\tau_1} \left(\begin{bmatrix} \tilde{i}_\ell(nT) \\ \tilde{v}_c(nT) \end{bmatrix} + d_n \begin{bmatrix} -T\,\dfrac{\bar{V}_c(T)}{L} \\ T\,\dfrac{\bar{I}_\ell(T)}{C} \end{bmatrix} \right) \tag{5.3}$$

Chapter 4 then showed that the application of the z-transform to Eqs. (5. 3) yields a set of steady state transfer functions G(z) defined by Eqs. (5. 4):

$$\begin{bmatrix} \tilde{i}_{\ell}^{*} \\ \tilde{v}_{c}^{*} \end{bmatrix} = G(z)d^{*} = (zI - M)^{-1} MKd^{*} = \begin{bmatrix} G_i(z) \\ G_v(z) \end{bmatrix} d^{*} \qquad (5.4)$$

where

$$M = e^{A_2 \tau_2} e^{A_1 \tau_1}$$

and

$$K = \begin{bmatrix} -T \dfrac{\bar{V}_c(T)}{L} \\ T \dfrac{\bar{I}_{\ell}(T)}{C} \end{bmatrix}$$

It was also noted in Chapter 4 that a simplification of Eqs. (5.4) is possible if a converter has only two states, as do most of the simple ones including our example, which results in

$$\begin{bmatrix} G_i(z) \\ G_v(z) \end{bmatrix} = (zI - M)^{-1} MK = \frac{[zM - z_1 z_2 I]}{(z - z_1)(z - z_2)} K \qquad (5.5)$$

where z_1 and z_2 are the eigenvalues of M.

The final exact results for the boost converter transfer functions as developed in Chapter 4 are:

$$\begin{bmatrix} G_i(z) \\ G_v(z) \end{bmatrix} = \frac{\left[z\, e^{A_2 \tau_2} e^{A_1 \tau_1} - z_1 z_2 I \right]}{(z - z_1)(z - z_2)} K \qquad (5.6)$$

It is noted that in the derivation of Eqs. (5.6) for the boost converter from its schematic of Fig. 5.1a, several equations were written but none was actually solved.

If one understands the small-signal approximations in the general derivation well enough, the transfer functions in the form of Eqs. (5.6) can be found in a matter of minutes for any two-state converter. However, Eqs. (5.6) are not in explicit form, and it is the last step of finding the explicit forms for $G_i(z)$ and $G_v(z)$ that is difficult.

To do this the transition matrix $M = e^{A_2 \tau_2} e^{A_1 \tau_1}$ must be found in explicit form. This may be done exactly through the very painstaking and tedious process of solution and multiplication of the exact exponential matrices. To find a single exponential matrix in closed form symbolically, one would have to take a Laplace transform, invert a matrix, and then take an inverse Laplace transform. Clearly, this effort would preclude investigation of systems of much higher than second order in symbolic form. Furthermore, the

resultant exact transition matrix would often contain many transcendental functions which tend to obscure the dependence of the converter's dynamic response on the filter elements.

This tedious process may be demonstrated by our boost converter example. With not much difficulty it can be shown that $e^{A_1 \tau_1}$ is given by:

$$e^{A_1 \tau_1} = \begin{bmatrix} 1 & 0 \\ 0 & e^{-\frac{\tau_1}{RC}} \end{bmatrix} \tag{5.7}$$

With considerably more difficulty $e^{A_2 \tau_2}$ may be found as:

$$e^{A_2 \tau_2} = \begin{bmatrix} e^{\frac{-\tau_2}{2RC}} \left[\cos \omega_f \tau_2 + \frac{1}{2RC\omega_f} \sin \omega_f \tau_2\right] & -e^{\frac{-\tau_2}{2RC}} \frac{1}{L\omega_f} \sin \omega_f \tau_2 \\ e^{\frac{-\tau_2}{2RC}} \frac{1}{C\omega_f} \sin \omega_f \tau_2 & e^{\frac{-\tau_2}{2RC}} \left[\cos \omega_f \tau_2 - \frac{1}{2RC\omega_f} \sin \omega_f \tau_2\right] \end{bmatrix} \tag{5.8}$$

$$\omega_f = \sqrt{\frac{1}{LC} - \frac{1}{(2RC)^2}}$$

The difficulty in derivation of Eqs. (5.8), and the mass of symbols that one has to manipulate to find Eqs. (5.6) explicitly, are sufficient to discourage further attempts along these lines. This is one

reason why current use of the discrete models is not widespread and is confined to computer analysis of specific cases.

This difficulty can be overcome by introduction of an approximation which we call the "straight-line" approximation. The approximation is stated as follows: since the switching frequencies of most practical converters are much higher than the natural frequencies of the converter filtering components, an accurate approximation for any exponential matrix $e^{A\tau}$ associated with a converter is found by

$$e^{A\tau} \simeq I + A\tau$$

A corollary to this is that if a transition matrix is of the form $e^{A_2\tau_2} e^{A_1\tau_1}$, then an accurate approximation to this matrix is

$$e^{A_2\tau_2} e^{A_1\tau_1} \simeq I + A_2\tau_2 + A_1\tau_1$$

To demonstrate this approximation for a particular case, we begin with the exact exponential matrices for the boost converter given in Eqs. (5. 7) and (5. 8), and note that if the switching frequency is much higher than the boost converter natural frequencies, then T and thus τ_1 and τ_2 are much shorter than the filter time constants. This implies that the following inequalities hold in Eqs. (5. 7) and (5. 8).

$$\frac{\tau_1}{RC} << 1 \qquad \frac{\tau_2}{2RC} << 1 \qquad \omega_f \tau_2 << 1$$

One may then approximate:

$$e^{-\frac{\tau_1}{RC}} \sim 1 - \frac{\tau_1}{RC} \qquad \cos \omega_f \tau_2 \sim 1$$

$$e^{-\frac{\tau_2}{2RC}} \sim 1 - \frac{\tau_2}{2RC} \qquad \sin \omega_f \tau_2 \sim \omega_f \tau_2$$

Insertion of these approximations into the exact expressions for $e^{A_1 \tau_1}$ and $e^{A_2 \tau_2}$ and retention of only first order terms in time yields:

$$e^{A_1 \tau_1} \sim \begin{bmatrix} 1 & 0 \\ 0 & 1 - \frac{\tau_1}{RC} \end{bmatrix} \tag{5.9}$$

$$e^{A_2 \tau_2} \sim \begin{bmatrix} 1 & -\frac{\tau_2}{L} \\ \frac{\tau_2}{C} & 1 - \frac{\tau_2}{RC} \end{bmatrix} \tag{5.10}$$

The multiplication of Eqs. (5.9) with Eqs. (5.10) and the retention of only first order terms in time yields the transition matrix.

$$e^{A_2\tau_2} e^{A_1\tau_1} \simeq \begin{bmatrix} 1 & \frac{-\tau_2}{L} \\ \frac{\tau_2}{C} & 1 - \frac{T}{RC} \end{bmatrix} \qquad (5.11)$$

However, this is seen to be the same result one obtains if the approximation $e^{A_2\tau_2} e^{A_1\tau_1} \simeq I + A_2\tau_2 + A_1\tau_1$ is made. This result is remarkably simple and easy to find.

From this example the general argument is clear. Because an exponential matrix represents a collection of time-domain solutions for any converter it always contains exponentially decaying sinusoidal functions which depend on the ratios of τ_1 and τ_2 to the filter time constants. Since converter switching frequencies are usually much higher than the natural frequencies of the filter components, the ratios of τ_1 and τ_2 to various filter time constants are much less than unity. The transcendental functions may then be accurately approximated by their truncated series which implies that any converter exponential matrix may be approximated by its truncated series as $e^{A\tau} \simeq I + A\tau$. The corollary result that $e^{A_2\tau_2} e^{A_1\tau_1} \simeq I + A_2\tau_2 + A_1\tau_1$ follows from this because second order terms in the matrix product $e^{A_2\tau_2} e^{A_1\tau_1}$ are negligible if they are negligible for the individual exponential matrices.

That keeping only the first order terms in time should give an accurate result for the transition matrix is really not surprising:

the approximation $e^{At} \sim I + At$ merely implies that the perturbation waveforms in the time domain are close to straight lines. This "straight-line" approximation has already been used in Chapter 1 to find the steady state waveforms; so, approximation of the transition matrix by retention only of its first order time terms constitutes a generalization of the approximations that are made to find the steady state converter waveforms. Indeed, Middlebrook and Cuk[14] show that this approximation is implicit in describing function converter models.

For an indication of the numerical accuracy of this approximation, we return to the boost converter example with element values chosen to be those used in Chapter 1.

$T = 10^{-4}$ sec. (switching frequency of 10 kHz)

$R = 60\ \Omega$

$L = 6.0$ mH

$C = 1/24 \times 10^{-3}$ F

$V_s = 60$ V

$\tau_1 = \tau_2 = 0.5 \times 10^{-4}$ sec. (50% duty cycle)

From these values, compute $\omega_f = 1.99 \times 10^3$ rad/sec (corner frequency of filter is then 316 Hz). With these values we compare exact and approximate transition matrices.

The exact solutions for the leading and trailing-edge transition matrices for the boost converter are:

$$e^{A_1\tau_1}e^{A_2\tau_2} = \begin{bmatrix} 0.995 & -8.24 \times 10^{-3} \\ 1.16 & 0.956 \end{bmatrix} \quad \text{(trailing-edge)}$$

$$e^{A_2\tau_2}e^{A_1\tau_1} = \begin{bmatrix} 0.995 & -8.07 \times 10^{-3} \\ 1.19 & 0.956 \end{bmatrix} \quad \text{(leading-edge)}$$

The first order approximation for either of these matrices from evaluation of Eqs. (5.11) is

$$\begin{bmatrix} 1 & \frac{-\tau_2}{L} \\ \frac{\tau_2}{C} & 1 - \frac{T}{RC} \end{bmatrix} = \begin{bmatrix} 1.00 & -8.33 \times 10^{-3} \\ 1.20 & 0.960 \end{bmatrix} \qquad (5.12)$$

In each component there is a relative error of from 1 to 3 percent. Another test of the accuracy of this result is to compare the eigenvalues of the exact transition matrices with those of the approximation. The results are:

exact eigenvalues: $0.9755 \pm j.097$

approximate eigenvalues: $0.9800 \pm j.098$

This example is an indication that the straight-line approximation is numerically sufficiently accurate for practical purposes. But, most important is the fact that with this approximation a converter transition matrix may now be found in the simple symbolic form of Eqs. (5.11). We apply this result to complete the explicit calculation of the boost converter transfer functions.

In the specific case of the boost converter transfer functions of Eqs. (5.6), the transition matrix can be evaluated in symbolic form with use of the straight-line approximation as Eqs. (5.11). Solution for the eigenvalues of the approximate transition matrix yields approximations for z_1 and z_2, the converter's z-plane poles.

$$z_1 \simeq 1 - \frac{T}{2RC} + j\sqrt{\frac{\tau_2^2}{LC} - \left[\frac{T}{2RC}\right]^2}$$

$$z_2 \simeq 1 - \frac{T}{2RC} - j\sqrt{\frac{\tau_2^2}{LC} - \left[\frac{T}{2RC}\right]^2} \qquad (5.13)$$

Use of the approximate transition matrix Eqs. (5.11) and the first order terms of $z_1 z_2$ in the transfer function Eqs. (5.6) gives explicit z-domain transfer functions of the boost converter to first order in time:

$$\begin{bmatrix} \tilde{i}_\ell^* \\ \tilde{v}_c^* \end{bmatrix} = \frac{1}{(z - z_1)(z - z_2)} \begin{bmatrix} z - 1 + \frac{T}{RC} & -z\frac{\tau_2}{L} \\ z\frac{\tau_2}{C} & (z-1)\left(1 - \frac{T}{RC}\right) \end{bmatrix} \begin{bmatrix} -T & \frac{\bar{V}_c(T)}{L} \\ T & \frac{\bar{I}_\ell(T)}{C} \end{bmatrix} d^*$$

The individual solutions are then

$$G_i(z) = \frac{\tilde{i}_\ell^*}{d^*} \simeq \frac{-T\left[\frac{\bar{V}_c(T)}{L}\left(z - 1 + \frac{T}{RC}\right) + z\frac{\bar{I}_\ell(T)\tau_2}{LC}\right]}{(z - z_1)(z - z_2)}$$

$$G_v(z) = \frac{\tilde{v}_c^*}{d^*} \simeq \frac{-T\left[z\frac{\bar{V}_c(T)\tau_2}{LC} - \frac{\bar{I}_\ell(T)}{C}(z-1)\left(1 - \frac{T}{RC}\right)\right]}{(z - z_1)(z - z_2)} \qquad (5.14)$$

A quick check on the accuracy of these expressions may be made by comparison of the modulation-to-output voltage transfer function $G_v(z)$ with that of Wester's averaged model.

If the ripple on the steady state waveforms $\bar{I}_\ell(t)$ and $\bar{V}_c(t)$ is small, then the relation $\bar{I}_\ell = \bar{V}_c/D'R$ between the average values $\bar{I}_\ell$ and $\bar{V}_c$, developed in Chapter 1, Eq. (1.2), may be used to write $G_v(z)$ as

$$G_v(z) \simeq \frac{\bar{V}_c}{D'} \frac{\left[1 - \left(\frac{z-1}{T}\right)\left(\frac{L}{D'^2R} - T\right)\right]}{\left[1 + \frac{1}{Q}\left(\frac{z-1}{\omega_o T}\right) + \left(\frac{z-1}{\omega_o T}\right)^2\right]} \qquad (5.15)$$

where

$$\omega_o = \frac{D'}{\sqrt{LC}}$$

$$D' = \frac{\tau_2}{T}$$

$$Q = \omega_o RC$$

It was stated in Chapter 4 that the s-plane is mapped into the z-plane by $z = e^{sT}$. At frequencies low compared to the switching frequency, $|sT| << 1$ so that the mapping is approximately $z = 1 + sT$. Substitution of this low-frequency approximation into Eq. (5.15) yields

$$G_v(z = 1 + sT) = -\frac{\bar{V}_c}{D'} \frac{\left[1 - s\left(\frac{L}{D'^2 R} - T\right)\right]}{\left[1 + \frac{1}{Q}\left(\frac{s}{\omega_o}\right) + \left(\frac{s}{\omega_o}\right)^2\right]}$$

which agrees with the df result except for the factor -T in the numerator. However, if the switching frequency is much higher than the radian frequency of the zero, then the df and discrete results agree for frequencies where $|sT| << 1$ is valid.

A number of interesting things can be done with the transfer functions $G_i(z)$ and $G_v(z)$. In Chapter 6 use of the transformation $z = e^{sT}$ is made to allow Bode plot comparison of transfer functions derived by both the discrete and describing function methods.

These comparisons allow one to see the range in frequency where the describing function approach is valid. However, the way in which the designer may be most interested in using the discrete functions is in evaluation of closed-loop response by means of the root locus.

Recall that in Chapter 4 in Eq. (4. 11) the true loop gain $T^*(z)$ was shown to be a linear combination of the transfer functions such as $G_i(z)$ and $G_v(z)$ for any of the modulators treated in Chapter 3. Since all the transfer functions of a converter have the converter's open-loop poles, then we conclude that the poles of the loop gain are always the open-loop poles of the converter -- z_1 and z_2 for the specific case of the boost converter. The zeros of $T^*(z)$ will depend on how $G_i(z)$ and $G_v(z)$ are combined. For example, suppose that the feedback and type of modulator were chosen such that $T^*(z) = kG_v(z)$. In other words, only the output voltage is effectively fed back. After some manipulation, the expression for $G_v(z)$ in (5. 14) may be expressed in the form:

$$G_v(z) = \frac{k'\left(\frac{z}{z_3} - 1\right)}{(z - z_1)(z - z_2)}$$

in which

$$k' = \frac{T\bar{I}_\ell(T)\left(1 - \frac{T}{RC}\right)}{C}$$

$$z_3 = \frac{1}{1 - \frac{\bar{V}_c(T)\tau_2}{\bar{I}_\ell(T)L\left(1 - \frac{T}{RC}\right)}}$$

For the boost converter element values given in Chapter 1, $z_3 = 1.39$. The open loop poles z_1 and z_2 are calculated to be:

$$z_1 = 0.98 + j.098$$

$$z_2 = 0.98 - j.098$$

Thus a pole-zero plot of $T^*(z)$ or $G_v(z)$ for this particular set of element values would appear as in Fig. 5.2. Since $T^*(z)$ is the loop gain, then as the scale factor k is varied from 0 to infinity, the closed-loop poles follow a root locus starting at the open-loop poles and ending at the open-loop zeros. This root locus, which for two poles and a zero makes a circle around the zero, is also shown in Fig. 5.3. The locus shows that with sufficient loop gain the boost regulator will oscillate at a frequency somewhat higher than its open-loop natural frequencies.

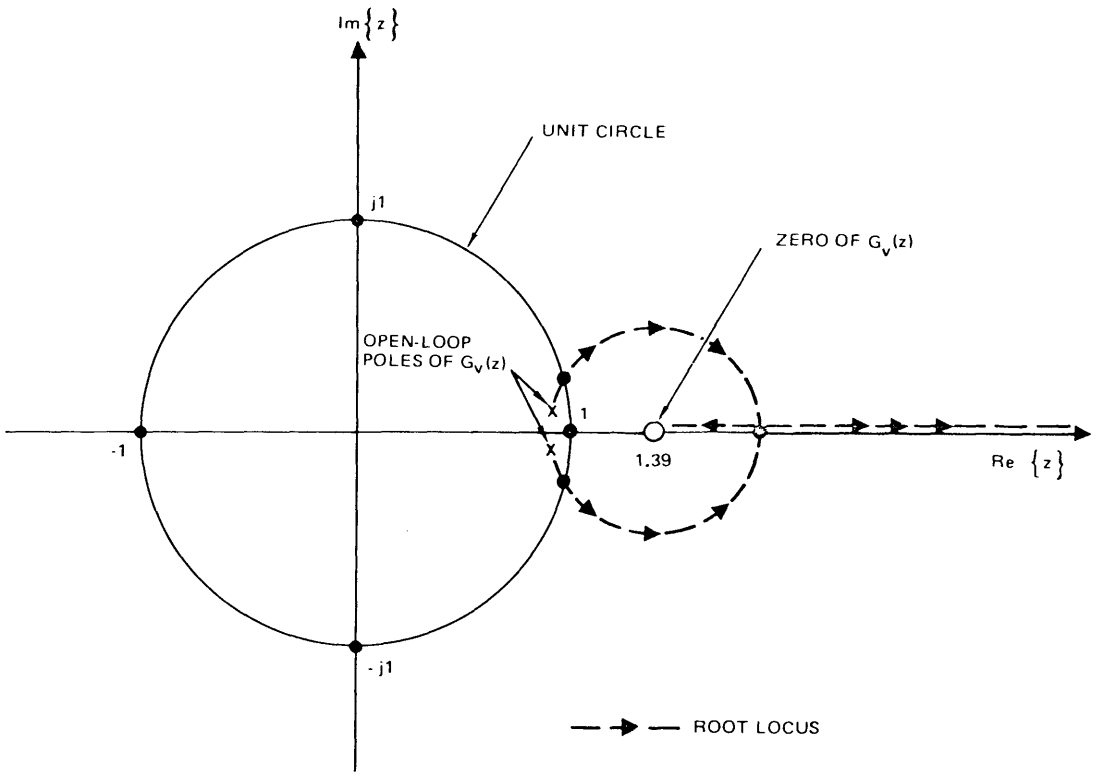

Fig. 5.3. Root locus of $T^*(z) = kG_v(z)$, boost regulator with voltage feedback.

Figure 5.4 is a pole-zero plot of the same transfer function in the s-plane obtained from Wester's describing function model. For the given set of parameters, the two models agree quite well qualitatively in predicting oscillatory behavior at slightly greater than the natural frequencies of the converter.

Since the transfer functions of modulators are constants, one can conclude that with simple voltage feedback a boost regulator at this operating point can never have a closed-loop bandwidth much beyond

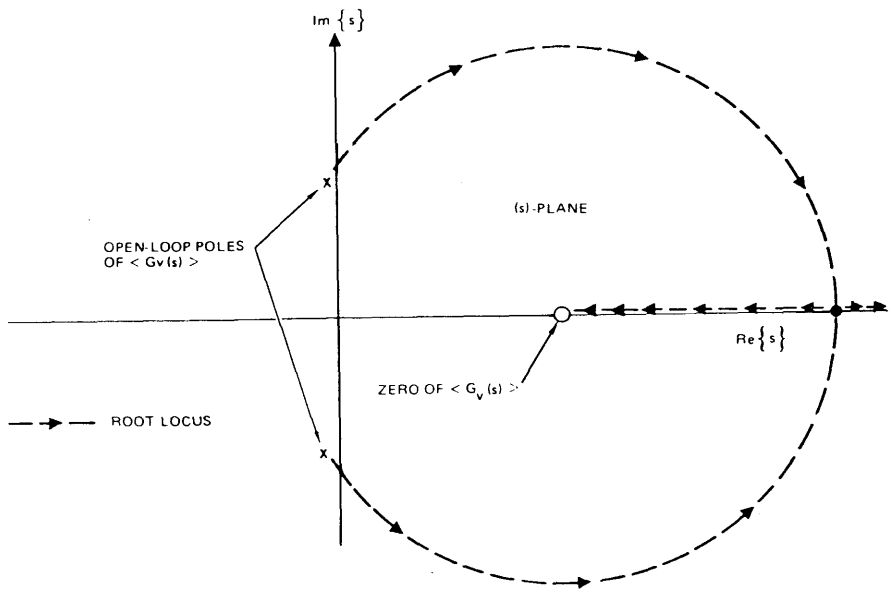

Fig. 5.4. Root locus of $T(s) = k\langle G_v(s)\rangle$, boost regulator with voltage feedback.

the effective resonant frequency of the output filter. This effective frequency can be found approximately by the relation mentioned in Chapter 4 relating the mapping of the s-plane to the z-plane:

$$z = e^{sT} \simeq 1 + sT$$

if

$$|sT| << 1$$

$$\therefore \quad s \simeq \frac{z - 1}{T}$$

So, for the boost converter with poles at z_1 and z_2 as given in Eqs. (5.13), the continuous poles are:

$$s_1 \simeq \frac{z_1 - 1}{T} = -\frac{1}{2RC} + j\sqrt{\left(\frac{\tau_2}{T}\right)^2 \frac{1}{LC} - \left[\frac{1}{2RC}\right]^2}$$

$$s_2 \simeq \frac{z_2 - 1}{T} = -\frac{1}{2RC} - j\sqrt{\left(\frac{\tau_2}{T}\right)^2 \frac{1}{LC} - \left[\frac{1}{2RC}\right]^2}$$

These agree precisely with the poles as derived by Wester's averaged model.

Several investigators have found that feeding back the current as well as the voltage seems to have a salutary effect on the converter's transient response [6, 8]. The root locus and the discrete model together provide an elegant way of explaining this.

First note that the current transfer function $G_i(z)$ as given in Eqs. (5.14) is of the form:

$$G_i(z) = \frac{k_i\left(\frac{z}{z_4} - 1\right)}{(z - z_1)(z - z_2)}$$

where

$$k_i = -\frac{T\bar{V}_c(T)\left(1 - \frac{T}{RC}\right)}{L}$$

$$z_4 = \frac{1}{1 + \frac{T}{RC} + \frac{\bar{I}_\ell(T)\tau_2}{\bar{V}_c(T)C}}$$

For the set of values used in this example, $z_4 = 0.928$.

If the feedback is made up of a linear combination of the inductor current and capacitor voltage, then the loop gain T*(z) is of the form:

$$T^*(z) = k\left[G_v(z) + hG_i(z)\right] \qquad (5.16)$$

where k and h are constants. Since $G_i(z)$ and $G_v(z)$ have the same poles, as h varies from zero to plus infinity the zero in the loop gain moves along a locus from the zero of $G_v(z)$ to the zero of $G_i(z)$ as shown in Fig. 5.5. Once h is chosen to place the zero in T*(z) then k, the overall gain, may be varied to move the closed-loop poles around this choice of zero. The partial loci of the closed-loop poles for four different zero placements are shown in Fig. 5.6.

Figure 5.6 indicates that with the right choice of h and k a boost regulator can oscillate at anywhere from near the output filter's resonant frequency to half the switching frequency. It also indicates the possibility of some interesting behavior which is incapable of being predicted by a continuous linear model.

For example, Fig. 5.7 is a root locus for a boost regulator when just the inductor current is fed back. This would be done if one wished to make the converter a current regulator. The pole which

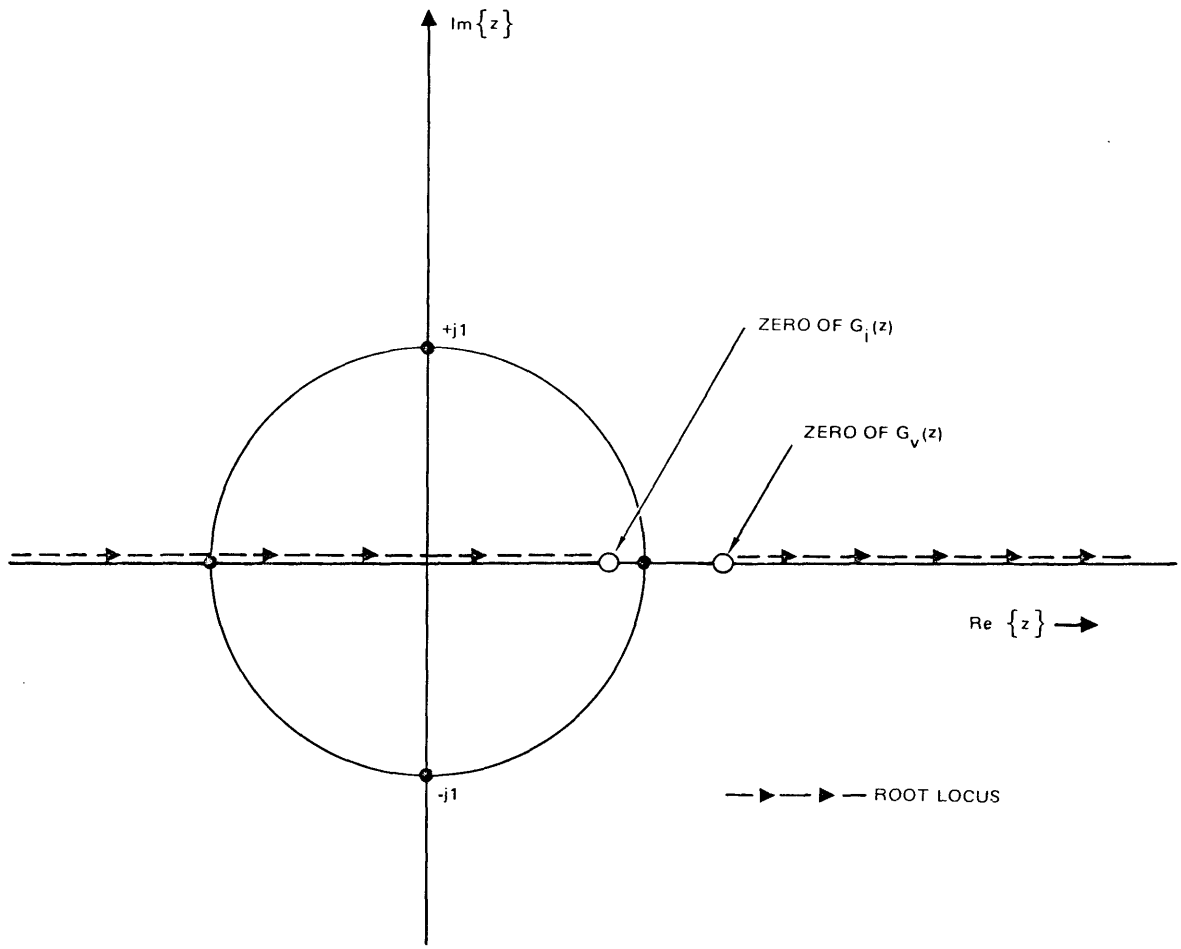

Fig. 5. 5. Root locus of the zero of T*(z) for increasing amounts of current feedback for boost converter.

heads toward the origin on the locus corresponds to a pole in the s-plane on the negative real axis which is heading for minus infinity. Thus, the part of the transient response corresponding to this pole decays more and more quickly.

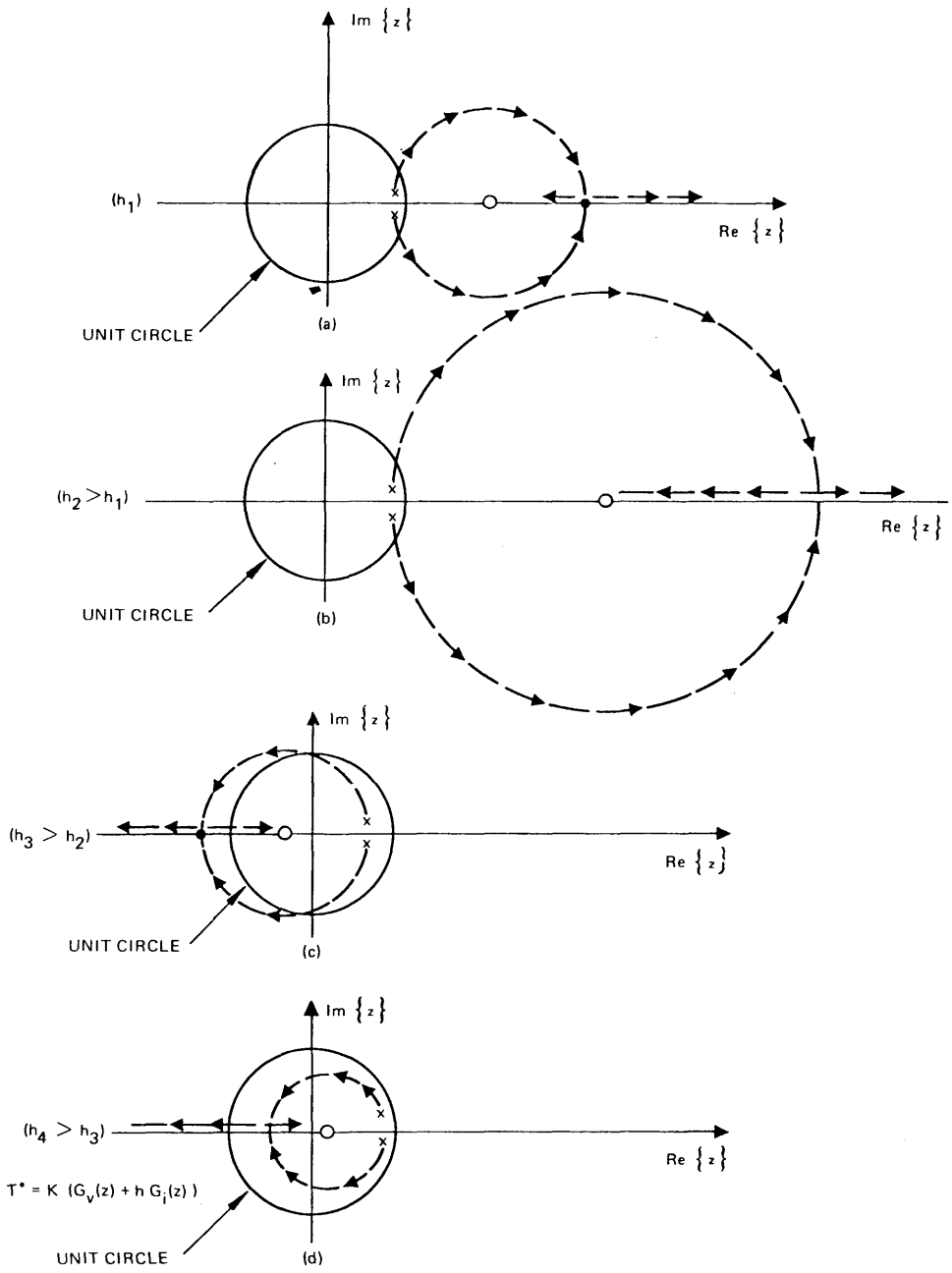

Fig. 5.6. Root loci for T*(z) with different zero locations corresponding to increasing amounts of current feedback.

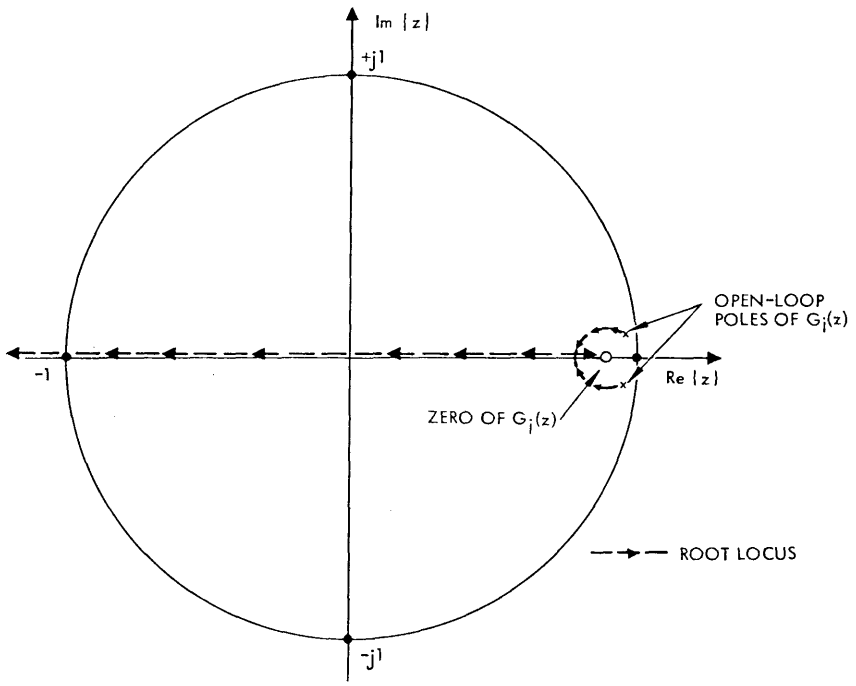

Fig. 5.7. Root locus for boost converter with current feedback.

Eventually, for a certain value of loop gain, the z-plane pole reaches the origin. This corresponds to a transient which is incapable of being predicted by the describing function approach. For a discrete system a pole at the origin means that part of the transient is over in a single cycle. In a practical sense it would appear that the closed-loop regulator only had a single pole in the s-plane.

As the loop gain is increased further, even stranger things happen. While the z-plane pole is on the negative real axis inside the unit circle it contributes a decaying oscillation at half the switching frequency. Thus a single pole can here effectively look like a

pair of complex conjugate poles in the s-plane. Now it may appear that the regulator has three s-plane poles.

An even further increase in the loop gain eventually drives the pole far enough so that it hits the unit circle. At this point the converter should sustain half-frequency oscillation according to the small signal discrete model. Actually, whether the converter will oscillate or not when the pole is precisely at -1 depends on second order nonlinear terms which were neglected in the derivation. Practically speaking, this is of little consequence, since at best the regulator would be only marginally stable.

This prediction of half-frequency or subharmonic oscillation comes with relative ease with the discrete model. For comparison one can refer to Yuh's work [13] where complicated Fourier techniques are used to make the describing function approach predict similar instability.

One final point of interest for the boost converter with both voltage and current feedback is that about any operating point there exists an optimal solution in the sense that the transient response is the fastest of all possibilities. Figure 5.8 is a root locus that illustrates the case.

Here h is chosen in Eq. (5.16) such that the zero of $T^*(z)$ is placed equidistant from the origin and the open-loop poles of $G_i(z)$ and $G_v(z)$.

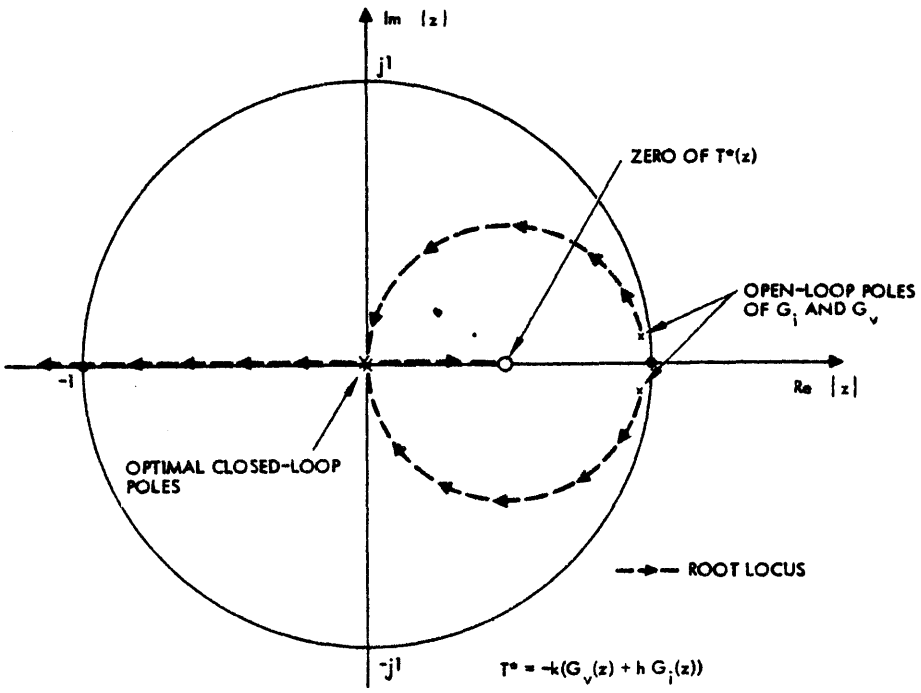

Fig. 5.8. Root locus for optimal transient response for boost converter.

Then an overall gain factor k in Eq. (5.16) is chosen for the loop gain such that the closed-loop poles coalesce at the origin.

The resultant closed-loop system then has an essentially finite transient response for small disturbances from its operating point. Sampled-data theory indicates that a pole of order n at the origin contributes a response that settles completely after n periods. Thus, this optimized two-pole system should settle in two converter cycles.

In Chapter 6 verification of the fascinating behavior predicted by the discrete model will be given by means of a digital computer program which solves the large-signal nonlinear boost converter equations.

To summarize this chapter, a boost converter has been used as an example of how one might use discrete modeling as a design analysis tool. Various assumptions were made about operating mode (continuous conduction) and type of modulation (leading-edge at beginning of $\overline{D}_1 = 1$). As a review of the earlier chapters the steps in the model derivation leading to an expression for the z-plane converter transfer functions were reviewed.

To find the converter transfer functions in explicit form a new "straight-line" approximation was introduced. It was shown that since the ratio of switching frequency to filter corner frequency is large, then the approximation $e^{At} \approx I + At$ can greatly simplify the task of finding a transition matrix. Because the most difficult part of the discrete model formulation is to find explicit forms for converter transition matrices, the straight-line approximation is a key step in the development of discrete techniques simple enough for use in initial design phases of a switching regulator.

A numerical example was given to indicate that the accuracy of this approximation is good. Since the requirements for this approximation to be accurate are met by most practical converters, we conclude that it should be of use in the discrete analysis of any switching converter. It is important to note that the straight-line approximation in no way limits the range of frequency validity of the discrete converter models, because $e^{A\tau}$ refers to the steady state solution and not to any perturbation frequency.

After this approximation was used to find explicit forms for the boost converter transfer functions, the root locus was then used to indicate the potential transient performance of a boost regulator with voltage or current feedback. This was done independently of the choice of modulator, because Chapter 3 showed that single-edge modulators contribute only constant gain factors to a regulator's z-plane loop gain. A natural by-product of these root loci was the prediction of half switching frequency oscillation for some cases. Similar predications with the describing function models are more difficult to derive. Finally, the root locus indicated that there exists a unique choice of the feedback which produces a regulator with optimal transient characteristics about the chosen operating point. From a design standpoint it is of great interest to know that this possibility exists.

Chapter 6

Verification of the Performance Analysis

In the previous chapters a small-signal modeling technique was introduced with the ultimate purpose of being used as an aid in the design of transient response for switching regulators. The essential claim for this technique is that a pulse-width modulated system, such as a switching regulator, is more accurately modeled for small signals by linear difference equations rather than linear differential equations. This is essentially proved by noting that in the mathematics of the discrete model derivation the only approximations made were "small-signal" type approximations. Nowhere was it assumed in the derivation that the switching frequency had to be "high" compared to filter resonant frequencies or closed-loop bandwidth.

With the exact derivation accomplished, it was then shown that the assumption of the switching frequency being much higher than the converter natural frequencies allowed simple "straight-line" approximations to be made to obtain the discrete model parameters. This approximation does not degrade the inherent perturbation high-frequency accuracy of the discrete converter models because it is only applied to find the steady state transition matrix. Consideration of various modulators in Chapter 3 led to the rather startling claim that as far as small-signal transient response is concerned, all modulators

offer the same potential performance. Use of the z-transform on the discrete model in Chapter 4 showed that closed-loop transient and stability performance could be inferred via the frequency domain concepts of transfer functions and loop gain. For the discrete model, though, the frequency domain is the z-plane rather than the s-plane.

By means of a simple example of a boost regulator in Chapter 5 some interesting transient behavior was predicted. Use of the root locus in this example showed that depending on the type and amount of feedback, the regulator has the potential for duty ratio oscillation from near the filter resonant frequencies to half the switching frequency. Even more important from a design standpoint is that negative infinity in the s-plane is in the middle of the z-plane at the origin and within the reach of the closed-loop regulator poles. This implies that an optimal transient response in the small-signal sense is possible provided the feedback is chosen to place all the closed-loop poles at the origin.

It is the aim of this chapter to lend credence to the validity of these conclusions by comparisons of the transient performance of a nonlinear large-signal boost regulator model with its small-signal discrete model by means of digital computer simulation. To indicate the ability of the approximate small-signal discrete models to predict the performance of a large-signal regulator, small-signal predictions and large-signal performances are compared at low frequencies and at frequencies comparable to the switching frequency. In addition,

particular emphasis is given to the optimal transient condition, since achievement of this response is of practical interest.

To begin we discuss the low frequency accuracy of the discrete models as represented by the approximate boost converter small-signal voltage transfer function $G_v(z)$ given in Eqs. (5. 14). This is compared with the comparable df result in a Bode plot, and then used to predict low-frequency oscillation of a boost regulator with voltage feedback.

Next, the approximate boost-converter small-signal current transfer function $G_i(z)$ of Eqs. (5. 14) is plotted and compared with its df counterpart. The high-frequency accuracy of the approximate discrete model is displayed by the ability to predict accurately from $G_i(z)$ the onset of half switching frequency oscillation in a regulator with current feedback.

Finally, the conditions for optimal transient response are examined. A section is presented on how to design the physical feedback for two different modulators so that the optimal response is achieved. Results of this section are then compared in a large-signal simulation to test the accuracy of the approximate models in a design mode.

The results presented here may be summarized as follows:

1. The small-signal difference equation model is a valid model. Actually this is plain from the mathematics of the earlier

chapters, but it will be demonstrated that if the large-signal regulator is slightly disturbed from its steady state, its transient performance closely follows that of the linear difference equation model.

2. The types of transient behavior indicated in Chapter 5 including the optimal response, do occur in various large-signal regulator configurations, and furthermore are accurately predicted by analysis with the linear discrete model. It will be shown that the linear discrete model including the "straight-line" approximation can quite accurately predict the onset of both low-frequency and half-switching-frequency oscillation as well as the conditions for the optimal response.

3. Different modulators can indeed yield the same transient response for "small" transients. Comparisons of the same regulator with a sawtooth modulator and a uniformly sampled modulator will show that although their large-signal performance can vary, for small signals both can produce similar transients. An example of this is that the optimal response is achieved with a uniformly sampled modulator, a modulator believed by many to have poor closed-loop bandwidth capability because of its delay.

For all the cases examined here the same basic converter and the same operating point were used. Except where mentioned otherwise, a sawtooth modulator is used in the large-signal model. The boost converter is described by the following parameters:

$T = 10^{-4}$ sec (switching frequency of 10 kHz)

$R = 60\ \Omega$

$L = 6.0$ mH

$C = 1/24 \times 10^{-3}$ F

$V_s = 60$ V

$\tau_1 = \tau_2 = 0.5 \times 10^{-4}$ sec (50% duty cycle)

$\frac{1}{\sqrt{LC}} = 2 \times 10^3$ radians per sec (318 Hz)

The effective resonant frequency, defined for Eqs. (5.15) is

$$\omega_o = \frac{\tau_2}{T} \frac{1}{\sqrt{LC}} \sim 159 \text{ Hz}$$

We begin with an investigation of the low-frequency accuracy of the discrete models. The goal is to test the accuracy of low-frequency oscillation prediction with $G_v(z)$ and to compare the averaged voltage transfer function $\langle G_v(s) \rangle$ with $G_v(z)$. A Bode plot of $G_v(z = e^{sT})$ is given in Fig. 6.1. Shown in x's in Fig. 6.1 is $\langle G_v(s) \rangle$ for Wester's averaged model. Both were easy enough to compute that a hand-held calculator was used for the task. It is seen that there is good agreement between these two different models at low frequencies. The most noticeable disparity between these transfer functions is that as half the switching frequency is approached, the discrete model shows an additional 90 degrees of phase lag. However, for voltage feedback this makes little difference in the prediction of oscillatory closed-loop transient behavior, because the frequency where the converter will first oscillate is much lower than the switching frequency.

In the case of voltage feedback the boost regulator loop gain $T^*(z)$ is given by

$$T^*(z) = kG_v(z)$$

where k is a constant. We can predict the value of k necessary for oscillation with voltage feedback k_o by finding the frequency f_o where the angle of $G_v(z)$ is -180 degrees in Fig. 6.1 and then choosing $k = 1/\left| G_v\left(z_o = e^{j2\pi f_o T}\right)\right| = k_o$.

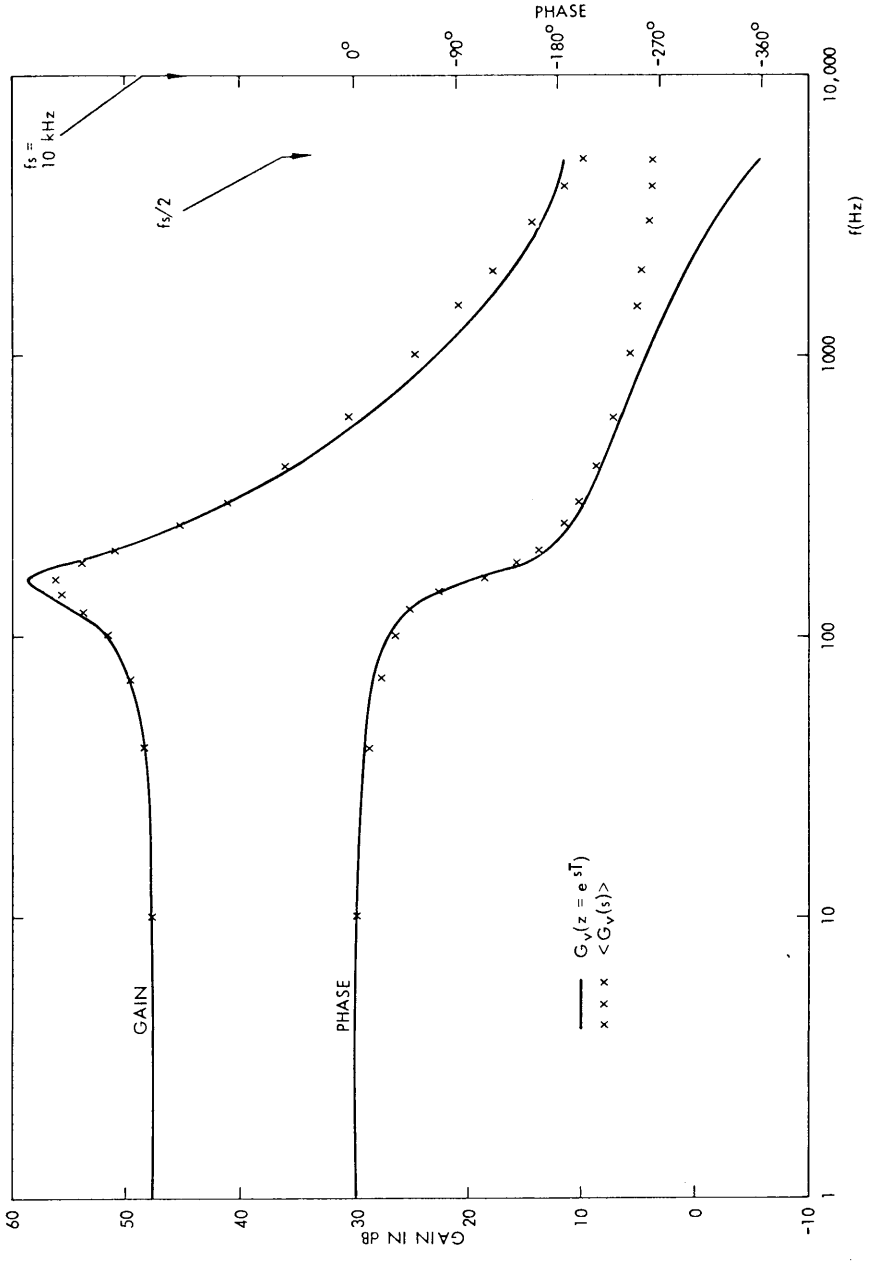

Fig. 6.1. Discrete and averaged modulation-to-capacitor voltage transfer functions.

This was done for the approximate $G_v(z)$ derived in Eq. (5.14) with the result that $k_o = 0.0034$ is the predicted gain necessary for oscillation. From simulation with a large-signal boost regulator with voltage feedback, an experimental value of $k_o = 0.00458$ was determined. This is a reasonable agreement if one considers the relevant time constant ratios necessary to validate the straight-line approximation given before Eqs. (5.9) and calculated here with the specific values taken for this boost converter.

$$\frac{\tau_1}{RC} = 0.02 \qquad \frac{\tau_2}{2RC} = 0.01 \qquad \omega_f \tau_2 = 0.226$$

Because the $\omega_f \tau_2 \ll 1$ inequality is not well satisfied for the regulator, it is not surprising that predicted and measured low frequency stability bounds differ somewhat from each other.

An additional low-frequency check on the accuracy of the straight line approximation for $G_v(z)$ is to compare the frequency of closed-loop oscillation for voltage feedback with the frequency where $G_v(z)$ is $-180°$ in Fig. 6.1.

Figure 6.2 is a plot of the discrete perturbations on the boost regulator capacitor voltage taken from a large-signal simulation with $k_o = 0.00458$. The plot indicates that the regulator is barely unstable. Examination of the period of the oscillation in Fig. 6.2 indicates that a full period would be 44T. Since the switching frequency is 10 kHz, $T = 10^{-4}$ sec. The period of the oscillation is then 4.4×10^{-3} sec

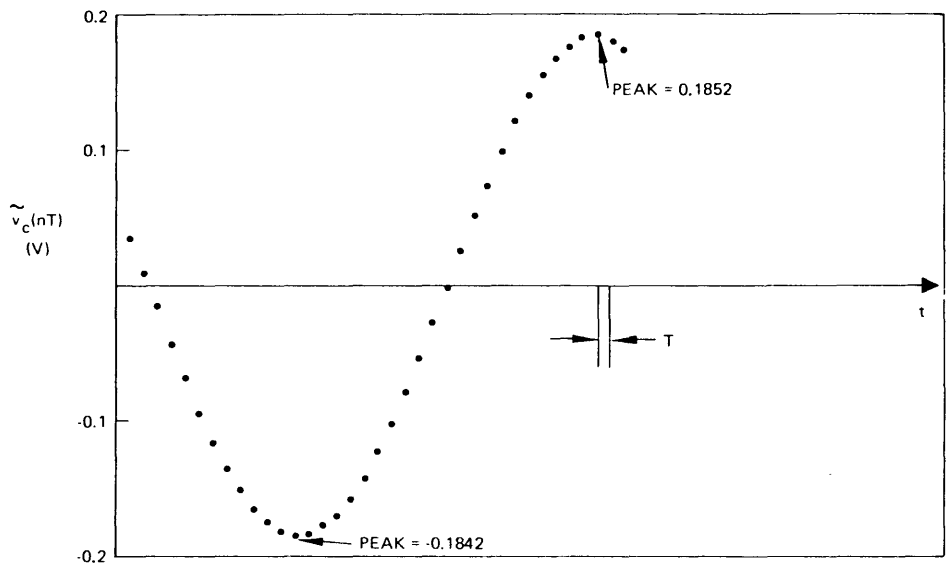

Fig. 6.2. Time response of perturbation on capacitor voltage.

indicating a frequency of about 230 Hz which agrees well with where the plot of $G_v(z = e^{sT})$ in Fig. 6.1 has -180 degrees of phase shift. Since both discrete and averaged models agree in this area it is not surprising that they can both be used successfully at low frequencies.

The divergence of results, and in fact the region where the accuracy of the discrete model is superior, occurs at frequencies approaching half the switching frequency.

A striking example of these effects is presented in the next example when a boost converter is made a current regulator by feeding the pulse-width modulator a measure of inductor

current. This example demonstrates the high-frequency accuracy of the discrete models.

Figure 6.3 is a Bode plot of the approximate discrete modulator-to-inductor current transfer function $G_i(z = e^{sT})$ given in Eq. (5.14). Also shown is the transfer function for the averaged model $\langle G_i(s) \rangle$. Again, there is close agreement at low frequencies, with the principal disparity being an extra 90 degrees of phase lag in $G_i(z)$ as frequencies approach half the switching frequency. In addition there is a distinct difference in the magnitudes of the two transfer functions near half the switching frequency.

For the case of current feedback the loop gain $T^*(z)$ is given by

$$T^*(z) = k\, G_i(z)$$

where k is a constant. From Fig. 6.3 we note that $G_i(z)$ has -180 degrees of phase shift at half the switching frequency. Since $z = -1$ at half the switching frequency a predicted stability bound for a boost current regulator is $k_o' = 1/|\, G_i(-1)\,|$. The predicted value for k_o' from the straight line approximation for $G_i(z)$ is $k_o' = 0.976$. Experimentally this bound was determined from large-signal regulator simulation to be $k_o' = 0.973$ which agrees well with the predicted bound.

Figure 6.4 is a picture of the resultant computer-simulated discrete perturbations in inductor current for an initial small disturbance in duty ratio with $k_o' = 0.973$. As predicted by the discrete

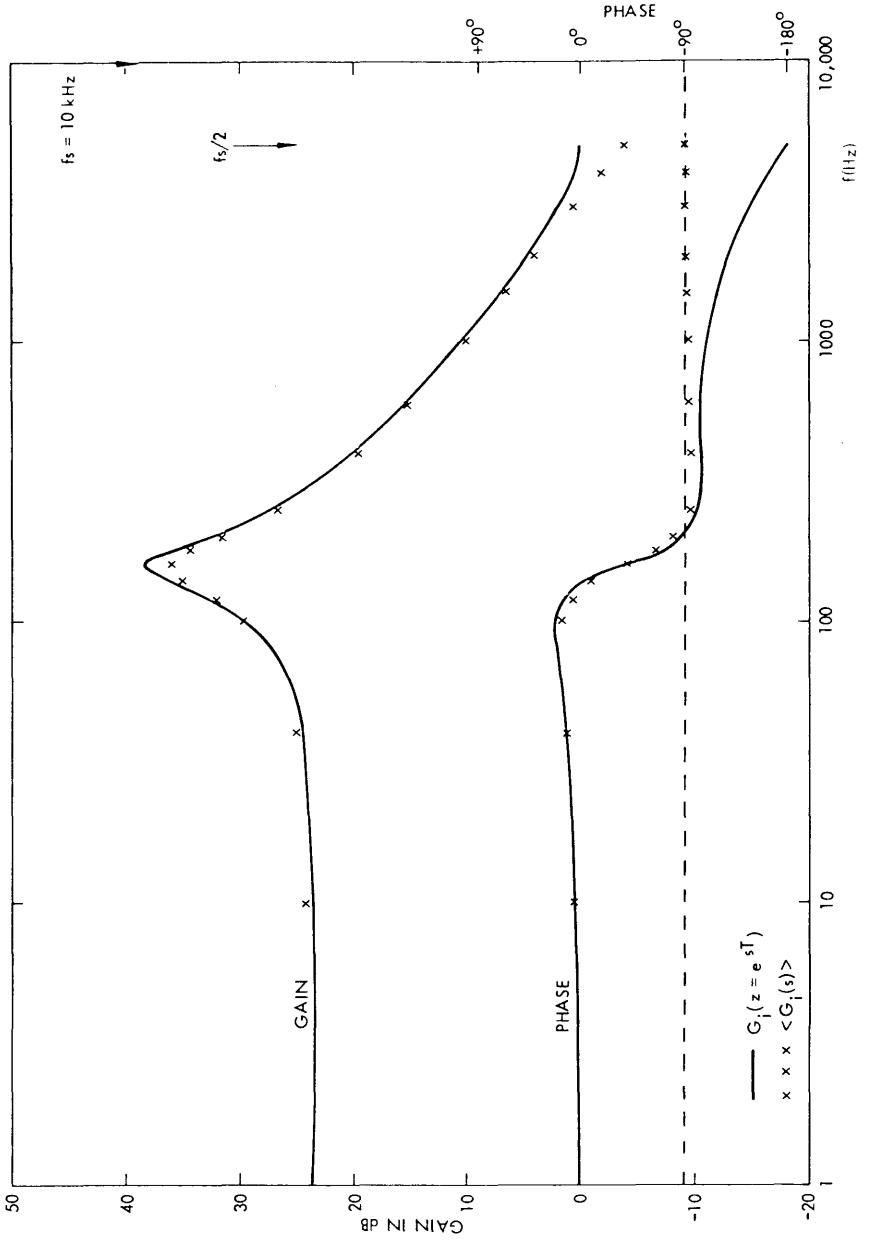

Fig. 6.3. Discrete and averaged modulation-to-inductor current transfer functions.

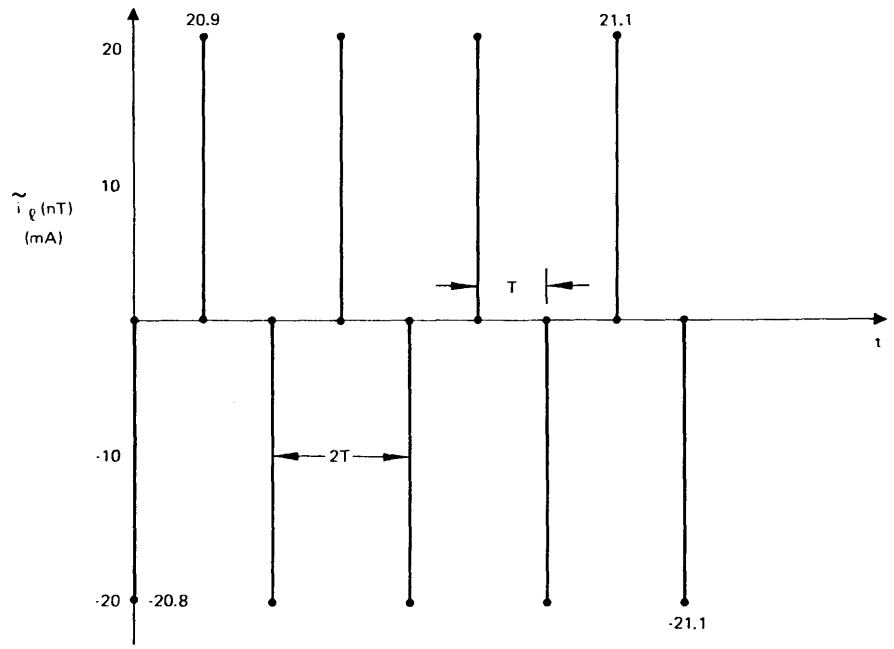

Fig. 6.4. Half frequency oscillation on inductor current.

current transfer function with the root locus in Chapter 5 and in the Bode plot of Fig. 6.3, the indicator current oscillates at half the switching frequency.

Figure 6.5 is a plot of the discrete capacitor voltage perturbations for the same case. In this figure we can see the effect of a stable pole as well as the unstable one. Recall that in Chapter 5 the argument was presented that since a single pole in the z-plane on the negative real axis gives rise to a ringing response at half the switching frequency, another pole can make the total system appear to have three poles if it were continuous. This effect is clearly evident in

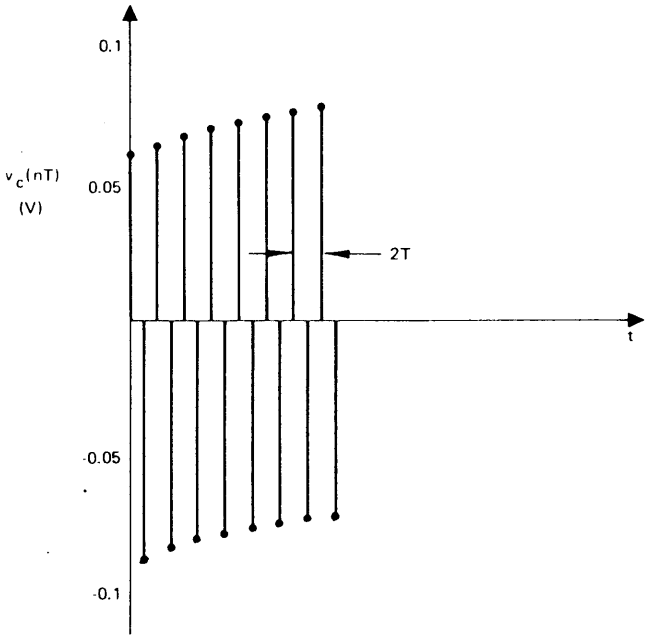

Fig. 6.5. Half frequency oscillation on capacitor voltage.

Fig. 6.5 as $\tilde{v}_c(nT)$ has a decaying component as well as the half frequency oscillation.

Although prediction of stability is a useful validation of an analytic technique, the more interesting and practical case from a design point of view is the optimal response condition.

In this last comparison a three-step procedure is outlined which shows how one can design the physical regulator feedback to achieve the optimal response. The procedure is then implemented on two boost regulators, one with a sawtooth modulator and one with a uniformly sampled modulator. Their transient responses are then

compared. To clarify this procedure we begin with a review of the notation in the development of the regulator loop gain $T^*(z)$.

The physical feedback for a regulator with converter state variable compensation is specified in general by Eq. (3.1) with a row vector H^T. For the case of the boost regulator H^T is defined by

$$V(t) = H^T \begin{bmatrix} I_\ell(t) \\ V_c(t) \end{bmatrix} + V_r = [a_1 \; b_1] \begin{bmatrix} I_\ell(t) \\ V_c(t) \end{bmatrix} + V_r$$

$$= a_1 I_\ell(t) + b_1 V_c(t) + V_r$$

where $V(t)$ is the signal input to a pulse-width modulator V_r is a dc reference signal and $I_\ell(t)$ and $V_c(t)$ are the boost converter state variables.

The modulator development of Chapter 3, summarized in Table 3.1, shows that any of the three modulators treated in that chapter may be characterized together with the compensation in the small-signal form

$$d_n = H_e^T \tilde{x}(nT)$$

where H_e^T is the "effective" feedback of the combination of modulator and compensation. For the case presented here we use the following notation for the effective feedback.

$$d_n = H_e^T \begin{bmatrix} \tilde{i}_\ell(nT) \\ \\ \tilde{v}_c(nT) \end{bmatrix} = [a \quad b] \begin{bmatrix} \tilde{i}_\ell(nT) \\ \\ \tilde{v}_c(nT) \end{bmatrix}$$

$$= a\,\tilde{i}_\ell(nT) + b\,\tilde{v}_c(nT) \qquad (6.2)$$

In Chapter 4 a general expression for the regulator loop-gain $T^*(z)$ was developed in terms of H_e^T in Eq. (4.11) as

$$T^*(z) = H_e^T\, G(z)$$

where $G(z)$ is a vector of the converter transfer functions. It is this form which enables the conclusion that for converter state variable feedback the loop gain is a linear combination of the converter transfer functions. With the notation of Eq. (6.2) the loop gain for a boost regulator is

$$T^*(z) = [a \quad b]\begin{bmatrix} G_i(z) \\ \\ G_v(z) \end{bmatrix} = a\,G_i(z) + b\,G_v(z) \qquad (6.3)$$

Finally from Eqs. (5.14) we note that G_i and G_v are each of the form of a linear polynomial in z over a quadratic in z which with Eq. (6.3) implies that $T^*(z)$ is of the form

$$T^*(z) = \frac{a'z + b'}{(z - z_1)(z - z_2)} \qquad (6.4)$$

where z_1 and z_2 are the poles of G_i and G_v given in Eqs. (5.13).

With all of the necessary notation defined we now list the three-step procedure one may use to find the physical feedback $H^T = [a_1, b_1]$ which will result in the optimal transient solution, where all of a regulator's closed-loop poles are at the origin in the z-plane.

1. Given a particular converter linearized about an operating point, find a' and b' in Eq. (6.4) in terms of the open-loop converter poles z_1 and z_2 such that $1 + T^*(z) = 0$ has a double root at $z = 0$.

From Eq. (6.4) $1 + T^*(z) = 0$ may be written as

$$(z - z_1)(z - z_2) + a'z + b' = 0$$

$$z^2 + (-z_1 - z_2 + a')z + b' + z_1 z_2 = 0 \qquad (6.5)$$

Clearly $a' = z_1 + z_2$ and $b' = -z_1 z_2$ result in the optimal response, because $1 + T^*(z) = 0$ reduces to $z^2 = 0$ for this choice.

2. With this optimal a' and b' known, find the optimal effective feedback $H_e^T = [a \quad b]$ by equating Eq. (6.3) with Eq. (6.4).

Because G_i and G_v have the same denominator $(z - z_1)(z - z_2)$ we may write

$$a \text{ (numerator of } G_i) + b \text{ (numerator of } G_v) = a'z + b' \qquad (6.6)$$

Equating the coefficients of z and the constant terms yields two equations from which we solve for a and b in terms of a' and b'.

3. Having found the optimal effective feedback $H_e^T = [ab]$ pick a modulator from Table 3.1 and find $H^T = [a_1 b_1]$ the optimal physical feedback using the formulas given for the individual modulators.

For example from Table 3.1 the formula for the uniformly sampled modulator relates H^T and H_e^T by

$$H_e^T = \frac{H^T e^{-A_2 \tau_2}}{TR'}$$

We may invert this expression to find H^T in terms of H_e^T as follows

$$H^T = TR' H_e^T e^{A_2 \tau_2}$$

$$[a_1 \quad b_1] = TR' [a \quad b] e^{A_2 \tau_2} \qquad (6.7)$$

Equation (6.7) expresses the final answer for the physical feedback into a uniformly sampled modulator.

As an additional example the sawtooth modulator relations between H^T and H_e^T are given in Table 3.1 as

$$H_e^T = \frac{H^T}{T\left(R' - H^T \bar{x}'(nT)\right)} \tag{6.8}$$

From Eq. (6.1) the term $H^T \bar{x}'(nT)$ for the boost converter is:

$$H^T \bar{x}'(nT) = [a_1 \quad b_1] \begin{bmatrix} \bar{I}_\ell'(nT) \\ \\ \bar{V}_c'(nT) \end{bmatrix} = a_1 \bar{I}_\ell'(nT) + b_1 \bar{V}_c(nT)$$

So Eqs. (6.8) may be expressed equivalently as

$$[a \quad b] = [a_1 \quad b_1] \frac{1}{T\left(R' - a_1 \bar{I}_\ell'(nT) - b_1 \bar{V}_c'(nT)\right)} \tag{6.9}$$

These equations may then be solved for a_1 and b_1 in terms of a, b, and the steady state conditions to find the optimal physical feedback into a sawtooth modulator.

These examples complete the presentation of the three-step design procedure for finding the physical feedback for the optimal transient case.

With the use of this procedure two different boost regulators were designed and simulated, one with a sawtooth pulse-width modulator and the other with a uniformly sampled modulator.

The converter parameter values used were those given at the beginning of this chapter. The clock ramp slope specified by R' in Eqs. (6.7) and (6.9) was arbitrarily set equal to 1000 for both modulators. The approximate expressions for $G_i(z)$ and $G_v(z)$ from Eqs. (5.14) were used for computation of the optimal effective gain from Eqs. (6.6). Then the straight-line approximation was used to simplify the exponential matrix of Eqs. (6.7) to find the physical gain into the uniformly sampled modulator. Next, to find the steady state derivatives $\bar{I}_\ell'(nT)$ and $\bar{V}_c'(nT)$ in Eqs. (6.9) the approximate techniques of Chapter 1 were used. These values then enabled the computation of the physical feedback into the sawtooth modulator with Eqs. (6.9). Large and small-signal regulator simulations of Eqs. (5.1) were then performed to investigate the accuracy of the approximate design techniques for the optimal response. Figures 6.6a and b are plots of the discrete transient current and voltage for an initial disturbance in duty ratio of 0.001, or 0.1 percent of the total period. These transients were computed for a small-signal linearized regulator model and for large-signal regulator models with sawtooth and uniformly sampled modulators. Agreement between the linearized model and the large-signal models with both types of modulators was good enough that to the eye their plots are indistinguishable in Fig. 6.6a

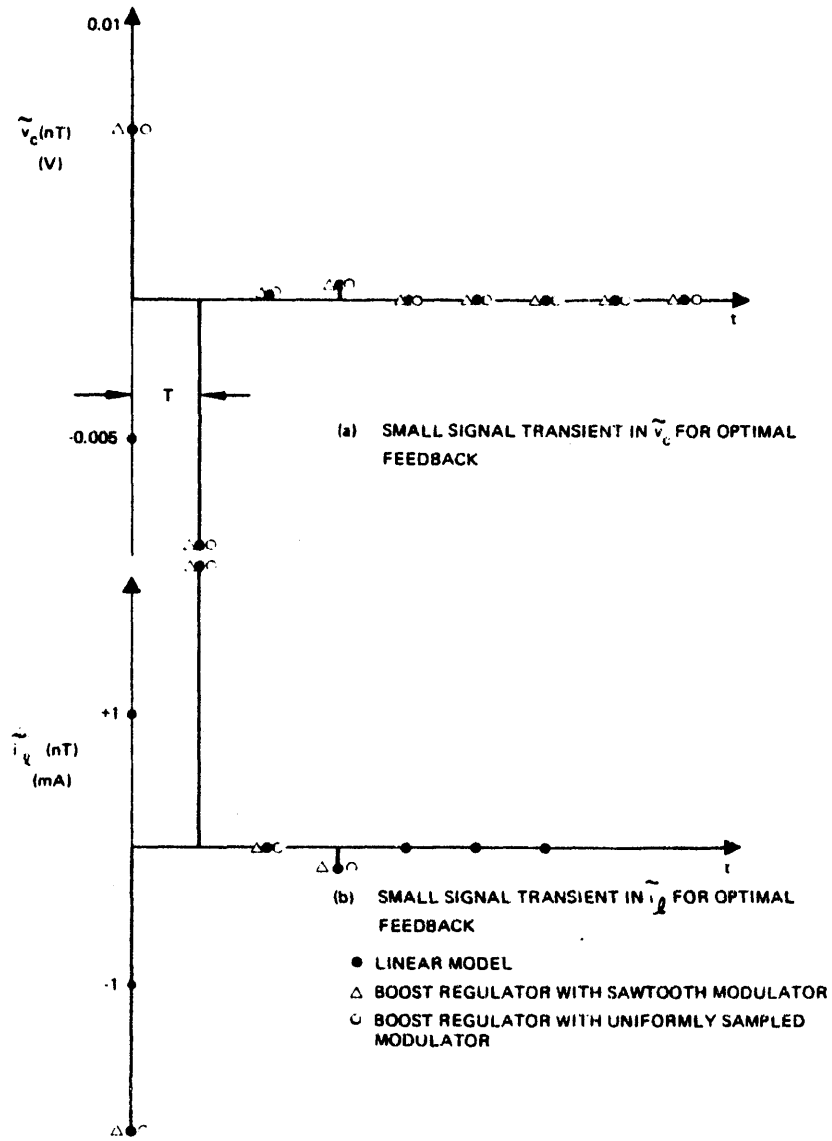

Fig. 6.6 Discrete perturbations $\tilde{v}_c(nT)$ and $i_\ell(nT)$ for a small disturbance from the optimal steady state solution.

and b. It is interesting to note that, except for a small residue in the fourth period, the transient is essentially finished in two periods as predicted in Chapter 5.

Agreement between the linearized and the large-signal regulators in Fig. 6.6 is not surprising because the initial perturbation from the steady state duty ratio was very small.

One would expect to see differences in the behavior of the linearized regulator model and the actual regulators for very large disturbances. However, it is to be expected that if the feedback is optimal for the small signal model, it will also be satisfactory for large disturbances as well, since real regulators are often subject to large source and load transients.

Figures 6.7 and 6.8 are plots of a large transient caused by an initial duty ratio perturbation of 10 percent (20 percent of either the $\bar{D}_1$ or $\bar{D}_2$ steady state pulse width). As anticipated, the linearized model and the two boost regulators all behave differently, but these differences are still not so great that the larger part of the transient is finished in the first two cycles. One might add that although these transients are large in the sense that the change in duty ratio is significant, the modulators do not saturate. Analysis of what happens with modulator saturation will vary from one regulator to the next, and it is doubtful that a linear model can yield useful design information in this case.

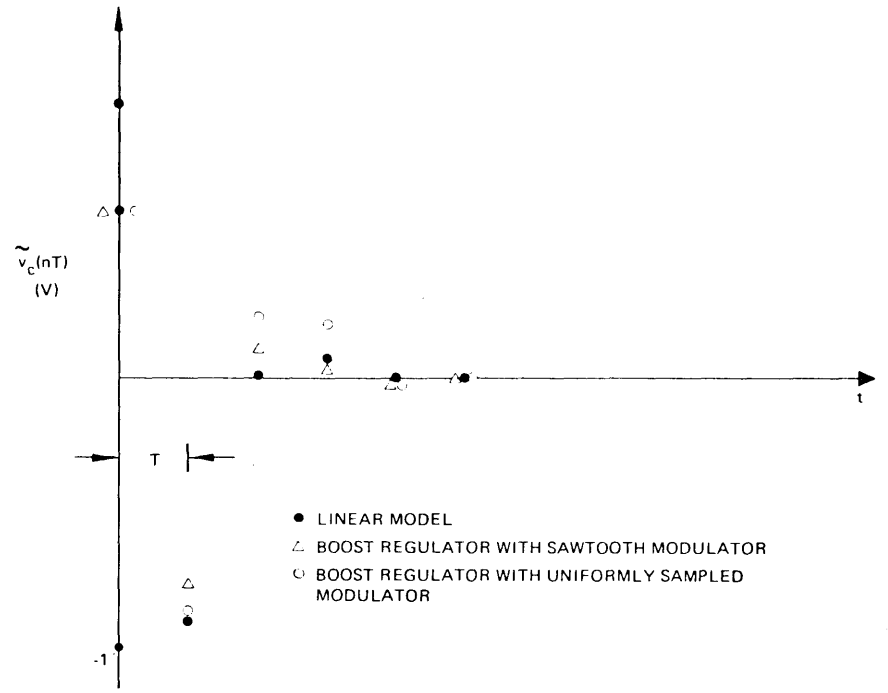

Fig. 6.7. Large-signal transient in $\tilde{v}_c(nT)$ for optimal feedback.

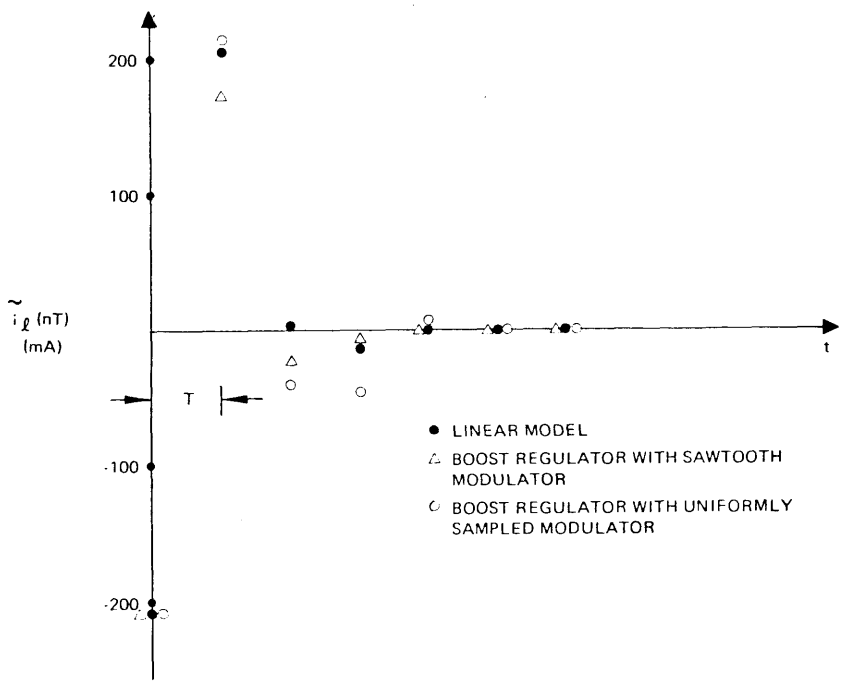

Fig. 6.8. Large-signal transient in $\tilde{i}_\ell(nT)$ for optimal feedback.

The results of this chapter may be briefly summarized as follows.

By the examination of three cases, voltage feedback, current feedback and optimal feedback, agreement has been shown between the behavior of large-signal regulators and their discrete models at low and high frequencies, and with two different types of modulators. From this it can be concluded that the discrete model is valid and useful for prediction of small transient behavior of a regulator about some steady state operating point.

The optimal response was shown to exist, and to be attainable even with a "delay" type modulator. Most important, though, is that use of the straight-line approximation together with the z-transform, allows one to design the physical feedback for a particular transient response such as the optimal response. A simple three-step procedure was introduced in this chapter to indicate the approach one might use to design for the optimal response. This is a clear indication that discrete modeling can indeed be useful as a synthesis tool which is the main goal of this thesis.

Also included in this chapter were a set of Bode plots comparing the discrete and df converter transfer functions. From these plots one may easily infer the high-frequency limitations of the df models.

Chapter 7

Review and Conclusions

The previous chapters have provided a number of useful results on the use of discrete models in the synthesis of switching regulators. It is the purpose of this last chapter to present the main conclusions and to add a few words on the application of this material.

The principal goal of this thesis is the development of simple discrete analysis techniques, for use in the initial design of switching regulators, which maintain the inherent accuracy of discrete methods over describing function methods at high frequencies.

A secondary goal is expression of the discrete models such that easy comparisons could be made between the discrete and the describing function results. This allows use of the discrete results as a yardstick to measure more explicitly the high frequency limitations of the df models.

The success in achieving these aims will be discussed after a review of the organization and results of each chapter.

In an attempt to make this work self-contained, the first chapter introduces the unfamiliar reader to a basic concept and functioning of a switching regulator. A simple analysis to find the steady state waveforms for a boost converter is presented to give the "feel" of a design-oriented approach. The main point of this chapter is that steady state converter waveforms are easily and quite accurately

found, so that their later inclusion as parameters in the discrete model should not be presumed to make the discrete models more difficult to find.

The second chapter contains the principal derivation of this work. It is shown that a generalized switching converter driven by a pulse-width modulated switch may be modeled about some steady state condition by a set of linear small-signal difference equations. A new symbol d_n is introduced in this derivation to model the normalized width of the small-signal modulation, and which later allows direct comparisons to be made between converter discrete and df transfer functions.

The main point of this chapter is to show that a small-signal difference equation converter model may be derived in a compact symbolic form almost by inspection of the converter state equations.

In Chapter 3 three different types of pulse-width modulators are shown to be characterized by small-signal difference equations compatible with those of the converter. With the assumption that the feedback is a linear combination of the converter state variables, detailed gain expressions are found for each modulator.

The key result of this chapter is that time delay of less than one cycle in a modulator only modifies the gain in the small-signal modulator models. It is also apparent from the derivations that small-signal discrete modulator models are usually easy to derive.

Chapter 4 shows that application of the z-transform to the difference equation models allows the regulator transient analysis problem to be treated in the frequency domain of the z-plane. For the case of converter state variable feedback, a loop gain quantity $T^*(z)$ is derived and shown to be composed of a linear combination of the converter transfer functions regardless of the type of modulator used. This means that the potential small-signal closed-loop dynamic behavior of a regulator is essentially independent of the choice of modulator.

A new identity is presented in this chapter for the case of a two-state converter which allows one to write, from the converter difference equations, the converter transfer functions directly without any matrix inversions, in terms of the converter transition matrix M and modulation gain K.

The most important conclusion of this chapter is that the potential transient performance of a switching regulator is strongly dependent on the converter transfer functions G(z). This in turn means that simplicity in the discrete modeling approach may be established by finding simple ways of deriving G(z).

Chapter 5 introduces a new approximation called the "straight-line" approximation, which enables G(z) to be explicitly evaluated in symbolic form with a minimal amount of computation. With the use of this approximation and the root locus, the potential transient performance of a boost regulator is investigated. Effects such as half

frequency oscillation and an optimal transient response are noted for various types of feedback.

The two key results of this chapter are that G(z) may be easily derived by use of the straight-line approximation, and that the resultant approximate G(ż) may then be used with the root locus in an exploratory manner to determine possible closed-loop transient responses.

In Chapter 6 verification of the effects predicted by the root locus is accomplished by means of a large-signal boost converter simulation. Comparisons between the discrete and df converter transfer functions are given in Bode plots which show explicitly the range of frequencies where the df models are valid. Also included in this chapter is a section covering the design of the physical feedback for two different types of pulse-width modulators. These methods are applied to the boost regulator example in order to achieve the optimal response with either modulator. The designs were then verified with a large-signal simulation.

The goal of Chapter 6 is to lend credence to the claims made in the earlier chapters. In particular the results predicted with the use of the approximate transfer functions are shown to be accurate in predicting high frequency closed-loop behavior. This indicates that use of the "straight-line" approximation does not degrade the accuracy inherent in the discrete regulator models.

In conclusion, the results of this thesis indicate that discrete models may be simplified to the point where it is possible to apply them in the initial design phases of switching regulators. We have seen that for the case of a two-state converter, it is possible to find the approximate discrete converter transfer functions with little more effort than the addition and subtraction of a few matrices. Furthermore, it has been shown that the closed-loop transient analysis problem may be intimately tied to solution of the discrete open-loop converter transfer functions by the introduction of a discrete loop gain and by application of the root locus to this loop gain.

A secondary goal, to provide a convenient way to gauge the accuracy of the df approach, was accomplished by introduction of the discrete equivalent d_n of the average modulation <d> into the discrete model formulation. One can show in general that if the "straight-line" approximation is valid, then, for frequencies where $|sT| \ll 1$, the transfer functions derived by either method agree with each other.

One of the most fruitful applications of the methods presented here is achievement of the optimal transient response for any given converter, through proper choice of feedback and modulator gain. Since the explicit results for the modulator and converter models show that the loop gain varies with the steady state condition, the objective is to design the loop gain to be insensitive to source and load changes so that the optimal response is achieved over a wide range of operating conditions.

In many systems measures of all the converter states may not be available for feedback purposes, in which case use of the root locus could indicate the limits on attainable transient performance.

Finally, it should be clear from this thesis that use of discrete models of switching regulators offers the designer substantial advantages in both accuracy and simplicity. In particular, this design approach permits an optimal transient response to be achieved.

References

1. I. M. H. Bábaá, T. G. Wilson, and Y. Yu, "Analytic Solutions of Limit Cycles in a Feedback-Regulated Converter System with Hysteresis," IEEE Trans. on Automatic Control, Vol. AC-13, No. 5, October 1968, pp. 524-531.

2. R. A. Skoog and G. L. Blankenship, "Generalized Pulse-Modulated Feedback Systems: Norms, Gains, Lipshitz Constants, and Stability," IEEE Trans. on Automatic Control, Vol. AC-15, No. 3, June 1970, pp. 300-315.

3. J. Rootenburg and R. Walk, "Stability of a General Type of Pulse-Width Modulated Feedback System," Bell Sys. Tech. J., Vol. 52, No. 11, December 1973, pp. 1811-1819.

4. R. D. Middlebrook and G. W. Wester, "Low-Frequency Characterization of Switched dc-dc Converters," IEEE Trans. on Aerospace and Electronic Systems, Vol. AES-9, No. 3, May 1973, pp. 376-385.

5. R. Prajoux, A. Capel, and J. G. Ferrante, "Stability Analysis of a P. W. M. Controlled DC/DC Regulator with DC and AC Feedback Loops," 1974 IEEE Power Electronics Specialists Conference Record, pp. 246-254 (IEEE Publication 74 CHO 863-1 AES).

6. R. Prajoux, A. Capel, and J. G. Ferrante, "State Variable Analysis of Multi-Loop PWM Controlled DC/DC Regulators in Light and Heavy Mode," 1975 IEEE Power Electronics Specialists Conference Record, pp. 91-103 (IEEE Publication 75 CHO 965-4 AES).

7. G. I. Cardwell and D. J. Packard, "A High Performance Line Regulator," 1974 IEEE Power Electronics Specialists Conference Record, pp. 106-113 (IEEE Publication 74 CHO 863-1 AES).

8. R. P. Iwens, Y. Yu, and J. E. Triner, "Time Domain Modelling and Stability Analysis of an Integral Pulse Frequency Modulated DC to DC Power Converter," 1975 IEEE Power Electronics Specialists Conference Record, pp. 80-90 (IEEE Publication 75 CHO 965-4 AES).

9. Y.S. Zypkin, "Theorie der Relaissysteme der Automatischen Regelung (book)," R. Oldenburg, Munich, Germany, 1958.

10. R. E. Andeen, "Analysis of Pulse Duration Sampled-Data Systems with Linear Elements," IRE Trans. on Automatic Control, Vol. AC-5, No. 4, September 1960, pp. 306-313.

11. E.S. McVey, and G.S. Nurre, "The Application of z-Transform Theory to the Analysis of Switched-Type Nonlinear Systems," IEEE Trans. on Applications and Inudstry, Vol. 83, No. 75, November 1964, pp. 353-360.

12. J.P. Sucena-Paiva, R. Hernandez, and L. L. Freris, "Stability Study of Controlled Rectifiers Using a new Discrete Model," IEEE Proceedings, Vol. 119, No. 9, September 1972, pp. 1285-1293.

13. J.M. Yuh, "Analysis and Comparative Study of Buck Regulators," PhD dissertation, Division of Engineering and Applied Science, California Institute of Technology, Pasadena, Calif., 1973.

14. R.D. Middlebrook and S. Cuk, "A General Unified Approach to Modelling Switching-Converter Power Stages," IEEE Power Electronics Specialists Conference, NASA Lewis Research Center, Cleveland, Ohio, June 8-10, 1976.

Appendix 1

Writing State Equations

Presented in this appendix is a review of a simple systematic way of finding the state equations for networks of the type commonly found in switching power converters.

The basic steps in finding the state equations of a converter during any switching interval may be summarized as follows:

1. In order to maintain state variable continuity across each switching instant, choose the state variables to be the current in each inductor and the voltage across each capacitor, giving each a reference direction on the circuit schematic.

2. Replace each inductor with an independent current source, and replace each capacitor with an independent voltage source.

3. Solve the resultant resistive network for the voltage across each inductive current source and the current through each capacitive voltage source.

4. Note that the voltage V_ℓ across each inductive current source is equal to $L\frac{dI_\ell}{dt}$ and the current I_c through each capacitive voltage is $C\frac{dV_c}{dt}$.

5. Divide each state equation by its respective L or C to get the standard form as presented in Chapter 2.

As an example of this technique, consider the boost converter of Fig. A1. 1. This converter is shown with parasitic elements representing loss in the inductor and capacitor to make the final state equations less trivial. Also, the converter is assumed to be operating in the interval where the transistor switch is open and the commutating diode (shown in dashed lines) is effectively closed. Note the inductor current I_l and capacitor voltage V_c are chosen as the state variables.

Next, Fig. A1. 2 shows the reactive elements replaced by independent sources. The input power supply, V_s, is also an independent source. This corresponds to step 2.

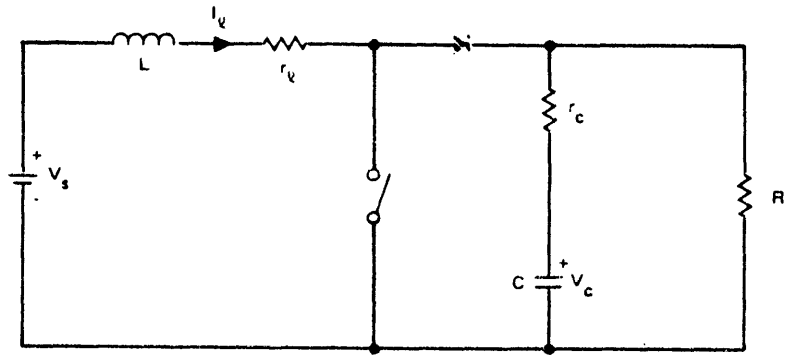

Fig. A1. 1. Boost converter with parasitic loss elements.

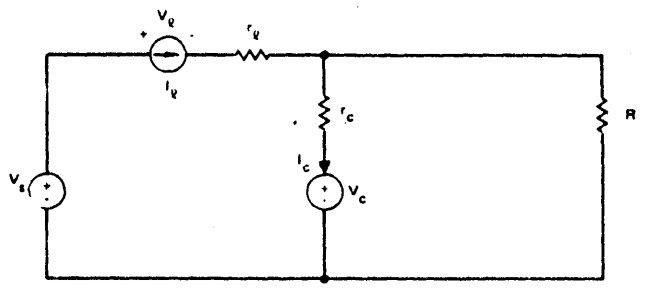

Fig. A1. 2. Source replacement of state variables.

The next step is to solve for the current through V_c (labeled I_c) and the voltage across I_ℓ (labeled V_ℓ). By superposition, these equations are of the form:

$$V_\ell = K_1 I_\ell + K_2 V_c + K_3 V_s$$

$$I_c = K_4 I_\ell + K_5 V_c + K_6 V_s$$

To find the K_i simply turn off the other sources (i. e., short the voltage sources and open the current sources) and compute V_ℓ or I_c as a function of the remaining source.

For example, to find K_1, turn off V_c and V_s as shown in Fig. A1. 3. Compute V_ℓ and hence K_1 as follows:

$$V_\ell = -\left[r_\ell + r_c || R\right] I_\ell = K_1 I_\ell$$

$$K_1 = -\left[r_\ell + r_c || R\right]$$

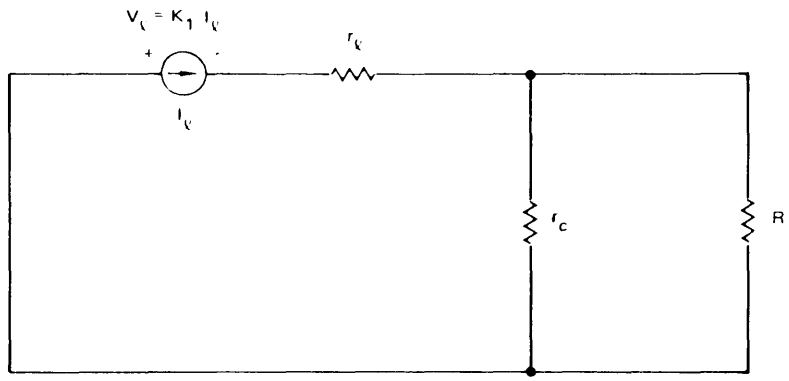

Fig. A1.3. Circuit for computation of K_1.

In a similar manner, the other K's may be found to yield:

$$V_\ell = -\left[r_\ell + r_c \,||\, R\right] I_\ell - \left(\frac{R}{r_c + R}\right) V_c + V_s$$

$$I_c = \left(\frac{R}{r_c + R}\right) I_\ell - \left(\frac{1}{r_c + R}\right) V_c \qquad \text{(A1.1)}$$

Finally, note that the relations between I_ℓ, V_ℓ and I_c, V_c are:

$$V_\ell = L \frac{dI_\ell}{dt}$$

$$I_c = C \frac{dV_c}{dt}$$

Substitution of these relations for V_ℓ and I_c in eq. (A1.1) gives:

$$L\frac{dI_\ell}{dt} = -\left[r_\ell + r_c \,||\, R\right] I_\ell - \left(\frac{R}{r_c + R}\right) V_c + V_s$$

$$C\frac{dV_c}{dt} = \left(\frac{R}{r_c + R}\right) I_\ell - \left(\frac{1}{r_c + R}\right) V_c$$

Division by L and C finally puts the state equations in standard form:

$$\begin{bmatrix} \dot{I}_\ell \\ \dot{V}_c \end{bmatrix} = \begin{bmatrix} -\dfrac{r_\ell + r_c \,||\, R}{L} & -\dfrac{R}{(r_c + R)L} \\ \dfrac{R}{(r_c + R)C} & -\dfrac{1}{(r_c + R)C} \end{bmatrix} \begin{bmatrix} I_\ell \\ V_c \end{bmatrix} + \begin{bmatrix} \dfrac{1}{L} \\ 0 \end{bmatrix} \begin{bmatrix} V_s \end{bmatrix}$$

This method will always work provided there are no loops of capacitors or nodes with only inductors connected to them, cases which typically never occur in converter models.

Appendix 2

Analysis of Reactive Compensation

A simplified way of handling regulator compensation for the discrete models is presented in this appendix. Discussion of the problem is followed by a general and a specific example to indicate the method.

To begin, compensation as it is used here will mean the addition of reactive elements, usually capacitors, in the feedback of a regulator to improve performance either in transient response or regulation. With the discrete model there are two ways to tackle the additional complexity that reactive compensation introduces.

The most direct approach is to consider each additional reactive element in the compensation as an additional state variable of the converter. Then, this new, more complex converter could be treated by the methods of Chapter 2 to derive small-signal linear difference equations about some operating point.

The main problem is that to find the z-transform transfer functions of the modulation to each of the state variables (now including the compensation) requires the evaluation of $(zI - M)^{-1} M$, where M is the transition matrix now of the converter-plus-compensation. If M is 2 x 2, evaluation is easy as shown in Chapter 4. For M of order 3 or higher (which a two-pole converter plus reactive compensation would be) the evaluation of the inverse in symbolic form would be quite complicated. Furthermore, if one wished to see the effect of

a change in the type of compensation, the whole model development procedure would have to be repeated. A general example will be first used to show a simpler alternative method based on a "non-loading" approximation.

The small-signal nonlinear state equations for a two-mode converter-plus-compensation may be represented by Eqs. (A2. 1), assuming single edge modulation.

$$\begin{bmatrix} \tilde{x} \\ \hline \tilde{x}_c \end{bmatrix} = (\bar{D}_1 A_1' + \bar{D}_2 A'_2) \begin{bmatrix} \tilde{x} \\ \hline \tilde{x}_c \end{bmatrix} + \begin{bmatrix} K \\ \hline K_c \end{bmatrix} d \qquad \text{(A2. 1)}$$

This corresponds to Eqs. (2. 5) with the product terms of d and the perturbation neglected, because they do not contribute to the small-signal difference equations.

In Eqs. (A2. 1) the state variables are partitioned into two groups $\tilde{x}$, to represent the state variables of the converter, and $\tilde{x}_c$ to represent the state variables of the compensation,

$$\begin{bmatrix} \tilde{x} \\ \hline \tilde{x}_c \end{bmatrix} = \begin{bmatrix} \tilde{x}_1(t) \\ \vdots \\ \tilde{x}_m(t) \\ \hline \tilde{x}_{c1}(t) \\ \vdots \\ \tilde{x}_{cj}(t) \end{bmatrix}$$

In a similar fashion K and K_c are sets of constants, derived as shown in Chapter 2, which represent the effect of the modulation on each of the state variables. As mentioned at the beginning of the appendix, Eqs. (A2. 1) could be treated as just a bigger, more complicated converter. Quite often, however, one can take advantage of the fact that in practical systems the converter voltages and currents affect those of the compensation, but not vice-versa. In other words, one can often assume that the compensation does not load the converter sufficiently to affect the operation.

Figures A2. 1a and b are two typical examples of this case. In Fig. A2. 1a it should be clear that small changes in the filter capacitor voltage (a converter state variable) will have much more effect on the compensation capacitor voltage (a compensation state variable)

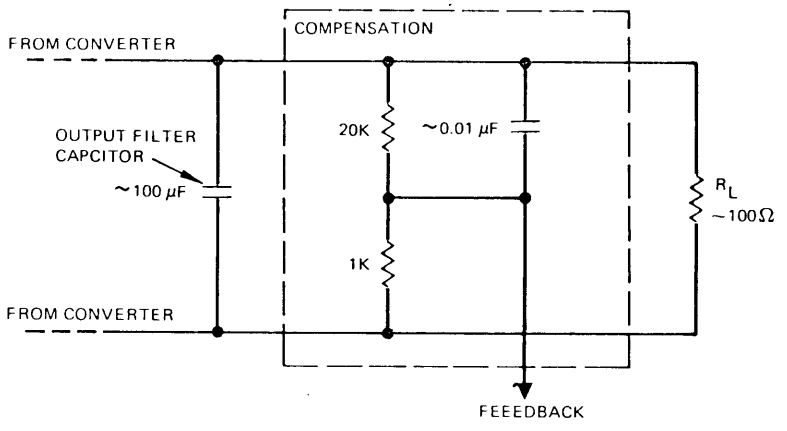

(a) LEAD-LAG COMPENSATION

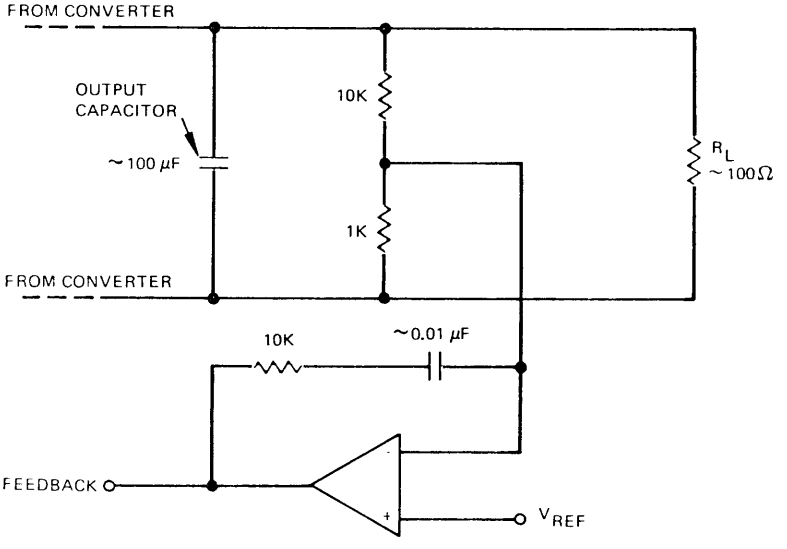

(b) LAG-LEAD COMPENSATION

Fig. A2.1. Typical compensation configurations for switching regulators.

than vice versa because of the relative component sizes. In Fig. A2.1b the op-amp makes this reverse signal flow even more negligible.

These examples help to indicate that although the non-loading assumption is an approximation, it is an extremely good one for most converters and most kinds of compensation.

The mathematical ramifications of the non-loading assumption are that the converter-plus-compensation state matrices A'_1 and A'_2 of Eqs. (A2.1) have the partition property as shown,

$$A'_1 = \left[\begin{array}{c|c} A_1 & \sim 0 \\ \hline H & A_c \end{array}\right]$$

$$A'_2 = \left[\begin{array}{c|c} A_2 & \sim 0 \\ \hline H & A_c \end{array}\right]$$

where A_1 and A_2 specify the topology of the converter by itself, A_c the topology of the compensation by itself, and H indicates how the converter states couple to the compensation.

Most important is the matrix block which is approximately all zeros, which specifies the back coupling from the compensation to the converter. If the compensation topology is altered in the two intervals then there would be an A_{c1} and A_{c2} instead of A_c in A'_1 and A'_2. Also, if the forward coupling were switched, H would have to be replaced by H_1 and H_2. For simplicity, it will be assumed that H and A_c are sufficient to model the coupling.

If the modulation is single-edged and located at the beginning of the $\bar{D}_1 = 1$ interval, then Eqs. (A2. 1) may be integrated as in Chapter 2 to find the linear difference equations for the converter-plus-compensation. The result is shown in Eqs. (A2. 2):

$$\begin{bmatrix} \tilde{x} \\ \hline \tilde{x}_c \end{bmatrix}_{(n+1)T} = e^{\left[\begin{array}{c|c} A_2 & 0 \\ \hline H & A_c \end{array}\right]\tau_2} e^{\left[\begin{array}{c|c} A_1 & 0 \\ \hline H & A_c \end{array}\right]\tau_1} \left(\begin{bmatrix} \tilde{x} \\ \hline \tilde{x}_c \end{bmatrix}_{nT} + \begin{bmatrix} K \\ \hline K_c \end{bmatrix} d_n T \right) \qquad \text{(A2. 2)}$$

With use of the series definition of the exponential matrix, it can easily be shown that the following equalities hold:

$$e^{\begin{bmatrix} A_1 & 0 \\ H & A_c \end{bmatrix}\tau_1} = \begin{bmatrix} e^{A_1\tau_1} & 0 \\ M_{c1} & e^{A_c\tau_1} \end{bmatrix}$$

$$e^{\begin{bmatrix} A_2 & 0 \\ H & A_c \end{bmatrix}\tau_1} = \begin{bmatrix} e^{A_2\tau_2} & 0 \\ M_{c2} & e^{A_c\tau_2} \end{bmatrix}$$

where

$$M_{c1} = H\tau_1 + (HA_1 + A_cH)\frac{\tau_1^2}{2} + \ldots$$

and

$$M_{c2} = H\tau_2 + (HA_2 + A_cH)\frac{\tau_2^2}{2} + \ldots$$

Substitution of these relations in (A2. 2) yields:

$$\begin{bmatrix} \tilde{x} \\ \hline \tilde{x}_c \end{bmatrix}_{(n+1)T} = \left[\begin{array}{c|c} e^{A_2\tau_2} \cdot e^{A_1\tau_1} & 0 \\ \hline M_{c2}e^{A_1\tau_1} + e^{A_c\tau_2}M_{c1} & e^{A_c T} \end{array}\right] \begin{bmatrix} \tilde{x} \\ \hline \tilde{x}_c \end{bmatrix}_{nT} + \begin{bmatrix} K \\ \hline K_c \end{bmatrix} d_n T$$

This shows that the partitioning property of A'_1 and A'_2 allows the difference equations to be partitioned into two sets. The first set is the original description of the converter by itself:

$$\tilde{x}\left((n+1)T\right) = e^{A_2\tau_2} \cdot e^{A_1\tau_1}\left[\tilde{x}(nT) + Kd_nT\right] \quad (A2.3)$$

The second set describes the compensation and how the converter is coupled to the compensation:

$$\tilde{x}_c\left((n+1)T\right) = e^{A_c T}\left[\tilde{x}_c(nT) + K_c d_n T\right] + \left[M_{c2}\, e^{A_1\tau_1} + e^{A_c\tau_2}M_{c1}\right]$$

$$\left[\tilde{x}(nT) + Kd_nT\right] \quad (A2.4)$$

This partitioning property can save a great deal of effort on the part of the designer. First, the converter can be characterized independently of any compensation and its z-transfer functions found.

Changing compensation only requires reevaluation of the set of difference equations describing the compensation and its coupling with the converter.

Also, since the converter-plus-compensation problem is split into two parts, the order of each part is reduced making it easier to work in symbolic form.

To illustrate how this result might be applied to a particular regulator, consider the boost converter used as an example in Chapter 5. It was shown that for a particular operating point, if the proper sum of inductor current I_ℓ and capacitor voltage V_c were fed back, an optimal transient response could be achieved. The feedback tends to hold this sum of I_ℓ and V_c constant, so if I_ℓ increases, V_c decreases, yielding a regulator with a closed loop output impedance typically too high to be a good voltage regulator and too low to be a good current regulator. In essence what one has is a regulator that has excellent transient properties, but with an unacceptable output impedance.

This situation may be remedied by integration compensation. To make the regulator a good voltage regulator, for example, one could integrate the difference between the output capacitor voltage V_c and some reference V_{ref}. Feeding this integrated voltage error back should insure a good voltage regulation regardless of any other feedback.

The new state variable V_p, the voltage across the compensation capacitance, then satisfies Eq. (A2.5):

$$V_p = k_p \int_o^t (V_c(t) - V_{ref})\, dt \qquad \text{(A2.5)}$$

or

$$\dot{V}_p = k_p (V_c(t) - V_{ref})$$

The small-signal version of Eq. (A2.5) is then:

$$\dot{\tilde{v}}_p = k_p \tilde{v}_c(t)$$

Insertion of the equation for the compensation state variable $\tilde{v}_p$ together with the state equations of the boost converter yields Eqs. (A2.6). The dashed lines are drawn to indicate how the matrices in Eqs. (A2.6) are partitioned.

$$\begin{bmatrix} \tilde{i}_\ell \\ \tilde{v}_c \\ \hline \tilde{v}_p \end{bmatrix} = \bar{D}_1 \left[\begin{array}{cc:c} 0 & 0 & 0 \\ 0 & -\frac{1}{RC} & 0 \\ \hline 0 & k_p & 0 \end{array}\right] \begin{bmatrix} \tilde{i}_\ell \\ \tilde{v}_c \\ \hline \tilde{v}_p \end{bmatrix} + \bar{D}_2 \left[\begin{array}{cc:c} 0 & -\frac{1}{L} & 0 \\ \frac{1}{C} & -\frac{1}{RC} & 0 \\ \hline 0 & k_p & 0 \end{array}\right] \begin{bmatrix} \tilde{i}_\ell \\ \tilde{v}_c \\ \hline \tilde{v}_p \end{bmatrix}$$

$$+ \begin{bmatrix} -\frac{\bar{V}_c(T)}{L} \\ +\frac{\bar{I}_\ell(T)}{C} \\ 0 \end{bmatrix} d \qquad \text{(A2.6)}$$

From Eqs. (A2.6) the following quantities used in the compensation difference equations may be identified:

$$A_c = 0 \qquad K = \begin{bmatrix} -\frac{\bar{V}_c(T)}{L} \\ +\frac{\bar{I}_\ell(T)}{C} \end{bmatrix}$$

$$H = \begin{bmatrix} 0 & k_p \end{bmatrix} \qquad K_c = 0$$

For typical parameter values for the boost converter, the coupling coefficients in the compensation difference equation are well approximated by retention of only the first order terms in time as shown below:

$$\left[M_{c2} e^{A_1 \tau_1} + e^{A_c \tau_2} M_{c1} \right] = \left[H\tau_2 I + IH\tau_1 \right] = HT$$

$$= \begin{bmatrix} 0 & k_p T \end{bmatrix}$$

Using these results, the approximate compensation difference equation for this case in the form of Eqs. (A2.4) is given by Eq. (A2.7).

$$\tilde{v}_p\left((n+1)T\right) = \tilde{v}_p(nT) + k_p T\left[\tilde{v}_c(nT) + \frac{T\bar{I}_\ell(T)}{C} d_n\right] \qquad (A2.7)$$

Application of the z-transform to (A2.7), with $v_p(0) = 0$ for transfer function calculation, leads to

$$\tilde{v}_p^*(z) = \frac{k_p T\left(\tilde{v}_c^* + \frac{T\bar{I}_\ell(T)}{C} d^*\right)}{(z - 1)}$$

The transfer function of the boost converter is known from the analysis of Chapter 5 to be $v_c^* = G_v(z)d^*$. This is then used to write the transfer function from d^* to v_p^* as:

$$\frac{v_p^*}{d^*} = \frac{k_p T\left(G_v(z) + \frac{T\bar{I}_\ell(T)}{C}\right)}{(z - 1)}$$

With the expression developed in Chapter 5 for $G_v(z)$, one can then show that the expression for the compensation transfer function $G_p(z)$ is of the form

$$\frac{v_p^*}{d^*} = G_p(z) = \frac{k'' z\left(\frac{z}{z_p} + 1\right)}{(z - 1)(z - z_1)(z - z_2)} \qquad \text{(A2.8)}$$

where

$$k'' = k_p T^2 \frac{\bar{I}_\ell(T)}{C}\left(1 + \frac{\bar{V}_c(T)}{\bar{I}_\ell(T)}\frac{\tau_2}{L}\right); \qquad z_p = \left(1 + \frac{\bar{V}_c(T)}{\bar{I}_\ell(T)}\frac{\tau_2}{L}\right)$$

For the parameters of Chapter 6, $z_p = 1.25$.

From this example, it should be clear that the compensation problem can be greatly simplified by the non-loading approximation. The derivation of the transfer function of Eq. (A2.8) required no matrix inversions nor any additional analysis on the basic converter by itself. With its simplicity this approximation should extend the capability of the designer to the point where nearly any converter with reactive compensation can be symbolically analyzed.

Appendix 3

An Invariant Property of the Transition Matrix

In this appendix we show a property of transition matrices that is invariant with problem formulation, that all transition matrices for a particular converter have the same eigenvalues. The physical argument is as follows:

Consider a converter of the general type introduced in Chapter 2 and operating at a steady state condition. If it is disturbed and allowed to settle back to its steady state, without any pulse-width modulation, the dynamic behavior of this transient should be the same regardless of how we formulate the difference equations to describe it.

The difference equation model for a converter is not unique because it only describes converter behavior at a particular set of time points. In Chapter 2 Eqs. (2.13) showed that by taking a time reference at the beginning of the $\bar{D}_1 = 1$ interval a specific set of linear difference equations describes the converter problem of perturbations on a steady state solution. An equally valid description of the problem would be Eqs. (2.14), obtained by taking the reference time at the beginning of the $\bar{D}_2 = 1$ interval as in Fig. A3.1. When

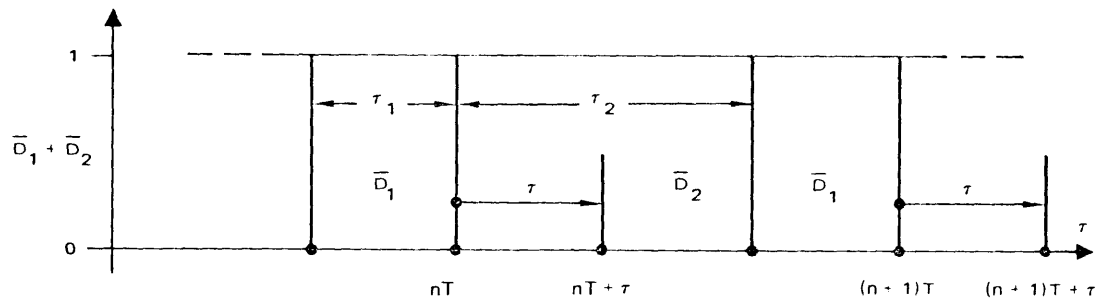

Fig. A3.1. Converter timing diagram.

there is no modulation Eqs. (2.13) and (2.14) reduce to Eqs. (A3.1) and (A3.2):

$$\tilde{x}\left((n+1)T\right) = e^{A_2\tau_2} e^{A_1\tau_1} \tilde{x}(nT) \qquad \text{(A3.1)}$$

$$\tilde{x}\left((n+1)T\right) = e^{A_1\tau_1} e^{A_2\tau_2} \tilde{x}(nT) \qquad \text{(A3.2)}$$

If the matrices A_1 and A_2 are not identical, then the transition matrices of Eqs. (A3.1) and (A3.2) will usually be different. Yet, if the formulation of the problem is correct, both matrices must indicate that the converter has the same dynamic behavior. One way of solving difference equations such as Eqs. (A3.1) is through the use of the z-transform. The procedure is quite analogous to using Laplace transform to solve sets of linear differential equations. A basic result of this approach is that poles in the z-plane indicate natural frequencies of the discrete system in the same way that poles in the s-plane correspond to natural frequencies of a continuous system. The z-plane poles occur at eigenvalues of the transition matrix. Thus,

if the discrete formulation of the converter problem is correct, then all transition matrices for the same converter must have the same eigenvalues. This is easily proved because of the structure of the problem. First we show that if a time τ later than the reference time is chosen for a new formulation of the homogeneous converter problem, the new transition matrix is formed by splitting a matrix off one side of the old transition matrix and multiplying it on the other side.

With reference to Fig. A3.1 the original problem formulation is:

$$\begin{aligned}
\tilde{x}\left((n+1)T\right) &= e^{A_1\tau_1}\, e^{A_2\tau_2}\, \tilde{x}(nT) \\
&= e^{A_1\tau_1}\, e^{A_2(\tau_2+\tau-\tau)}\, \tilde{x}(nT) \\
&= \left[e^{A_1\tau_1}\, e^{A_2(\tau_2-\tau)}\right]\left[e^{A_2\tau}\right]\tilde{x}(nT) \\
&= [A][B]\,\tilde{x}(nT)
\end{aligned}$$

Using $nT + \tau$ at the reference time, the new formulation is:

$$\begin{aligned}
\tilde{x}\left((n+1)T+\tau\right) &= \left[e^{A_2\tau}\right]\left[e^{A_1\tau}\, e^{A_2(\tau_2-\tau)}\right]\tilde{x}(nT+\tau) \\
&= [B][A]\,\tilde{x}(nT+\tau)
\end{aligned}$$

Clearly then, for a particular converter given any two transition matrices, one can find two nonsingular (because they are products of exponential matrices which are nonsingular) matrices A and B such that AB is one transition matrix and BA is the other.

Therefore, to show that the eigenvalues and hence the system dynamics remain invariant with regard to when the reference time is chosen, one only need show that the eigenvalues of AB are identical to those of BA for square nonsingular A and B.

Note, the following equality holds, since A is invertible:

$$\lambda I - AB = A[\lambda I - BA]A^{-1}$$

Taking the determinant of both sides we find:

$$\text{Det. } (\lambda I - AB) = \text{Det. } \left(A\,(\lambda I - BA)\,A^{-1}\right)$$

$$= \text{Det. } (A)\ \text{Det. } (\lambda I - BA)\ \text{Det. } (A^{-1})$$

$$= \text{Det. } (\lambda I - BA)$$

The characteristic equations and hence the eigenvalues are identical.

This result tells us two things: First, that the discrete converter model behaves in a way compatible with the physical converter, and second, that if we somehow can find the eigenvalues for a particular converter transition matrix, then we know them for any other transition matrix for the same converter provided the operating point stays the same.